Practical Fault Simulation on an Earthing Transformer using SFRA

A unique analysis approach towards simplifying SFRA results
to assist with deformation diagnosis in Earthing Transformers

Hayden Sherwood

Undergraduate Electrical Power Engineer

Supervisor: Dr.Gareth Lee

A thesis submitted to the School of Engineering and Energy, **Murdoch University**
in partial fulfilment of the requirements for the degree of

Bachelor of Engineering Honours [BE(Hons)]
Electrical Power Engineering

Perth, 2017

Author's Declaration

I, Hayden Neville Kok Sherwood, certify that this work contains no material which has been accepted for the award of any other degree or diploma in my name, in any university or other tertiary institution and, to the best of my knowledge and belief, contains no material previously published or written by another person, except where due reference has been made in the text.

In addition, I certify that no part of this work will, in the future, be used in a submission in my name, for any other degree or diploma in any university or other tertiary institution without the prior approval of the Murdoch University.

I give consent to this copy of my thesis, when deposited in the University Library, being made available for loan and photocopying, subject to the provisions of the Copyright Act 1968.

I also give permission for the digital version of my thesis to be made available on the web, via the University's digital research repository, the Library Search and also through web search engines, unless permission has been granted by the University to restrict access for a period of time.

Signed: …………………………………………….

Name: …………………………………………..

Date: …………………………………………..

Abstract

Earthing Transformers are an integral part of power and distribution systems around the world, although, little consideration is given to their ongoing monitoring and maintenance. The failure of an earthing transformer can cause a multitude of issues including compromised stability and safety of the electrical network. The necessity to maintain both safety and stability of electrical networks highlights valuable real world applications for an SFRA earthing transformer testing toolkit.

As a starting point, the project adopted a review of existing research along with an analysis of earthing transformer design principles. Research found that because of an inherent design strategy, many ZN wound earthing transformers have a unique failure type in common; axial displacement of the inner and outer windings.

The second project stage involved physical simulation of an earthing transformer's axial windings displacement using SFRA as a diagnosis tool. Simulation results provided evidence that (for the given test subject) defect detection is possible using SFRA benchmarked comparisons.

Analysis of benchmarked comparisons found deviation only at select resonances with general spectral shape retention for all other points along the SFRA trace. Spectral consistency of benchmarked comparisons allowed the implementation of a speech processing technique known as Mel-Frequency Cepstral Coefficients (MFCC). An adaption of the MFCC process introduced a way of encoding and distilling the SFRA trace data while exaggerating critical points of deviation.

The third major project stage involved the development of code using Mathworks MATLAB as a platform to the fulfil data management and computational requirements of the adapted MFCC. Select variables were isolated throughout the code to ensure that the process was tune-able on multiple levels for future optimisation.

By selecting and mapping the appropriate resultant cepstral coefficients against each other, it was found that a meaningful representation of the SFRA trace can be graphically presented as a single point on a two-dimensional plot. Simulated transformer defect scenarios had notable deviation on both the x and y axis when processed and plotted together.

Analysis, processing and comparison of 28 different earthing transformer SFRA traces found possible real world applications for a single point spectrum classifier. The spectrum classifier was proposed as a substitution for pre-existing subjective analysis techniques, potentially building on the communal engineering toolbox for SFRA analysis.

Acknowledgements

Table of Contents

List of Figures

List of Tables

List of Abbreviations

Table 1.1 – List of Abbreviations used throughout the report.

Abbreviation	Meaning	Category
A	Ampares	Electrical
APU	Australian power utility	Organisation
BIL	Basic Impulse Level	Electrical
CIGRE	Conference Internationale des Grandes Reseaux Electriques	Organisation
CSV	Comma Separated Value	Software
CT	Current Transformer	Electrical
DGA	Dissolve Gas Analysis	Electrical
Dyn*	Delta Primary windings connection & Star Secondary winding connection (Transformer Vector group for a step-down Tx with unknown phase angle)	Electrical
EPE	Excess Power Equipment	Organisation
FAT	Factory Acceptance Testing	Electrical
FFT	Fast Fourier Transform	Mathematical
HV	High Voltage	Electrical
Hz	Hertz	Electrical
IDCT	Inverse Descrete Cosine Transform	Mathamatical
IEEE	Institute of Electrical and Electronics Engineers	Organisation
kVA	Kilo Volt Ampares	Electrical
LFCC	Linear-frequency cepstral coefficients	Speech Analysis
LPC	Linear predictive coding analysis	Speech Analysis
LV	Low Voltage	Electrical
MEN	Multiple Earthed Neutral	Electrical
MFCC	Mel-frequency cepstral coefficients	Speech Analysis
OC	Open circuit	Electrical
PLP	Perceptual linear predictive coefficients	Speech Analysis
RLC	Resistive, Inductive and capacitive	Electrical
SC	Short circuit	Electrical
SFRA	Sweep Frequency Response Analysis	Electrical
V	Voltage	Electrical
VA	Volt Ampares	Electrical
Zn	Zig-Zag winding configuration	Electrical

Chapter 1   Introduction

Earthing Transformers are an integral part of power and distribution systems around the world, although, little consideration is given to their ongoing monitoring and maintenance. These transformers provide network operators both an earth point for delta systems and a method of limiting the fault levels within the power system. The focus on maintenance and monitoring is generally aimed at the larger power transformer which have a high capital cost, yet the earthing transformer provides a level of protection to the main unit. The failure of an earthing transformer can have a significant adverse impact on the main transformer and so understanding the changing state of the internals over time is of importance in helping preserve the main transformer throughout its service life.

Over the past decade, Sweep Frequency Response Analysis (SFRA) has become a popular method for detecting physical changes inside power and distribution transformers. Very little documented research, however, has been invested in SFRA of three phase zig-zag (ZN) wound earthing transformers.

This thesis proposes the use of SFRA to detect mechanical defects in ZN wound earthing transformers, prior to a potentially hazardous and costly asset failure. One of the main project goals is to determine if it is possible to diagnose developing faults in an earthing transformer using SFRA alone. A detailed analysis of specific faults that most commonly affect earthing transformers will be presented, followed by practical fault case simulations. Fault case simulations, benchmarked and compared using SFRA, will be offered to solidify communal understanding of fault diagnosis in earthing transformers.

A secondary goal of the project is to develop a tool to assist in deciding if an earthing transformer needs to be serviced, refurbished or replaced from an asset management standpoint. Research will consider existing SFRA analysis methods, leading to the proposal of a unique approach to processing raw SFRA data for assistive fault diagnosis. Design requirements for the assistive tool are defined as follows:

- Simple interface,
- Automatic data management & simple intuitive data acquisition,
- Multiple trace entry and processing capability,
- Automated processing with minimal user variable inputs,
- Refinable process,
- Simple output display,
- Meaningful output to assist with fault diagnosis.

2

The design requirements listed above provide a metrics for the successful completion of the defined second stage of this project.

The use of SFRA as an input interface in conjunction with a specific knowledge base of fault responses aims to enable the creation of a customised assistive fault diagnosis tool. Collectively, the objective of this project is to highlight the value of implementing ongoing monitoring and maintenance strategies for earthing transformers, while simplifying the analysis process.

The outcomes here will be a clear benefit to network operators who may be able to predict when to remove an earthing transformer from service prior to failure and thereby saving the main transformer from unwarranted fault currents that may in turn damage or destroy the transformer prematurely.

Chapter 2   Background

This chapter presents an overview of the key concepts, relevant to earthing transformers, sweep frequency response analysis, transformer faults and data analysis techniques has been presented below. A fundamental understanding of the highlighted topics is required to develop an appreciation for justifications made later in this report. Although a basic understanding of electrical principles has been assumed, earthing transformers are a relatively unique component of any substation arrangement and so the question arises; why do we need earthing transformers?

2.1   Why do we need earthing transformers?

An earth (ground) reference point must be present in almost all electrical systems to ensure local safety compliance and integrity of equipment is maintained [1]. AS/NZS 3000 calls for a Multiple Earthed Neutral (MEN) system in which the Star (Wye) connected windings of a transformer (Neutral point) is bonded at Ground potential [2]. The MEN connection provides a return path for currents flowing from a phase conductor to earth (typically under fault conditions).

Electrical system protection is often formed using monitoring current transformers (CT's) on the transformers MEN connection. An imbalance in phase loading will cause currents to flow back through the transformers neutral bushing via the MEN connection. If the current flowing through a neutral connection is above safe working levels (typically under phase to ground fault conditions), the corresponding upstream protection relay is designed to trip (Isolating the transformer or substations feed) after a graded time setting [3].

The lack of a MEN connection means that no fault current can flow back through the neutral conductor and the respective upstream protection (neutral CT dependant) would not trip. If, for instance, an earth fault was present in a star connected supply without a MEN connection - even for a delta-connected load - one ramification would be high phase to neutral voltages. In this instance, high phase to neutral voltages are caused by unbalanced phase loading and could potentially damage connected loads, other electrical infrastructure and the transformers winding insulation [4]. Unprotected line to ground faults can also cause large safety risks to Persons and livestock as detailed in AS2067, making specific reference to step and touch considerations from AS/NZS 60479.1 [5]. The Victorian government has invested $750 million in the Powerline Bushfire Safety program (PBSP), recognising that as an un-isolated, fallen power line can cause fires [6].

For systems that do not have an earthing reference (such as a Delta connected supply) an Earthing Transformer with a three phase, "zig-zag (ZN)" winding configuration can be used to create an artificial neutral point and in turn, an earthing reference point [7]. In such a system, if the earthing transformer were to fail, any wye-connected loads would be inoperable and the system will no longer have an earthing reference point [3]. As established above, a missing earth reference means the substation is no longer compliant with Australian Standards and poses sizeable safety risks to electrical infrastructure, connected loads, livestock and persons.

By nature, Earthing transformers are most commonly subjected to fault currents where phase to ground short circuit faults exist [3]. As a result, the internal core and windings of the transformer are exposed to large forces throughout their lifetime. It is difficult to determine how many faults an Earthing Tx can withstand given a large variance in the duration and severity of the faults themselves. Figure 2.1 below provides a visual representation of a transformer's insulation strength over time. In reality, not all fault events will damage a transformer's insulation; however, mechanical deformation within a transformer can be thought of in a similar same way [8]. Over time, winding packing material can become loose and move as a result of large fault current forces or damage during transport. Once structural bracing is no longer tight, a transformer's windings can move because of the same forces until irreparable damage is done.
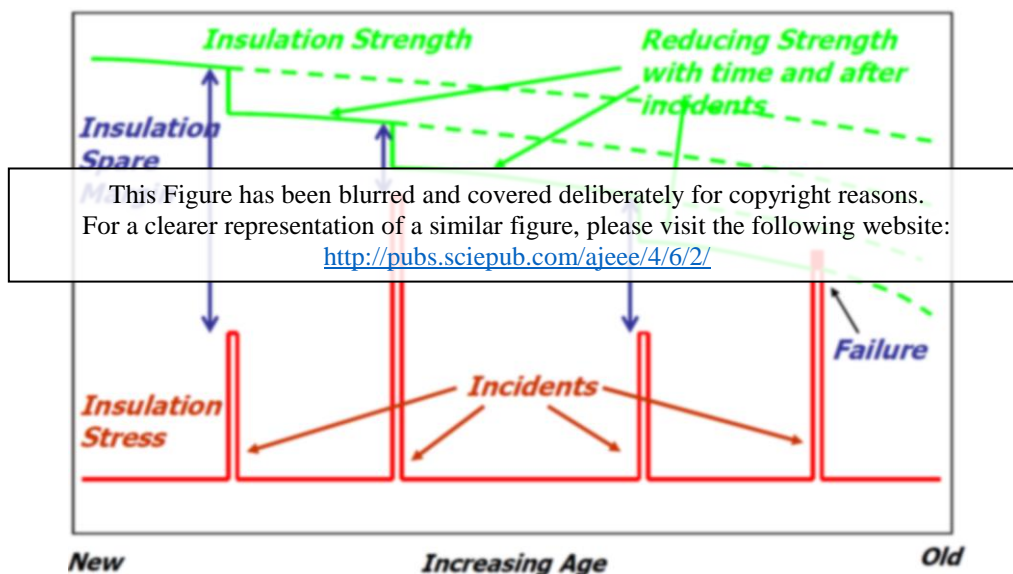
Figure 2.1 – A conceptual transformer failure model. [8]

IEEE's Standard 32, "Test Procedure for Neutral Grounding Devices" Chapter 6 provides a detailed specification for the manufacturing of earthing transformers. Chapter 6.4.2.2 makes specific reference to the mechanical failure withstand requirements associated with "asymmetrical peak currents" [9]. Mechanical and electrical withstand requirements, however, only apply to the design life of a transformer (Typically around 20 years) and do not take into consideration many factors. Some undesirable factors may include:

- Misspecification,

- Elongated fault duration (because of incorrect protection relay trip time settings/failure),

- Adverse ambient temperature conditions,

- Lightning Strikes,

- Inconsistent manufacturing process,

- Mishandling of the transformer during transport.

Factors such as the above mentioned, reinforce the requirement for periodic/systematic electrical and mechanical testing of earthing transformers. Current recommendations for conditional monitoring of earthing transformers includes; Ratio testing, Insulation Resistance testing and Dissolve Gas Analysis (DGA) testing [1]. Sweep Frequency Response Analysis (SFRA) testing is one of the industry's most commonly used methods for comparative, structural and electrical, testing of the internal workings of a transformer. By overlaying historical and new SFRA output trace responses, the user can determine if any internal mechanical shift has occurred [7]. SFRA testing is most commonly used for situational monitoring of large power transformers following transport or electrical fault events.

2.2   SFRA basic principles

2.2.1   Introduction

As the name suggests, an SFRA tester sweeps the frequency of an injected ac voltage signal on an input-connected terminal from 20Hz through to approximately 2MHZ, measuring the output voltage waveform on the secondary-connected terminal. The transformers internal resistance, inductance and capacitive (RLC) are responsible for the unique SFRA output signal for the connected transformer 'circuit' [7]. Within a transformer, capacitance if formed between almost all internal structural and electrical components as seen in
Figure 2.2 below.

This Figure has been blurred and covered deliberately for copyright reasons.
For a clearer representation of a similar figure, please visit the following website:
http://accentsjournals.org/PaperDirectory/Journal/IJATEE/2017/5/1.pdf
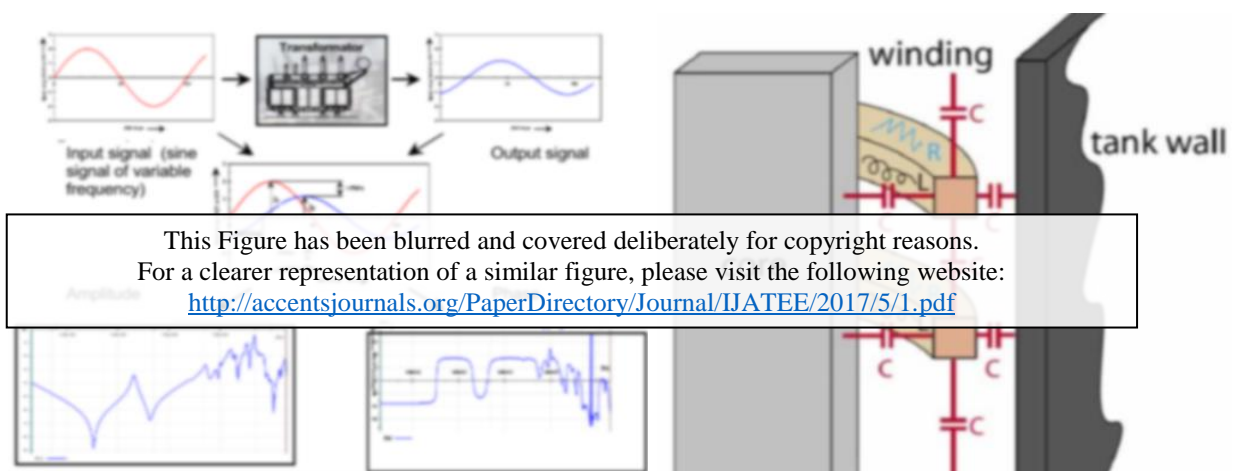
Figure 2.2 - Principle operation of SFRA (top) and simplified network behaviour of a transformer's active part (bottom) [10]

Inductance is formed in the transformer windings and Resistance is based on the resistivity of the winding material, length and cross sectional area. In theory, a Capacitor acts as an open circuit at low frequencies and a short circuit at high frequencies. Conversely, an inductor tends to act like a short circuit at low frequencies and an open circuit at high frequencies [11]. Because a transformer can be thought of as a complex network of RLC components, sweeping an input signal from a low frequency to a High frequency provides a complex output response.

To display the output response in a meaningful way, most SFRA testers perform the calculation seen below in Equation 2.1 to determine the transformer's piecewise magnitude transfer function. When all the individual magnitude transfer functions are plotted on a graph, the resultant line is known as a transformer's 'magnitude trace'. Examples of a transformer's magnitude trace response can be seen in Figure 2.2 above and the Figure 2.3 below.

Similarly, Equation 2.2 below is the standard formula used by SFRA software to generate a piecewise phase transfer function, collectively known as the transformers 'phase trace'. An example of a transformers phase trace response can be seen on the right of Figure 2.2 above.

When describing the spectral shape of an SFRA trace, the relative minima and maxima along the graph are reffered to as resonant points. After a resonant point, an increase of amplitude reffered to as a 'capacitive climb-back' while conversly, a decrece of amplitude into the resonant point is called 'inductive roll-off'.

There exists a relationship between phase angle and the location of resonant peaks in the corresponding magnitude plot of an SFRA trace. A sharp change in the output phase trace for a transformer around a specific frequency indicates that the magnitude trace has changed from inductive to capacitive in nature. This inductive to capacitive shift indicates the presence of a resonant point along the corresponding SFRA magnitude trace.

Equation 2.1 – Two port magnitude transfer function formula typically used by SFRA software [12].

$$H(dB) = 20\log_{10}\left(\frac{V_{out}}{V_{in}}\right) \tag{2.1}$$

Equation 2.2 - Two port phase transfer function formula typically used by SFRA software [12].

$$H(\theta) = \tan^{-1}\left(\frac{V_{out}}{V_{in}}\right) \tag{2.2}$$

Each trace is unique, not only to the transformer, but also to each winding. The unique trace response (conceptually thought of as a transformer's 'fingerprint') is as a result of inherent non-uniformity in phase layout and manufacturing inconsistencies. Detailed transformer design considerations are given throughout the work of S.V.Kulkarni & S.A.Khaparade, highlighting the magnetic and electrical effects of non-uniform transformer layouts [13].

A transformer trace typically has an overall capacitive trending nature in the frequency domain as seen below in Figure 2.3. The complex RLC circuit interaction of a transformer's windings structure provides a series of resonances along the frequency sweep. There exists some similarities in the spectral shape of many transformer SFRA trace response's depending heavily on the connection configuration (Star or Delta), the voltage rating, current rating and the test set connections [14].

This Figure has been blurred and covered deliberately for copyright reasons. For a clearer representation the figure, please visit the following website: http://ieeexplore.ieee.org/document/6554237/
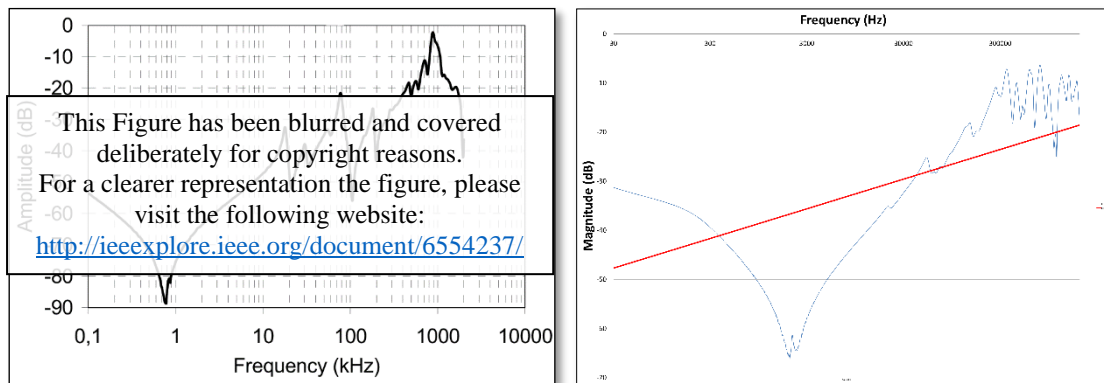
Figure 2.3 - Examples of end-to-end SFRA transformer traces. Left = 266 MVA, 420/ $\sqrt{3}$ / 21 / 21 kV Power Transformer [15] Right = 22kV Earthing transformer with a log trend-line (Red) Generated from The Australian power utility (APU) data (introduced properly later in this report).

2.2.2   Methods for analysing SFRA traces

Simply put, differences between SFRA traces are indicative of a change in the transformer's RLC "circuit". A variation in the RLC circuit suggests that the physical and/or electrical construction of the transformer has changed, possibly indicating a fault. SFRA guidelines suggest using a hierarchy of preference when comparing and analysing results. This hierarchy is as follows;

1. Time based benchmark comparisons,
2. Type or 'Sister Transformer' comparisons,
3. Phase to phase comparisons [10, 15, 16].

A breakdown of the different analysis methods can be found below in sections 2.2.2.1, 2.2.2.2 and 2.2.2.3 respectively. Detailed recommendations can be found in IEEE's Std. 57.149 [16] and CIGRE's technical brochure 342 [15].

2.2.2.1   Time Based SFRA benchmark comparisons

Time based SFRA benchmark comparisons inherently require a baseline SFRA trace of the test subject. Benchmark SFRA testing is recommended to be incorporated into any large power transformer manufacturers factory acceptance testing (FAT). FAT SFRA is known to be the best working practice as it provides an RLC fingerprint of the transformer, immediately after completion. SFRA testing, however is not often considered to be a standard FAT for distribution transformers [15].
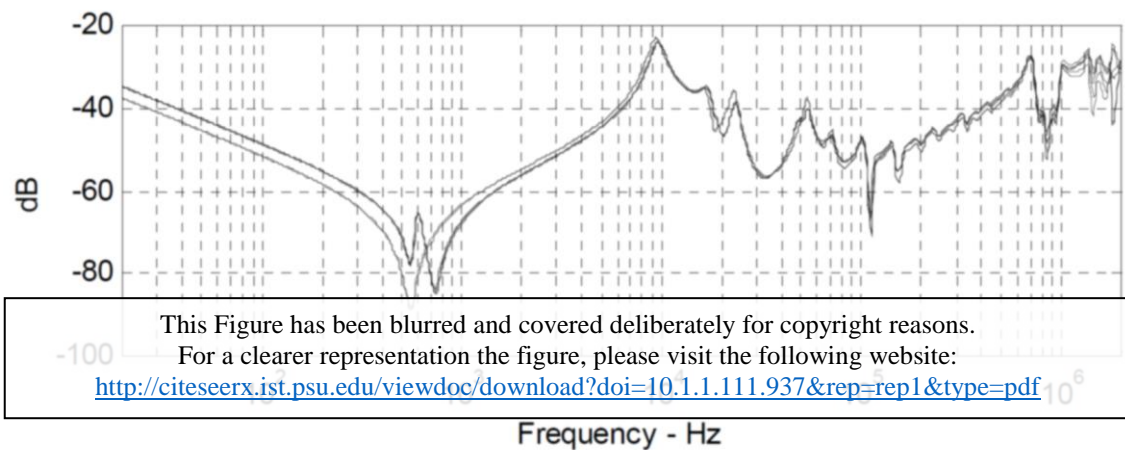
Figure 2.4 – An example of a transformers time based SFRA (HV winding) trace comparison with all phases present [12].

A shift in the resonant frequency location(s) and/or magnitude between the baseline trace and a new trace taken at a later point in time can be indicative of an internal fault [16]. Figure 2.4 above is an example of three benchmark SFRA transformer traces compared to three new SFRA transformer traces taken as a later date. All new traces have very close correlation to the benchmark trace results suggesting that no internal changes have occurred between tests.

2.2.2.2 Type or Sister Transformer SFRA comparisons

Comparing different transformer SFRA trace results for fault identification is difficult as each transformer has a unique response based on several factors. Primarily, different manufacturers use different designs, construction methods and bracing to name just a few. Because of these characteristic differences, the output SFRA trace is often vastly different. Some other factors that greatly affect a transformers frequency response are the voltage and current ratings. Internal layouts are predominantly dictated by minimum voltage clearance and conductor thickness requirements for a given power and voltage specification. In principle, sister transformer comparisons are possible between transformers of the same manufacturer, power rating and voltage rating.

10
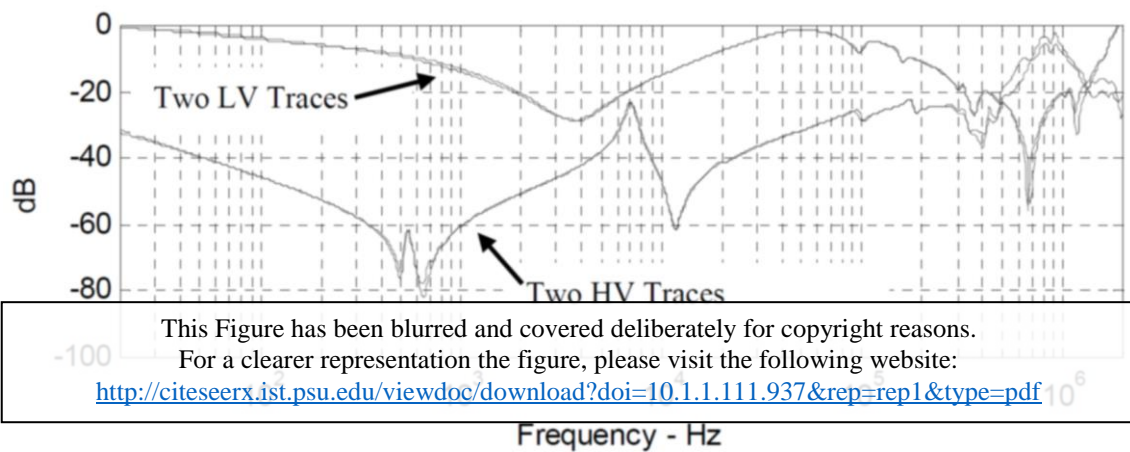
Figure 2.5 - An example of four 'sister' transformer SFRA trace responses (two HV and Two LV) plotted on the same axis [12].

An example of a sister comparison SFRA trace of both high voltage and low voltage has been provided in Figure 2.5 above. In this instance, close correlation between both transformer open circuit tests indicates that the transformer is safe to return to service. This type of transformer comparison, however, is known to be greatly subjective and prone to misdiagnosis. One of the key reasons that this method is subjective and prone to misdiagnosis is the inability to easily compare more than one set of traces at a time.

2.2.2.3   SFRA Transformer Phase to Phase comparisons

When conducting SFRA tests on a transformer, recommendations for the connection arrangements are provided by the test equipment manufacturer. An example of a manufacturers recommendations for the different test connections can be found on pages 97 and 98 of the Doble M5200 SFRA user manual [17]. Doble recommends conducting as many tests as possible including multiple phase testing.

As mentioned above in section 2.2.1, most transformers have inherent non-uniformity their windings layout. Non-uniformity in conjunction with manufacturing inconsistencies often results in an SFRA phase to phase comparison trace with large deviations. Large deviation can be misdiagnosed as an internal fault making phase to phase comparisons subjective and less consistent [15]. While displaying time based transformer SFRA comparisons, Figure 2.4 above also provides an example of phase to phase comparisons with large centre phase deviation.

2.2.3　　　SFRA Interface

SFRA testers rely on a computer interface to run their software and are currently known as an "offline", isolated test to ensure that parallel impedances do not provide misleading results [15]. Dr. Shawn Nielsen and his team at the Queensland University of Technology, however, are currently working on a method for online FRA fault diagnosis. This method effectively measures the change in impedance (both magnitude and phase) around a significant resonant point in the winding FRA spectra.

Almost all SFRA testing software can export a graphical trace output in a comma separated value (CSV) format. Interchangeable datasets enable users to globally compare and share information in a format that is easy to import and analyse using a variety of software packages.
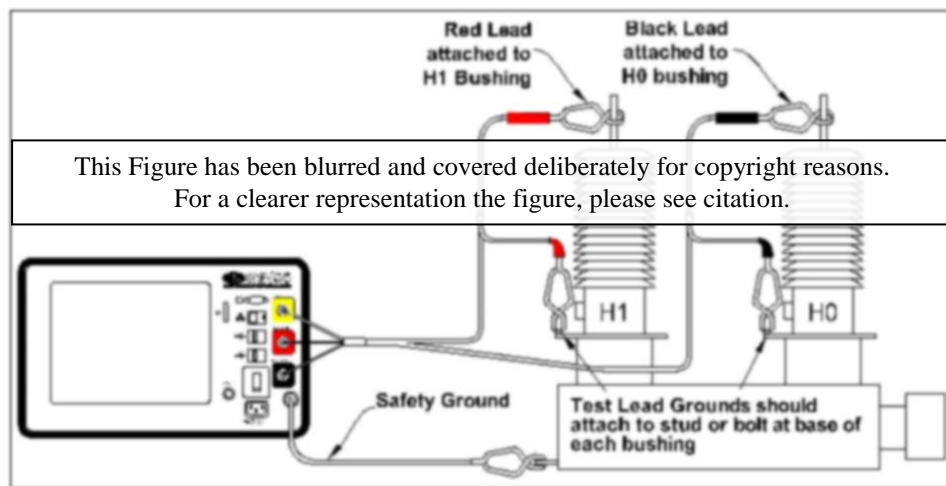
Figure 2.6 – Typical test set connections for a Doble SFRA tester [17].

An example of a typical Doble manufactured SFRA test set connection configuration can be seen above in Figure 2.6. Most manufacturers use a three lead test configuration with a known impedance, typically 50Ω [17], [14], [18]. Figure 2.7 below provides the basic test circuit for an SFRA tester where the 'Impedance, Z' is the test subject (in our case the transformer).
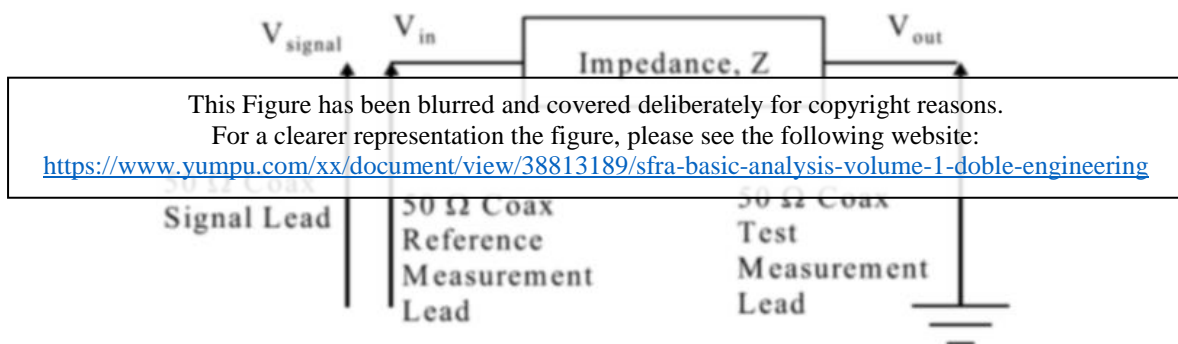
Figure 2.7 – Basic test circuit for an SFRA tester [19]

12

Having the same impedance for the input signal, input measurement and output measurement leads as seen in Figure 2.7 helps to mitigate the risk of skewed results from additive lead impedance.

2.2.4   Previous Research

Power authorities have been using SFRA testing for over a decade now; however, there is very limited literature available for the conditional SFRA testing of earthing transformers. Historically, most available literature looks at the use of SFRA testing to diagnose issues in large Power Transformers. In 2008, S. Sanchez, J. Rico and A. Avalos, C. Perez published a paper on field and laboratory SFRA testing of relatively large power transformers. The paper concluded that SFRA testing could be used to detect a variety of incipient faults in large power transformers [20]. Their 2008 paper also reinforced the cited work of Luwendran Moodley and Brian de Klerk. Moodley and Klerk's 2006 paper using power transformer case studies to establish the value of SFRA testing as a diagnostic tool in the local power network [7]. CIGRE's technical brochure 342 presents a case study where SFRA results from an auto transformer that suffered "Axial collapse after clamping failure" [15] was compared with data from years before. SFRA was key in the decision to remove the auto-transformer from service as other tests provided inconclusive results. An internal forensic assessment of the transformer confirmed that irreparable damage had occurred confirming the SFRA trace diagnosis.

Simon A. Ryder published a paper in 2003 on the use of SFRA testing for the analysis of small distribution transformers. Ryder simulated typical faults found in large power transformers and concluded that most of these faults could be detected using SFRA on smaller distribution transformers [9]. As introduced in Chapter 1, Earthing transformers are physically and electrically small assets. Ryder's research supports the theory that faults in earthing transformers should be detectable using SFRA.

2.3   Fault and Failure modes for Earthing Transformers

As introduced in 0 above, Earthing transformers typically use a Zig-Zag (Zn) winding configuration. Research found that Zn wound transformers are of a unique winding layout design. Each electrical winding is split in half and wound on different core legs as seen in Figure 2.8 below [3]. The inner and outer core leg windings are wound in opposite directions with the same number of turns so that under normal system operation, the magnetic flux produced by each winding cancels out. Ideally, with a net winding magnet flux equal to zero, no current will flow through the earthed star point of the transformer [21], as per Faradays Law [11].

This Figure has been blurred and covered deliberately for copyright reasons.
For a clearer representation the figure, please see the following website:
https://www.l-3.com/wp-content/uploads/2014/04/Georgia-Tech-Zig-Zag-Grounding-Transformers.pdf
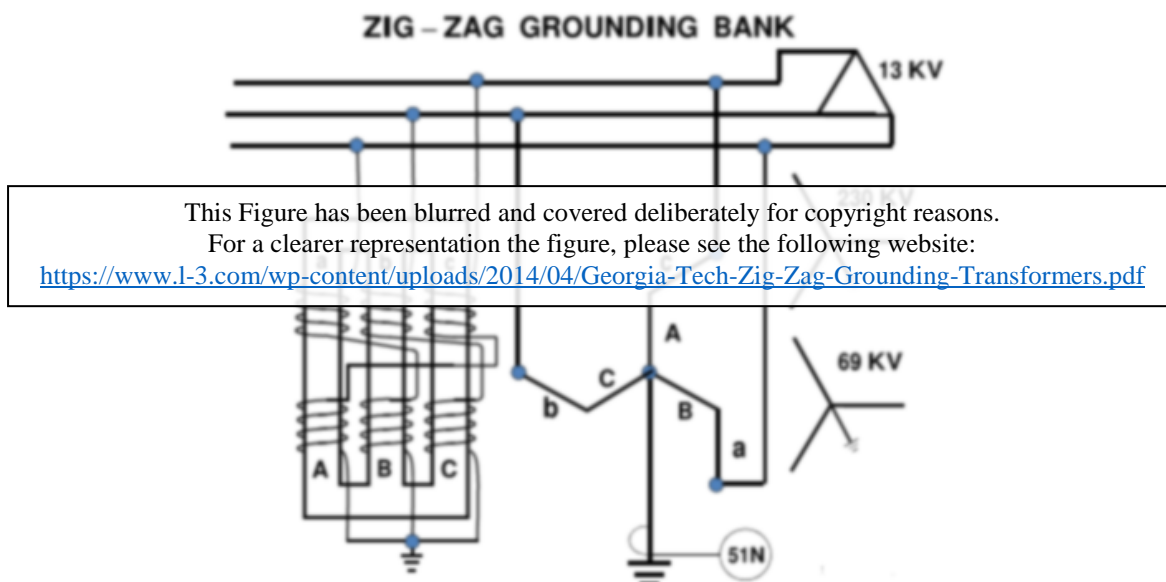
Figure 2.8 – Typical Zig-Zag (Zn) winding layout for an earthing transformer [3].

2.3.1 Known Transformer Faults

Known oil-filled transformer internal "failure modes" are outlined and defined by IEEE's Standard C57.149, Section 6.5 to be the following:

- "Radial "Hoop Buckling" Deformation of Winding
- Axial Winding Elongation "Telescoping"
- Overall- Bulk & Localized Movement
- Core Defects
- Contact Resistance
- Winding Turn-to-Turn Short Circuit
- Open Circuited Winding
- Winding Looseness due to Transportation
- Residual Magnetization
- Floating Shield" [16]

Each of the known oil-filled internal failure modes listed above have been discussed in sections later in this report. Discussions in each respective section highlight the relevance of each to earthing transformers specifically. The immediate sub sections below include Hoop Buckling, Axial windings displacement and bulk movement. An understanding of each failure mode is required for some of the later report sections. Discussions for each of the remainder failure modes subsections can be found in Appendix A below.

14

2.3.1.1 Radial "Hoop Buckling" Deformation of Winding

As introduced in section 2.1 above, Earthing transformers are designed to be able to withstand large fault currents for a short duration. Radial forces are the greatest in magnitude during a short circuit fault as is discussed in the works of [15], [12], [16], [17] (to name a few) and displayed diagrammatically with force vectors in Figure 2.9 below. Research found a unique design decision that is common in almost all earthing transformers to reduce the effects of hoop buckling. By removing the inter-layer oil ports in a transformer winding (typically vertical spacers insulated pressboard 'sticks' positioned evenly around the windings between layers), the radial strength of the core is greatly increased [22], [13]. Consequently, removing inter-layer oil ports greatly reduces a transformer's winding heat dissipation capability; however, the resulting increase in radial strength mitigates the risk of hoop buckling as a potential failure mode.

2.3.1.2 Axial Winding Elongation "Telescoping"

Research found that historically, Axial winding elongation (also known as "Telescoping") is the most common failure mode for earthing transformers. Axial forces on transformer windings are generated as a result of miss-alignment of the windings magnetic centre [22]. Earthing transformers do not need any tapings along each winging for voltage compensation making it easier to align the magnetic centre of the inner and outer winding. Figure 2.9 below shows a typical transformer winding with force vectors, defined by the direction of current flow as per Lenz's Law [11]. The example in section 5.4 of John J. Winders, Jr.'s Power Transformers, Principles and Applications provides an ideal template for a basic understanding of the forces acting on the earthing transformers' windings. The example in section 5.4 utilises symmetrical windings with no taps and the same number of ampere-turns on the inner and outer windings, wound in opposite directions. [22].

This Figure has been blurred and covered deliberately for copyright reasons.
For a clearer representation the figure, please see the following website (pages 171 and 172):
http://bbs.hwrf.com.cn/downmte/Power%20Transformers%20Principles%20and%20Applications.pdf
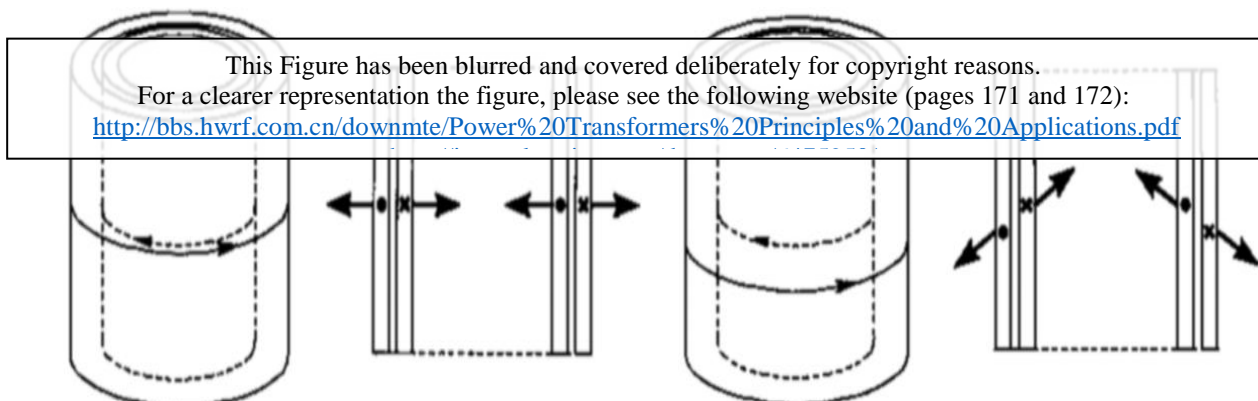
Figure 2.9 – (Left) "A pair of cylindrical concentric windings with their magnetic centres perfectly aligned."
(Right) "A pair of cylindrical concentric windings with their magnetic centres offset in the vertical direction, resulting in net vertical forces on the windings." [22]

When the magnetic centres of the inner and outer windings are perfectly aligned, no axial forces are acting on the windings as seen in the Left side of Figure 2.9 above. The right side of Figure 2.9 shows that when the magnetic centres are not aligned, a vertical component of the force vector is present, pushing the inner winding upwards and the outer winding downwards. The vertical component of the force is intuitively made greater by further axial displacement suggesting that this failure mode somewhat self-perpetuating.

A survey conducted by the CIGRE workgroup 13.19, taskforce #1 found that of the 24,292 power transformers involved, only 15 of them were known to have failed over the 5-year investigation period. Of these transformers, however, it was noted that over 50% of them involved windings failure because of axial forces.

IEEE's Standard C57.149, Section 6.5.2 has broken down the typical effects of axial winding deformation on transformer SFRA traces into frequency regions and can be seen below in Figure 2.10. As discussed in section 2.2 above, the frequency regions of an SFRA trace are known to relate to different RLC circuit interactions within a transformer. Figure 2.11 and Figure 2.12 below provide examples of the expected power transformer SFRA trace response to axial winding deformation for open and short circuit tests respectively.

Frequency range	Axial winding deformation Assuming, no other failure modes exist:
20 Hz – 10 kHz	**Open Circuit Tests:** This region (core region) is generally unaffected during axial winding deformation. **Short Circuit Tests:** Results in a change in impedance. The FRA trace for the affected winding causes a difference between phases or previous results in the inductive roll-off portion.
5 kHz – 100 kHz	**Open Circuit and Short Circuit Tests:** Axial winding deformation is most obvious in this range. The bulk winding range can shift or produce new resonance peaks and valleys depending of the severity of the deformation. The changes will be greater for the affected winding, but it is still possible to have the effects transferred to the other winding(s).
50 kHz – 1 MHz	**Open Circuit and Short Circuit Tests:** Axial winding deformation can shift or produce new resonance peaks and valleys depending of the severity of the deformation. The changes will be greater for the affected winding, but it is still possible to have the effects transferred to the other winding(s).
> 1 MHz	**Open Circuit and Short Circuit Tests:** The response to axial winding deformation is unpredictable.

Figure 2.10 – Snipping from IEEE Standard C57.149 showing the effects of Axial winding deformation on transformer SFRA response broken down into frequency regions [16].

The expected LV Open circuit and HV short circuit tests can be seen below, also as extracts from section 5.6.2 of IEEE Standard C57.149.
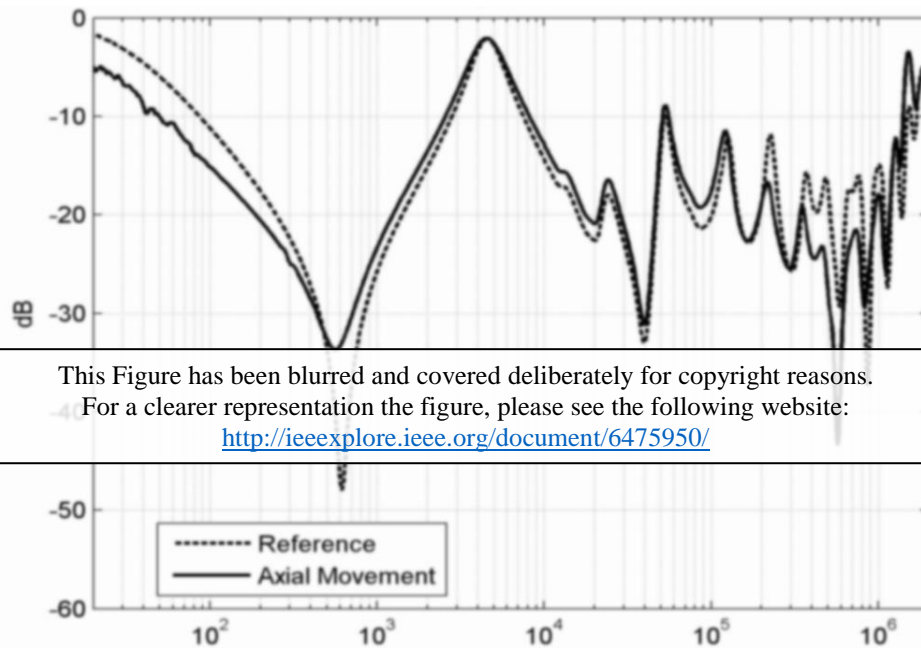
16

Figure 2.11 – Snipping from IEEE Standard C57.149 showing a SFRA comparative trace of Axial movement for tertiary open-circuit winding tests [16].
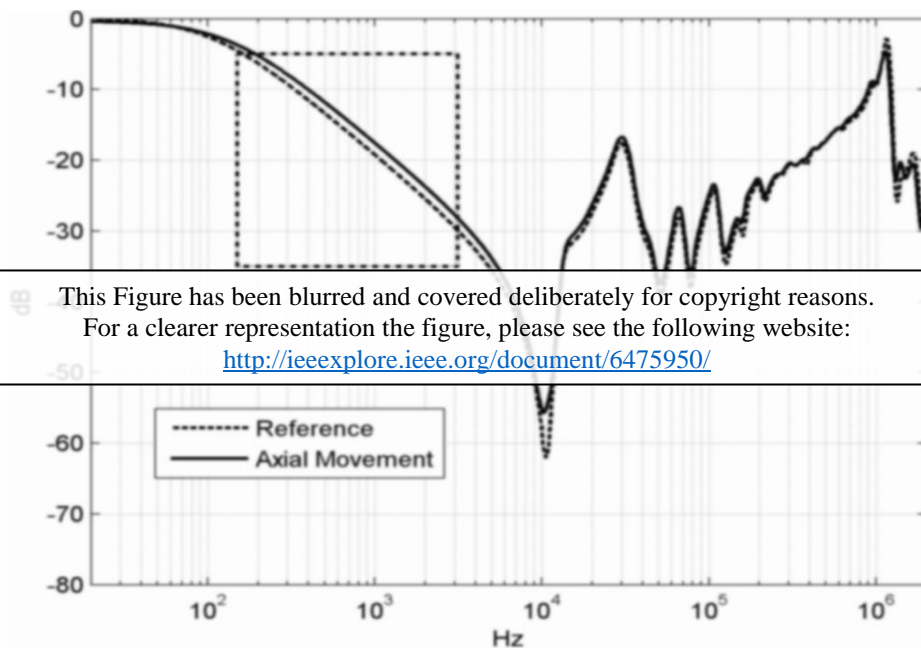
Figure 2.12 - Snipping from IEEE Standard C57.149 showing a SFRA comparative trace of Axial movement for tertiary HV short-circuit winding tests [16].

2.3.1.3 Overall- Bulk & Localized Movement

Standard C57.149, Section 6.5.3 states that high current forces and transportation are the most common causes for overall- bulk and localized movement in transformers [16]. Figure 2.13 below is an extract from the work of N. Hashemnia, Ali S. Masoum, A. Abu-Siada and Syed M. Islam. Figure 2.13 provides a possible transformer SFRA response to an axial shift of the bulk windings at 2% and 5% of its magnetic centre position. The presented results were attained through transformer finite element model manipulation.

This Figure has been blurred and covered deliberately for copyright reasons.
For a clearer representation the figure, please see the following website:
http://ieeexplore.ieee.org/document/6966530/
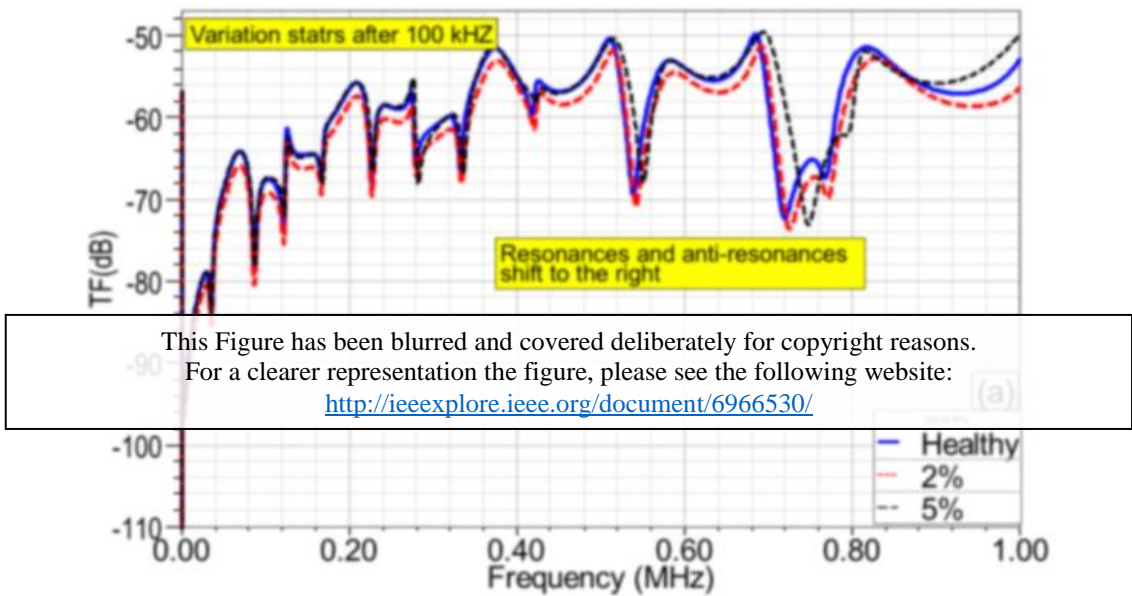
Figure 2.13 – Snipping of a simulated Axial displacement SFRA trace for a finite element model of a single phase Power transformer looking at bulk windings movement [23].

Yet another extract from section 5.6.2 of the IEEE Standard C57.149 can be found in Figure 2.14 below, defining the expected SFRA response for a bulk winding shift fault mode.

Frequency range	**Bulk winding deformation** Assuming, no other failure modes exist:
20 Hz – 10 kHz	**Open Circuit Tests:** This region (core region) is generally unaffected during bulk winding movement. **Short Circuit Tests:** This region is generally unaffected during bulk winding movement. All phases should be similar.
5 kHz – 100 kHz	**Open Circuit and Short Circuit Tests:** Bulk winding movement is most obvious in this range. Newly created resonance peaks or valleys are the key indicator. The bulk winding range can shift or produce new resonance peaks and valleys depending of the magnitude of the movement. The changes will be greater for the affected phase.
50 kHz – 1 MHz	**Open Circuit and Short Circuit Tests:** Generally, this range remains unaffected. However, changes to the CL capacitance can cause resonance shifts in the upper portion of this range.
> 1 MHz	**Open Circuit and Short Circuit Tests:** Changes to the CL capacitance can cause resonance shifts.

Figure 2.14 – Snipping from IEEE Standard C57.149 showing the effects of Bulk winding movement on a transformer SFRA response broken down into frequency regions [16].

2.4   Data analysis techniques

Given the subjective nature of SFRA trace analysis as discussed in Section 2.2.2 above, the development of a tool that can analyse SFRA trace data in an efficient and precise manner has been the focal point of research for some time now [15].

Some established techniques found for identifying faults through automated SFRA trace analysis include:

- Difference Plotting [16],
- Correlation coefficients (CCF) [16], [15], [17],
- Error functions [15],
- Co-variances [24].
- Pole-Zero Representation [24], [15]. Some tools for the creation and analysis of pole-zero plots include:
  - Expert systems
  - Artificial Neural Networks (ANN)
  - Bayesian classifiers
  - Support Vector Machines
  - Fuzzy logic classifiers
  - Self-organising maps

The techniques listed above were found to have limited success in detecting faults by analysing SFRA trace data and all have restrictions that can be further researched through the corresponding citations. One of the focal point of this project was to develop a **unique**, customised tool for the assisted detection of faults in Earthing Transformers. It was deemed important to be aware of existing SFRA analysis techniques to solidify conceptual novelty, however, a detailed analysis of each would not serve relevant to this report.

2.4.1   Speech Signal Processing

Section 2.2 discussed the general spectral shape of any given transformer's SFRA response (based on a common connection configuration and specification), to be relatively consistent. The idea that a transformer's response can be relatively consistent in spectral shape draws parallels with that of a digitised speech signal. Although people often speak any given language with different accents, tones, speeds and pronunciations, almost any digitised speech signal has enough consistency in spectral shape to identify what has been said. Technology integrating automatic speech recognition software provides a way to identify the sounds, words and sentences being processed. In the same way that speech can be automatically identified, it may be possible to build on and adapt existing signal feature extraction techniques to analyse and classify transformer SFRA responses.

The process of collecting speech data is vastly different from transformer SFRA analysis and involves what is known as analogue-to-digital conversion as a first step of signal processing. Analogue-to-digital signal conversion requires both sampling and quantization. To sample a signal, the amplitude of the input is taken at a given time with a 'sample rate' defined in samples-per-second. Quantization is the process of digitising the range of a signal or rather making the range of the signal discrete [25]. Once digitised, the next step of processing a speech signal is what is known as 'feature extraction'.

2.4.1.1 Feature extraction introduction

The main goal of feature extraction in speech processing is to efficiently distil a large amount of digitised speech signal data into only a few vectors that represent the 'important' information [26]. As a first stage of almost all feature extraction techniques, the digitised speech signal data (time domain based) is converted into the frequency domain. The frequency domain data is collectively known as the speech signals' Spectrum. A sample's speech signal spectrum is shown at the top of Figure 2.15 below. Once in the frequency domain, it is possible to separate the spectrum into the 'spectral envelope' and the 'spectral details' as shown in the lower traces of Figure 2.15 respectively.
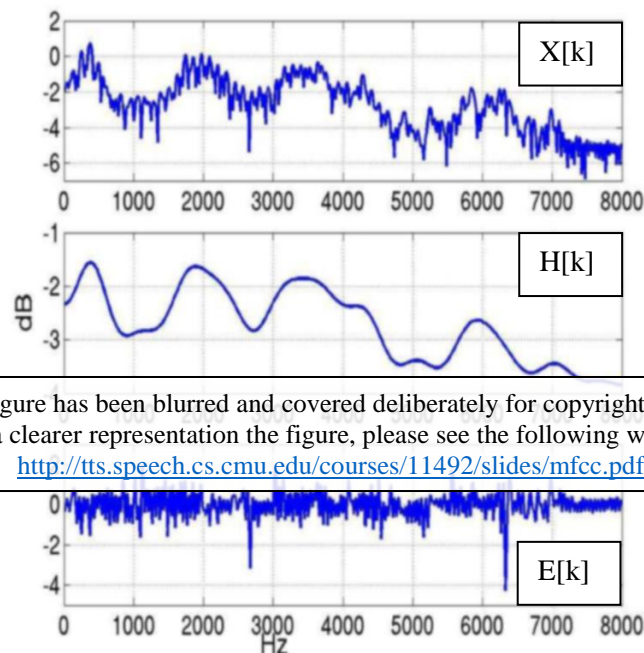
This Figure has been blurred and covered deliberately for copyright reasons.
For a clearer representation the figure, please see the following website:
http://tts.speech.cs.cmu.edu/courses/11492/slides/mfcc.pdf

Figure 2.15 – The top graph displays a sample speech signal's spectrum, the middle graph is the spectral envelope of the top spectrum along with the spectral details at the bottom [27].

Separation can be achieved by exploiting the fact that the Inverse Fast Fourier Transform (IFFT) of the log-spectrum is the sum of the IFFT of spectral envelope and the spectral details as mathematically shown below in Equation 2.3. The pseudo-frequency mapped resultant (Cepstrum) can be filtered at a low frequency to isolate the spectral envelope components [27].

20

Equation 2.3 – Mathematical identity useful to help separate a spectrum into its spectral envelope and spectral details [27].

$$IFFT(\log X[k]) = IFFT(\log H[k]) + IFFT(\log E[k]) \tag{2.3}$$

From Equation 2.3, the spectral envelope of a speech signal is essentially a log of the low frequency magnitude spectrum with resonances (known as 'Formants'), representing its main frequency components [26]. Section 2.2.1 above describes the output data from an SFRA tester as a log-magnitude plot, much like a speech signal's digitised spectrum, representing the transformers unique internal layout.

2.4.1.2   Techniques

There exists a variety of techniques commonly used for feature extraction in automatic speech processing applications. Some of the more common and well proven techniques for feature extraction are as listed below:

- Linear predictive coding analysis (LPC)
- Perceptual linear predictive coefficients (PLP),
- Mel-frequency cepstral coefficients (MFCC),
- Linear-frequency cepstral coefficients (LFCC) [28]

A conceptual overview of LPC, PLP and LFCC can be found in Appendix A below. Background into MFCC along with a process overview has been provided in section 2.4.1.3 below, given that it was the primary method chosen for this project.

2.4.1.3   Mel-frequency cepstral coefficients (MFCC)

Mel-frequency cepstral coefficients (MFCC) is arguably the most commonly used feature extraction technique available. MFCC is widely used because of its simplicity, computational speed and manageable output coefficients [26]. Feature extraction using MFCC relies on the spectral form of an input signal making it sensitive to small variations in the spectral data (noise). In speech processing, MFCC can be implemented using several steps as detailed in Figure 2.16 below.
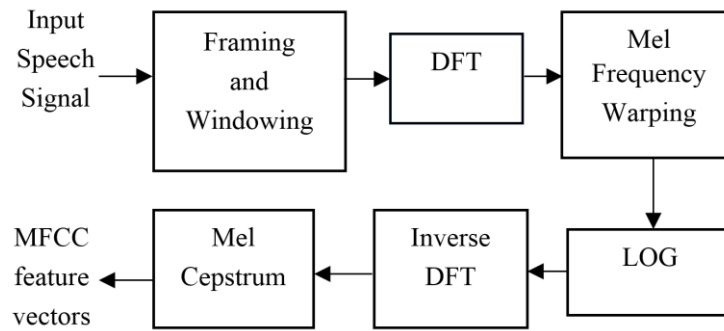
Figure 2.16 – The MFCC computational process graphically presented for simple analysis [29].

MFCC makes use of human speech limitations by setting the sampling frequency to approximately 20kHz, known as the Nyquist frequency. The Nyquist frequency for human speech is twice the maximum frequency that information can be conveyed (10kHz) [26].

Pre-emphasis is applied to compensate for the natural 'spectral tilt' of human speech, boosting the signals high frequency energy to assist with the inclusion of all the spectral information available. The emphasised signal is then split into small windows to minimise any non-statutory spectral features. Windowing of the signal is applied to compensate for the human auditory system's sensitivity to time evolving spectral content [26].

As discussed in section 2.4.1.1 above, each windowed signal is converted into the frequency domain, most commonly using a Fast Fourier Transform (FFT) for its computational speed. The absolute value of the resultant is then filtered using a bank of Hamming windows, spaced along a 'Mel-scale' axis to tailor the output coefficients for human hearing characteristics (less sensitive at higher frequencies). The use of a Hamming window for the filter bank is required to ensure that the output function is continuous for all data points (necessary for Fourier transforms).

A logarithm function is applied to the filtered spectrum as this assist in dampening the effects of unwanted magnitude changes from the input signal. Finally, an Inverse Transform is applied to the log-filtered spectrum. Typically, the function used for this operation is the Inverse Discrete Cosine Transform (IDCT). IDCT is typically used instead of a 'Sine' based Inverse Fast Fourier Transform (IFFT) for comparative data purposes given fewer computational iterations are required for signal approximation [30]. The application of an IDCT on the log spectrum data results in what is known as the signals cepstrum, mapped on a 'persuado-frequency' axis.

The number of output cepstrum coefficients is equal to the number of filters applied in the in the Hamming filter bank. A change in magnitude of any given coefficient is uncorrelated to the other output coefficients which is a feature that is unique to the cepstrum (not true for the spectrum). Each uncorrelated output coefficient subsequently represents a different frequency band for the transform making it possible to isolate lower or higher frequency components of the signal as required. It is also possible to exploit the independent magnitude nature of each cepstrum coefficient for analysis purposes as most of the information is typically stored in a select few filter coefficients [26], [29].

2.4.2   Application requirements for fault analysis

Modification of any analysis technique for fault identification within earthing transformers requires an intimate understanding of the characteristic SFRA changes that result from specific faults. Section's 2.2 and 2.3 above cover some of the key research papers that have been published in the space of SFRA testing. Both sections surmise that SFRA fault analysis of earthing transformers is a relatively untouched area of study. To gather an intimate understanding of the characteristic SFRA changes that result from specific faults in earthing transformers, practical simulation of the most common fault scenario could be used to gather real world data. Section 2.3.1 above provides an overview of known transformer faults, essentially concluding that the most likely fault to occur in an earthing transformer is 'axial windings displacement'.

Chapter 3   Practical Transformer Fault Simulation Testing

3.1   Introduction

As introduced in section 2.2.4 above, Simon A. Ryder published a paper in 2003 on "TRANSFORMER DIAGNOSTICS USING FREQUENCY RESPONSE ANALYSIS" [9]. Ryder's fault simulation work was carried out at the Alstom transformer research centre in France with the facilities to simulate several faults, typical power transformers. Although specific simulation methodology was not disclosed in his 2003 paper, fault simulation on transformer windings displacement was deemed to be of particular relevance to this project. Ryder suggests that from experience, a winding shift of over 2% in power transformers is detectable using SFRA. To prove this, a 3% permissible core-window HV windings movement was applied to the 100kVA test subject, simulating a 'windings displacement' fault. The respective SFRA trace results from Ryder's paper can be seen in Figure 3.1 below. It is clear to see that from the time based SFRA comparison, a spectral resonance magnitude change along with frequency shift occurs because of the simulated fault.

This Figure has been blurred and covered deliberately for copyright reasons.
For a clearer representation the figure, please see the following website:
https://www.researchgate.net/publication/3973174_Transformer_diagnosis_using_frequency_response_analysis_results_from_fault_simulations
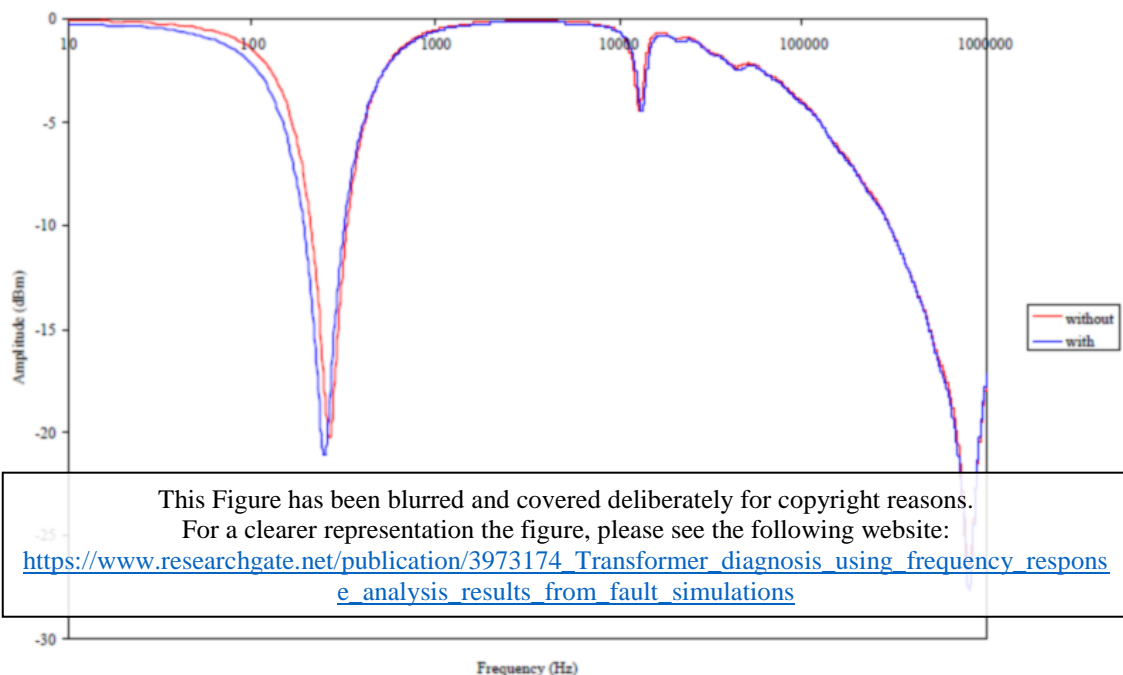
Figure 3.1 – An extract from Simon A. Ryder's 2003 paper showing a time based SFRA comparison from a simulated 3% windings displacement fault [9].

Fortunately, an Australian power utility (APU) made the decision to SFRA benchmark most of the earthing transformers throughout their electrical network. APU facilitated the raw SFRA trace data from these benchmarked Earthing transformers to the author for the completion of this project. APU earthing transformer data was initially analysed to determine the characteristic SFRA trace shape that would result from a zig-zag (Zn) wound transformer. Figure 3. below is a random sample of twenty Zn wound earthing transformer 'A phase', open circuit traces, mapped on the same axis. The sample of transformers included four different manufacturers and of various current, voltage and impedance nameplate ratings.
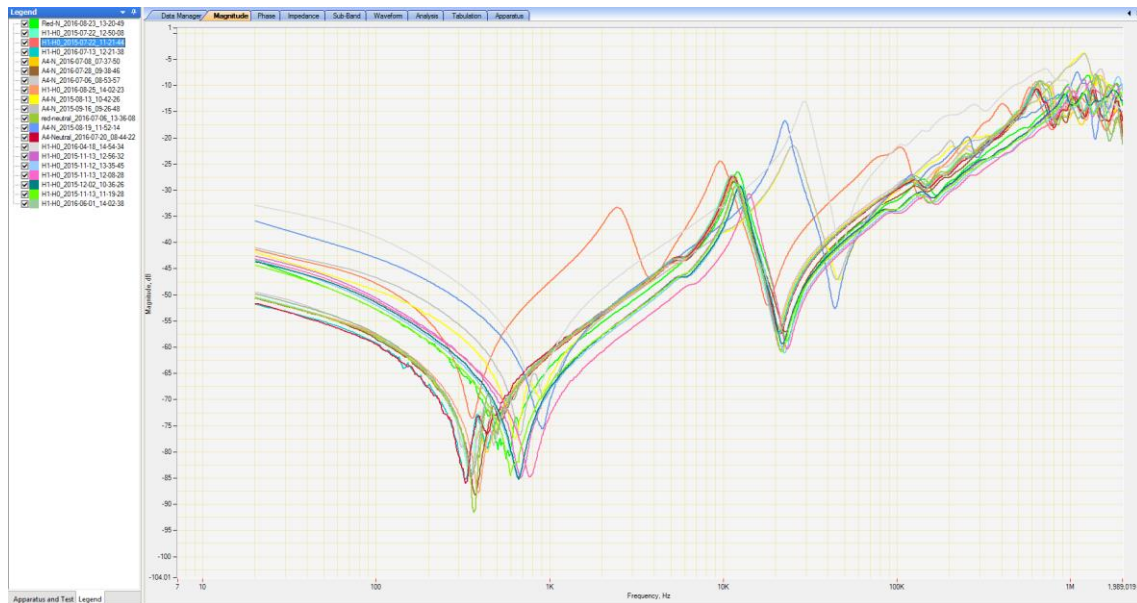
Figure 3.2 – Twenty randomly selected 'A phase', open circuit tested; Zn wound earthing transformer SFRA traces mapped on the same axis. Raw data provided by The Australian power utility.

Given differences in the windings configuration and connections between a Zn wound earthing transformer and Ryder's Dyn* vectored transformer, the SFRA fault response can be expected to be different. It was therefore proposed that SFRA analysis of a simulated windings axial displacement fault on an earthing transformer should be conducted.

3.1.1 Donated Earthing Transformer from Excess Power Equipment

Local power service and supply company, Excess Power Equipment (EPE) donated a stock Zn wound earthing transformer for the completion of this project as seen in Figure 3.3 below. An EPE transformer datasheet along with extensive photos of the transformer can be found in Figure 6.1 and Figure 6.2 of Appendix C below. EPE also facilitated Workshop space, tools, a Doble M5400 SFRA tester, insulation resistance tester (Fluke 1550B, SN 08813014), windings resistance meter (Sivananda TWRM10A, SN SE/002062014), Oil Dielectric tester (Foster Megger OTS/60SX, SN 97071810500797) and Dissolve Gas Analysis (DGA) tester (GE Energy Kelman Transport X: 80-2621). The additional test equipment was requested for the purpose of certifying the transformer test subject health as is recommended in the respective sections of AS/NZS 60076 – 6 [31], AS 2374 [32] and A.S.1767 [33], prior to SFRA benchmarking.

Figure 3.3 - Donated Earthing transformer from Excess Power Equipment for developing fault simulations.
Left – Transformer after refurbishment by EPE
Right – Transformer core and coils being de-tanked

Table 3.1 – Earthing transformer test subject electrical specifications

Number of Phases	3
Rated Voltage	11000V
Vector Group	Zn
Rated Neutral Current and Duration	75A for 10 seconds
Zero Sequence Impedance	9.2Ω/phase at 75°C
Rated Frequency	50Hz
BIL	75kV

As introduced in section 2.3 above, a Zn wound transformer has only one set of electrical windings per phase, separated into two half sections and wound on top of each other on the respective core legs. Figure 3.4 below is a zoomed extract of the test subject's nameplate, providing indication of the internal windings layout and inter-winding electrical connections. Convention suggests that the windings seen at the top of this layout and connection diagram have been wound on the inside of the windings seen at the bottom of Figure 3.4 respectively. Visual inspection of the winding found this convention to be true once the transformer was un-tanked, explained in further detail below. The alignment of each winding in Figure 3.4 represents the physical core leg location for each respectively.
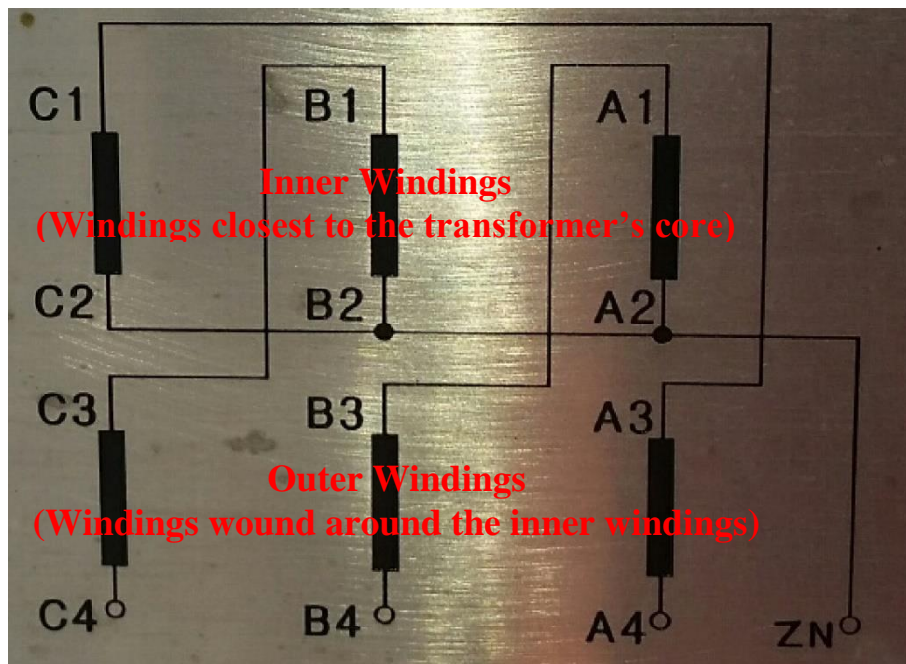
Figure 3.4 – An extract from the test subjects' full transformer nameplate (found in Figure 6.2, Appendix C) of the internal windings layout and inter-winding electrical connections with added

As diagrammatically shown in Figure 3.4 and introduced in 2.3 above, each transformer phase connection has one part of the electrically interconnected windings on a different core leg. It is interesting to note that B and 'C phase' have a very similar geometric windings layout while 'A phase' has the greatest physical separation between its interconnected windings.

3.2 Method

The purpose of this section is to define the method used to simulate a windings axial displacement fault on an earthing transformer using SFRA for benchmarking and analysis. The major objective of simulating an axial displacement fault on the earthing transformer is to determine if it is possible to detect this specific fault using SFRA alone. Results from the fault simulation will be used for justification of a filter placement convention for the proposed analysis process discussed in section 2.4.2 above. Fault simulations included only two different fault severity scenarios given workshop access limitations. The two fault severity scenarios were deemed adequate for the main purpose of determining if the fault itself can be detected using SFRA and what changes along the spectrum as a result.

3.2.1 Conditional testing and Benchmarking

Conditional benchmark testing of the earthing transformer consisted of the following:

1. Oil dielectric test
2. Dissolved gas analysis (DGA) test
3. Insulation resistance test
4. Windings Resistance test
5. Sweep Frequency Response Analysis (SFRA) tests

The testing method and results for points 1 to 4 listed above have been included in section C.2 of Appendix C below. Each test serves to ensure that a different component of the transformer is in good health, prior to SFRA testing. The respective sub-sections of C.2 present both method and justification behind each. Section 3.2.2 below present the method conducted to simulate an axial windings displacement fault using SFRA alone as a diagnosis tool.

3.2.2 Sweep Frequency Response Analysis (SFRA) tests

All sweep frequency response analysis (SFRA) tests were conducted using a Doble M5400. The test set lead connections and transformer bushing connections were repeated in full for all test iterations as per Table 3.2 below.

Table 3.2 – Lead Connections for every SFRA test

Red lead	A	B	C	A	B	C
Black Lead	N	N	N	N	N	N
Bushing Connections	Open Circuit	Open Circuit	Open Circuit	Short Circuit: B-C-N	Short Circuit: C-A-N	Short Circuit: A-B-N

SFRA tester frequency sweep setting – 20Hz to 2Mhz

Transformer SFRA test iterations were conducted exclusively in the order of the list below:

1. Baseline SFRA test when the transformer was fully assembled,
2. Comparative SFRA test when the transformer had been drained of oil with the lid placed back on top of the transformer,
3. Baseline and comparative SFRA test when the transformer core and coils had been fully un-tanked,
4. Comparative SFRA test with a core earth strap fitted to the transformer,
5. Comparative SFRA test with bulk movement of the A and 'C phase' outer core leg windings to the bottom of the core window,
6. 90% movement of the inner core windings towards the top of the core window,
7. 45% movement of the inner core windings towards the top of the core window.

Each of the listed steps has been elaborated on in the below sub sections:

3.2.2.1 Baseline SFRA test - Transformer fully assembled

Six SFRA tests were conducted on the fully assembled Earthing Transformer (Earth Tx), with the cable box cover removed, using the connections defined in Table 3.2 above. Photos of the respective connections made and the bushing short circuit leads configurations during testing can be found in section D.1 of Appendix D.

The purpose of conducting fully assembled SFRA tests was to provide a baseline set of data for time based, type based and sister Tx based comparisons.

3.2.2.2 Comparative SFRA test - Transformer oil removed

Next, the transformers tank lid was removed and all 166 Litres of oil was pumped from the transformer into a clean oil storage vessel. The transformers tank lid was then re-seated with four locating bolts (one in each corner). SFRA tests performed in section 3.2.2.1 were repeated in full. A photo of the Tx with all the oil removed can be found in Figure 3.5.
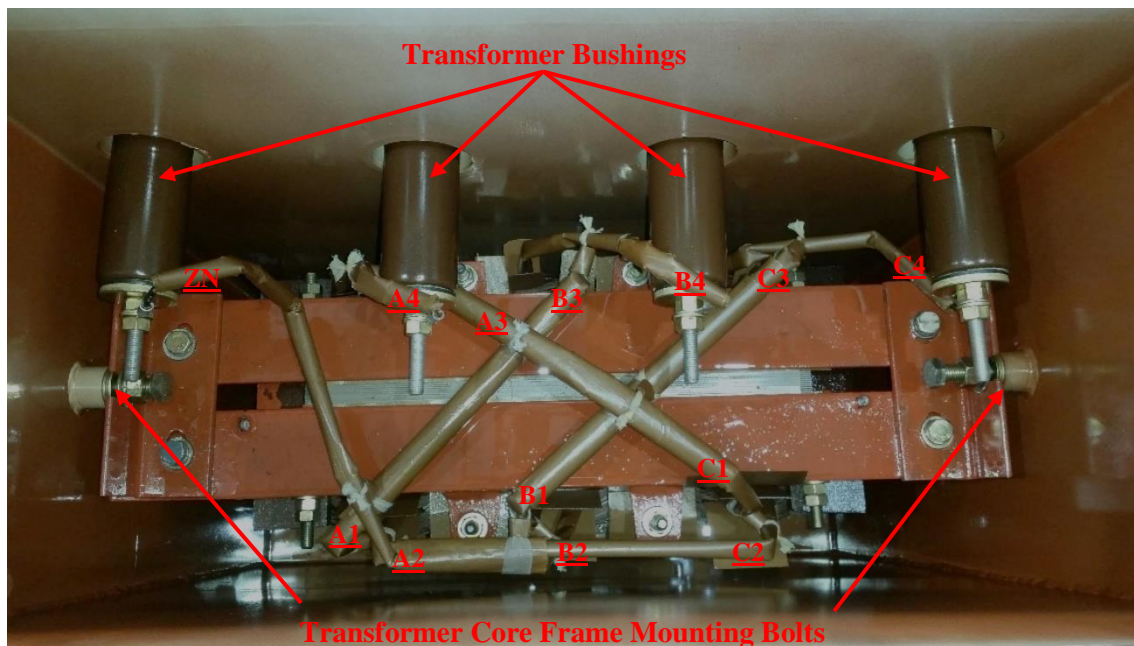
Figure 3.5 – Internal view of the earthing transformer with oil removed and labelling of the topical components and wiring interconnections.

SFRA tests with the oil drained from the transformer were conducted to isolate the effect that removing the oil would have on the transformers SFRA response. The isolated changes in SFRA response were deemed important for comparison purposes and for the potential normalisation of testing results when compared to other oil filled earthing transformers.

3.2.2.3 Baseline and comparative SFRA test - Transformer core and coils fully removed (un-tanked)

The transformers bushings were then electrically disconnected and removed. The core frame mounting bolts were removed from the tank fixings shown in Figure 3.5 above. The transformer core and coils assembly was then lifted out of the transformer tank by 'noosing' the core bracing frame with a gantry connected chain set as seen in Figure 3.3 above and section D.3 of Appendix D below. Once removed the Transformer core and coils assembly were placed on large wooden blocks in an oil drip tray. The coil leads were cleaned of oil using a small amount of sheltie on a scrap piece of cloth. All the SFRA tests from Table 3.2 above were once again repeated taking care to ensure that the now loose coil leads were not touching each other or the transformer ground potential frame. A photo of the un-tanked transformer can be found in Figure 3.6 below.

Figure 3.6 – Un-tanked earthing transformer core sitting on wooden blocks in an oil drip tray.

Bushings were disconnected and removed to enable the core and coils assembly to be lifted due to the overhang seen in Figure 3.5 above. Large wooden blocks were used to offset the transformer from the metal oil drip tray to remove the potential capacitive coupling effect that could skew SFRA results. To ensure that the testing process was un-biased, consistent testing conditions were required. To achieve consistent test conditions with the original 'baseline' taken in section 3.2.2.1 above, the transformer would need to be fully assembled and filled with oil every time a change was made, prior to re-testing. Given that the bushings overhang the transformer core and coils, it was deemed problematic to attempt to rebuild and re-fill the transformer for each test iteration. Foreseeable problems were brainstormed as follows;

- Movement of the core and coils as a result of the repetitive lifting stresses,
- Incorrect lead terminal connections (due to human error),
- Inconsistent bushing connection lead paths,
- Broken or stressed lead insulation due to constant movement,
- Movement of the windings test spacer while lifting the core and coils back in to the transformer tank.

For the reasons listed above, it was decided that all modifications to the core and coils, simulating a winding axial displacement fault, would be conducted and re-tested in an un-tanked state. The main purpose of the SFRA test when the transformer had been un-tanked was therefore to create a new baseline set of data. This data set was intended for direct comparisons with later test iterations to ensure that the simulated windings axial displacement faults could be detected using SFRA alone in an earthing transformer.

3.2.2.4 Comparative SFRA test with bulk movement of the A and 'C phase' outer core leg windings to the bottom of the core window

For the Bulk winding movement test iteration, the first step was to remove the lower and upper windings bracing chocks for the inner and outer C core leg windings (windings C1 to C2 and C3 to C4 as given in the nameplate windings layout diagram, Figure 3.4 above). The core-to-windings top and bottom insulation spacers were then cut in half and replaced under and above the 'B phase' windings. Both the inner and outer 'C phase' windings were then pushed down until the windings insulation was sitting on the bottom of the core window, ensuring that the inner and outer windings were still physically aligned. Another full set of SFRA measurements were then taken as per Table 3.2 above.
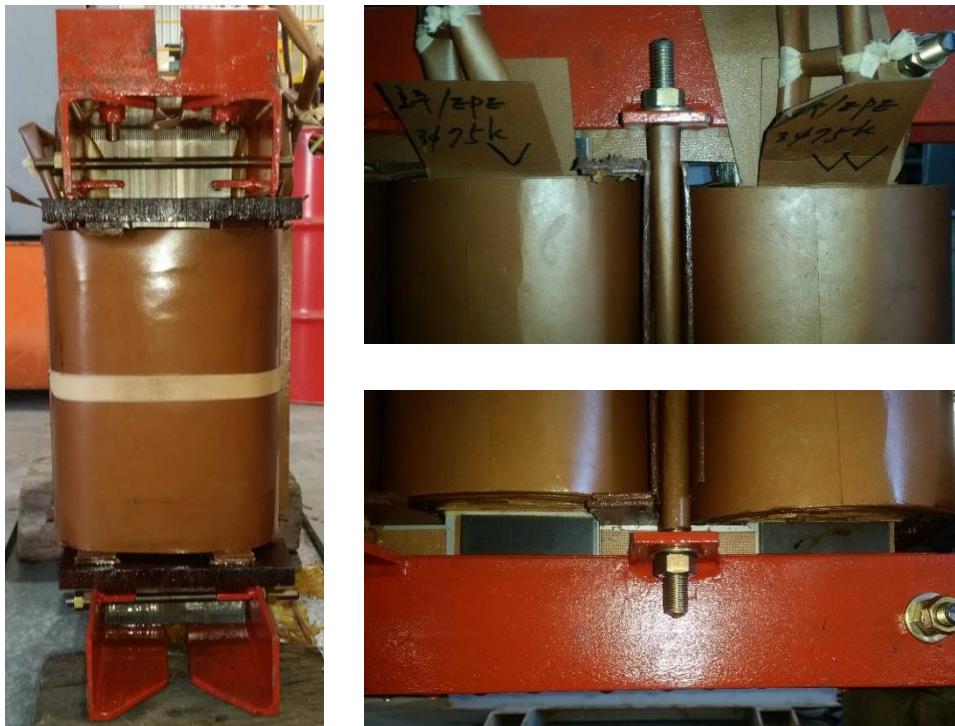
Figure 3.7 – Photos of the Earthing transformer core and coils
Left- Transformer core and coils assembly before any modification has been made.
Top Right – Top view of the C core leg windings bulk movement
Bottom Right – Bottom view of the C core leg windings bulk movement with 'C phase' sitting on the transformers core.

The 'C phase' outer core leg windings were chosen to reflect the greatest deviation in the SFRA response as discussed in section 3.1 above. The windings chocks were removed and modified to support the 'B phase' winding while enabling full axial movement of the 'C phase' winding as seen in Figure 3.7 above. The modifications made to the windings-to-core spacer can be seen in section D.4 of Appendix D below. Moving the windings as one piece to their lowest permissible point simulated a developing fault condition for the transformer and isolated the effects of bulk windings movement for the earthing transformers SFRA. The SFRA tests were conducted as above for direct comparison with the un-tanked baseline data collected in section 3.2.2.3.

3.2.2.5 90% movement of the inner core windings towards the top of the core window

Windings spacers, made of layered pressboard insulation, were fabricated to the specifications provided in section D.5.1 of Appendix D below. The actual windings displacement in this simulated fault case is 89.23% however, to simplify descriptions; this number will be referred to as 90% throughout the rest of the report. The inner and outer 'C phase' windings were then lifted to the top of the core window. The prefabricated pressboard spacers were then placed under the inner 'C phase' winding. The bulk windings were then pushed downwards allowing the outer winding to move to the bottom of the core window as seen in Figure 3.8. A full set of SFRA tests were then carried out as per the connections defined in Table 3.2.
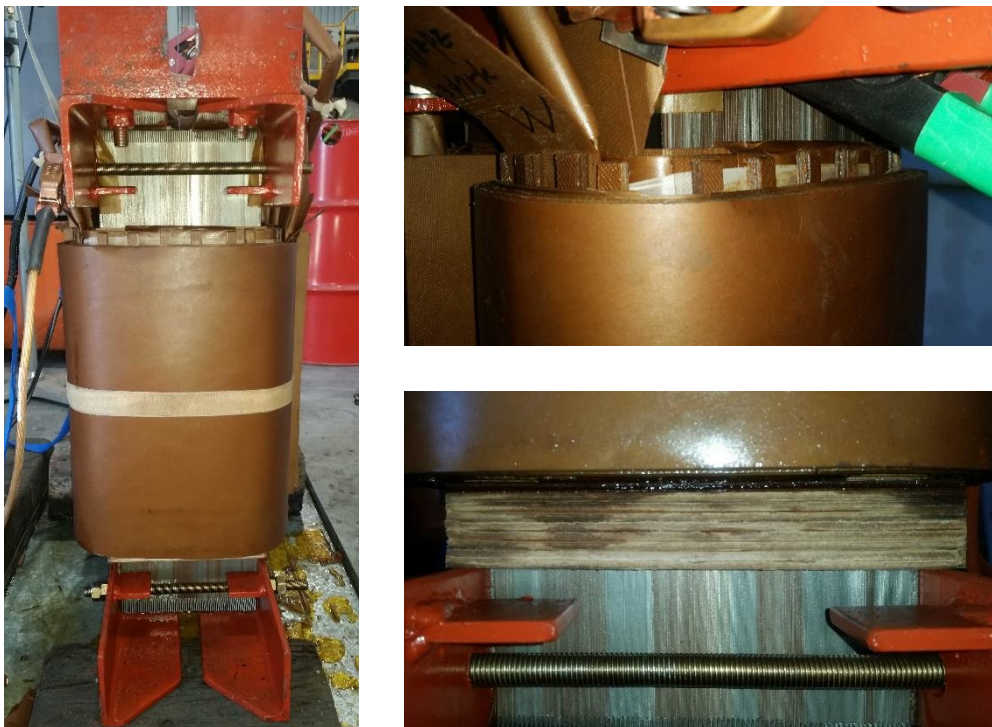
Figure 3.8 – Earthing transformer core & coils assemble after inner windings axial shift upwards of 90% of the total core window and outer 'C phase' winding at the bottom of the core window.
Top Right – Close view of the 90% axial windings displacement.
Bottom Right – Spacer under 'C phase' prior to inner winding axial displacement.

The windings spacers were fabricated out of pressboard insulation for its rigid form and nonmagnetic properties. Rigidness was required as for the windings spacers as the available mounting points for the spacer on the core clamping frame was spaced without middle support as seen in Figure 3.8. It was important that the spacer be made of a nonmagnetic material so that it did not introduce a new variable into the SFRA trace under testing conditions. Once again, the 'C phase' winding was selected as no further modifications were required of the windings support chocks than those made and discussed in section 3.2.2.4 above. The inner windings spacers were created with adequate width to push up and expose the oil port insulation sticks of the windings as they were found to be glued to the outer wrap of the inner coil. The height of the windings spacer (closer to 'B phase') was made to be smaller than the outer spacer as the bottom of the core window sat slightly higher than the core clamping frame.

3.2.2.6 45% movement of the inner core windings towards the top of the core window

The outer winding was then pushed back to the top of the core window, in line with the inner winding. The windings spacers were then removed and made shorter by removing layers of the pressboard insulation as per the specifications provided in section D.5.1 of Appendix D below. The actual windings displacement in this simulated fault case is 44.61% however, to simplify descriptions; this number will be referred to as 45% throughout the rest of the report. The pressboard spacers were then placed back in the same positions described in section 3.2.2.5 and seen in Figure 3.9. The windings were then pushed down the 'C phase' core leg until the outer winding was once again resting on the bottom of the core window. The final full set of SFRA tests were conducted as per the connections defined in Table 3.2.
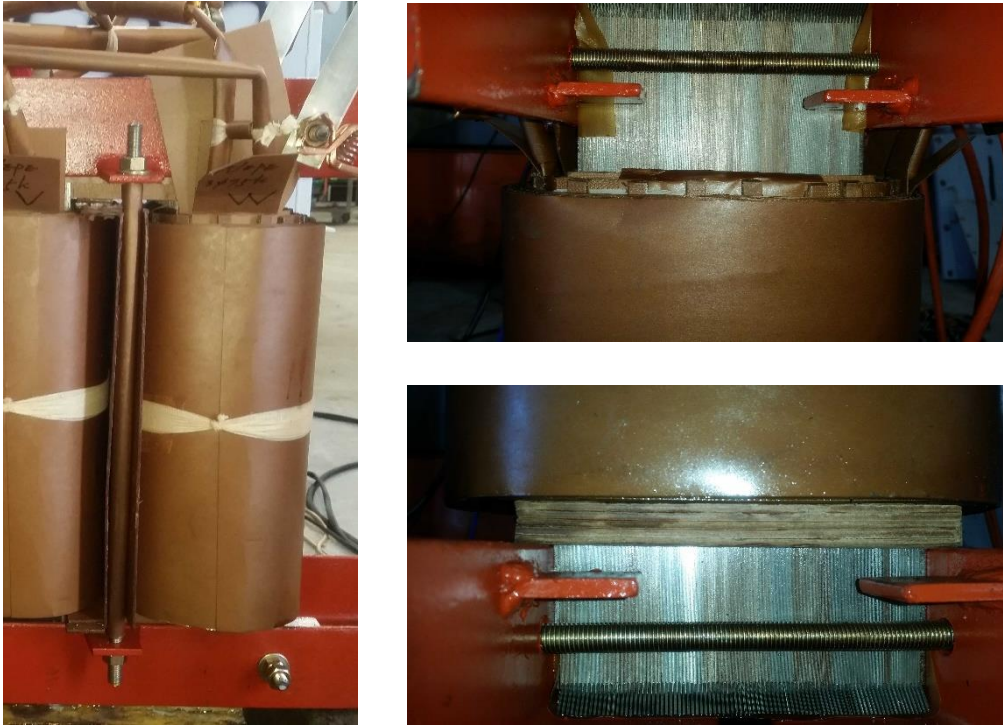
Figure 3.9 - The earthing transformer core and coils assemble after inner windings axial shift upwards of 45% of the total core window and outer 'C phase' winding at the bottom of the core window.

The inner winding pressboard spacers were made shorter to reflect a smaller axial displacement developing fault for the earthing transformer. This was conducted to see if it is possible to detect even small amounts of axial displacement between windings in an earthing transformer using SFRA as a diagnosis tool. Having two fault simulation cases of the same nature but varying in severity enables comparisons to see if a relationship exists between the fault severity and the SFRA trace for potential linear interpolation.

3.3   Results and Discussions

Results from the method presented in section 3.2.1 can be found in the form of a completed test certificates in Appendix C.2 (templates provided by Excess Power Equipment (EPE)). To surmise, The transformer and insulating fluid were found to pass all of the respective tests defined in section 3.2.1 above as per AS/NZS 60076 – 6 [31], AS 2374 [32] & A.S.1767 [33] respectively. Results and discussion from the method presented in section 3.2.2 above can be found in the subsections below.

3.3.1 Baseline SFRA test - Transformer fully assembled

Figure 3.10 below provides a full suite of SFRA traces results from benchmark testing method discussed in section 3.2.2.1 above. It is interesting to note that 'A phase' deviates the greatest at lower frequencies, contradicting the typical two winding transformer open circuit results discussed in section 2.2.1 above. 'C phase' open circuit trace results show an extra resonant point soon after the capacitive climb back from the lowest frequency resonance. The short circuit traces from Figure 3.10 has close correlation between phases with slight resonant point deviation at higher frequencies. Photos of the SFRA test set connections can be found in Appendix D.1.
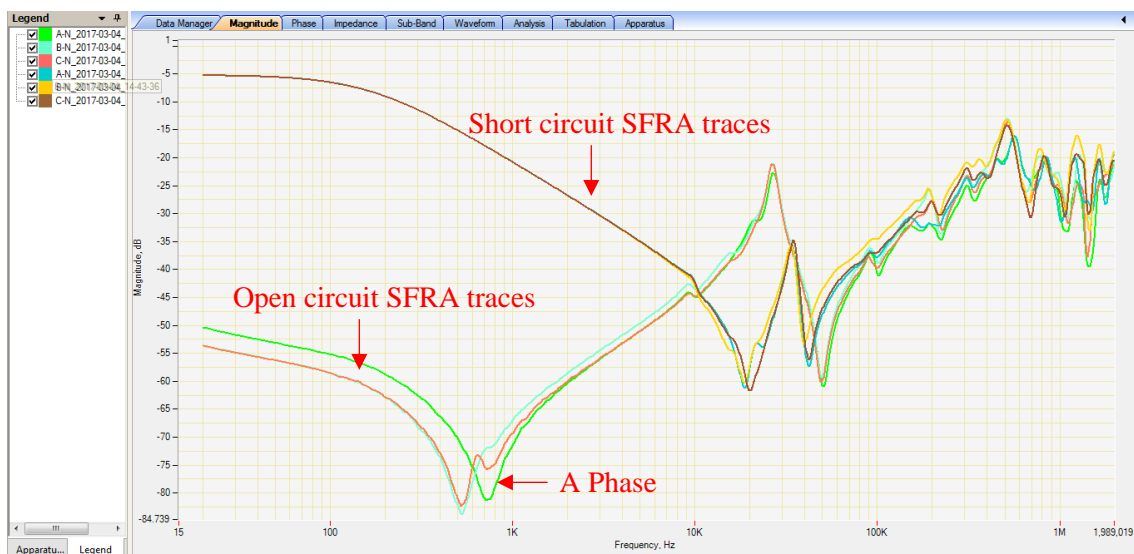
Figure 3.10 – Full suite of open circuit and short circuit SFRA trace results from the earthing transformer – Fully assembled (Benchmark Trace)

Benchmarked deviation of the 'A phase' winding, seen in the lower frequency region of Figure 3.10 above is likely the result of a common design layout choice for Zn wound earthing transformers. Section 3.1.1 above presented the test subject's windings layout and discussed interconnections in detail, noting that the 'A phase' interconnected windings have the greatest geometric separation from each other. The inter-windings capacitive relationship is therefore expected to deviate greatly from the B and 'C phase' interconnected windings.

Due once again to the multi-core-leg windings layout of this Zn wound earthing transformer, the extra 'C phase' resonance is likely because of inter-winding capacitive coupling. The capacitive coupling between 'C phase' and both the A and 'B phase' windings of the transformer result in a trace that tries to mimic both simultaneously providing averaging of data points to a certain degree.

36

By short circuiting all other bushing connections to the reference point for the SFRA tested transformer, it is possible to remove the effects of inter-winding capacitive coupling. For this reason, the short circuit benchmark phase comparison has a far closer correlation; supporting the normality of the A and 'C phase' open circuit benchmark SFRA results above.

3.3.2 Comparative SFRA test when the transformer had been drained of oil

Figure 3. shows the SFRA open circuit trace result from 'A phase' once the oil from the transformer has been removed. The "No Oil" SFRA trace response in grey has been mapped on the same axis as the green 'A phase' open circuit baseline trace, introduced in Figure 3.10 above. The method used to attain these results can be found in section 3.2.2.2 above. The no-oil SFRA trace has a relatively consistent frequency and magnitude offset on the logarithmic scale axis. The mid frequency region of this trace (800Hz to 700kHz) shows very similar spectral shape to the baseline with a consistent offset, most visible between the 800Hz and 28kHz range. The no-oil trace in Figure 3. also has large resonance deviation at the top frequency regions of the SFRA trace (900kHz to 2MHz). B and 'C phase' windings benchmark SFRA comparisons from removing the transformers oil can be found in Appendix D.2 below. Appendix D.2 also contains photos of the transformer before and after the oil had been removed.
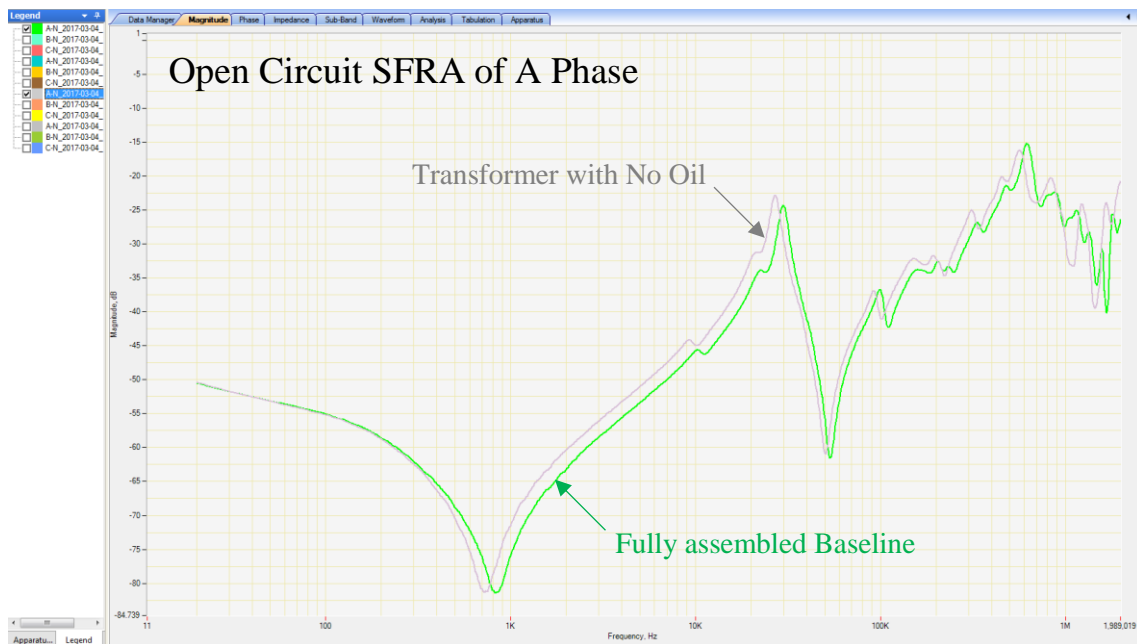
Figure 3.11 – Comparison of 'A phase' open-circuit SFRA trace responses.
Green Line – Fully assembled 'A phase' SFRA Benchmark
Grey Line – Earthing transformer 'A phase' SFRA trace after the oil has been removed.

Figure 3.12 below is the 'A phase' SFRA short circuit test result once again from the method detailed in section 3.2.2.2 above. The "No Oil" SFRA trace response in grey has been mapped on the same axis as the blue 'A phase' short circuit baseline trace. As seen in Figure 3. in the previous section, the trace shows very consistent spectral offset from approximately 10kHz through to 700kHz. Once again, the resonant peak deviation is more prominent in the higher frequency SFRA trace region (700kHz to 2MHz)
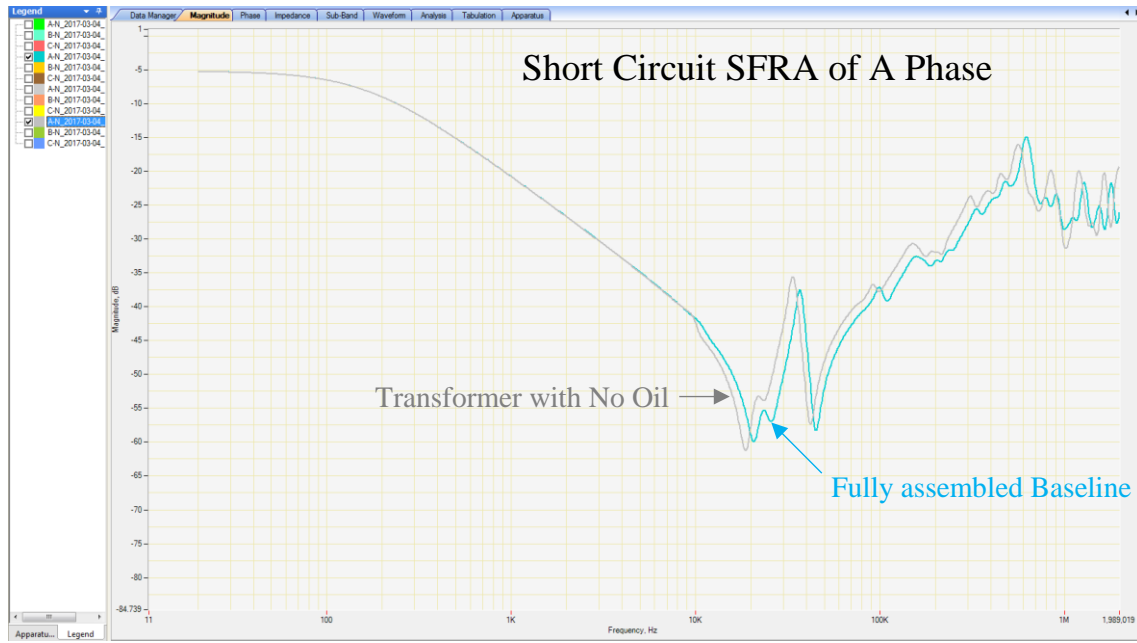
Figure 3.12 – Comparison of 'A phase' short-circuit SFRA trace responses.
Blue Line – Fully assembled 'A phase' SFRA Benchmark
Grey Line – Earthing transformer 'A phase' SFRA trace after the oil has been removed.

The frequency and magnitude offset seen in Figure 3. and Figure 3.12 above has a capacitive nature as a result of the oil being removed. Discussions in section 2.2.1 above introduced the concept that capacitive coupling occurs between the signal injected windings and all other internal components of the transformer. For the cases shown in Figure 3. and Figure 3.12, the capacitive coupling between the 'A phase' windings and other windings, the tank frame and the transformers core has changed with the insulation medium (from oil to air). The variations across almost the entire frequency sweep as a result of removing this earthing transformers oil aligns with section 4.8.2 of IEEE's standard 52.149 [16].

3.3.3 Baseline and comparative SFRA test when the transformer core and coils had been fully un-tanked

From the method defined in section 3.2.2.3 above, the grey line results of Figure 3.13 below were attained. The Earthing transformers fully assembled 'A phase' open circuit SFRA trace has been plotted in green on the same axis for comparison purposes. The general spectral shape of the un-tanked 'A phase' trace shows very little variation from the baseline trace. The un-tanked SFRA response appears to have a uniform higher frequency offset after approximately 300Hz when compared to the green baseline trace.
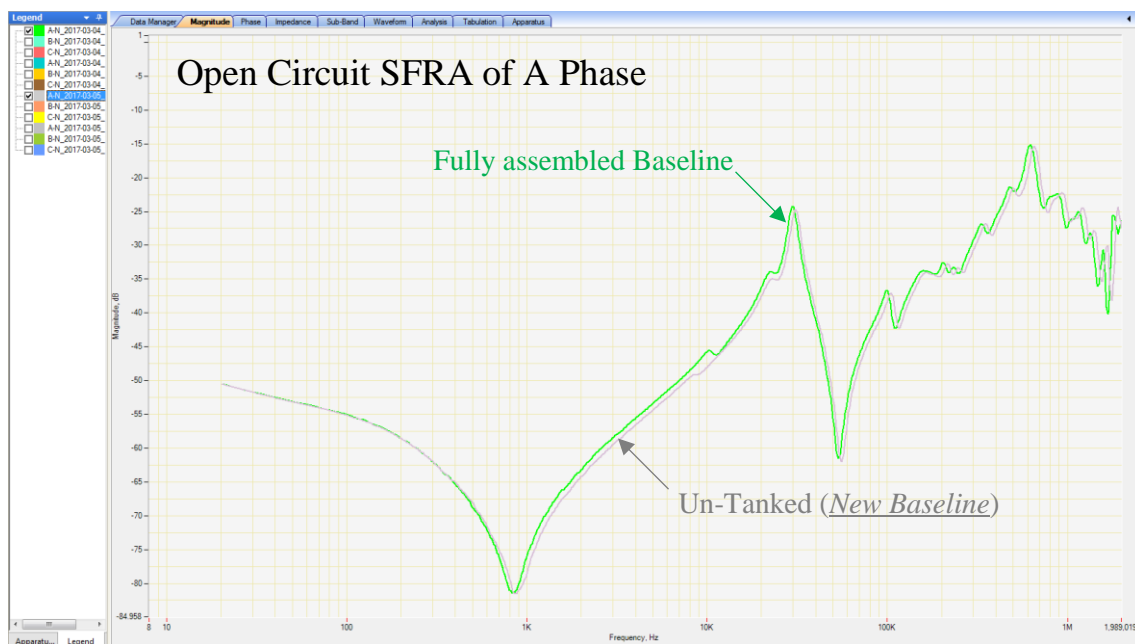
Figure 3.13 – Comparison of 'A phase' open-circuit SFRA trace responses.
Green Line – Fully assembled 'A phase' SFRA Benchmark
Grey Line – Transformer 'A phase' SFRA trace result after core and coils un-tanking.

An un-tanked short circuit SFRA results comparison can be found in Figure 3.14 below. The offset seen for the un-tanked short circuit test is proportionally similar to the open circuit comparison seen in Figure 3.13 above. Once again, retention of the spectral shape can be seen when compared with the baseline short-circuit trace with noticeable deviation starting at approximately 6kHz for the short circuit case.
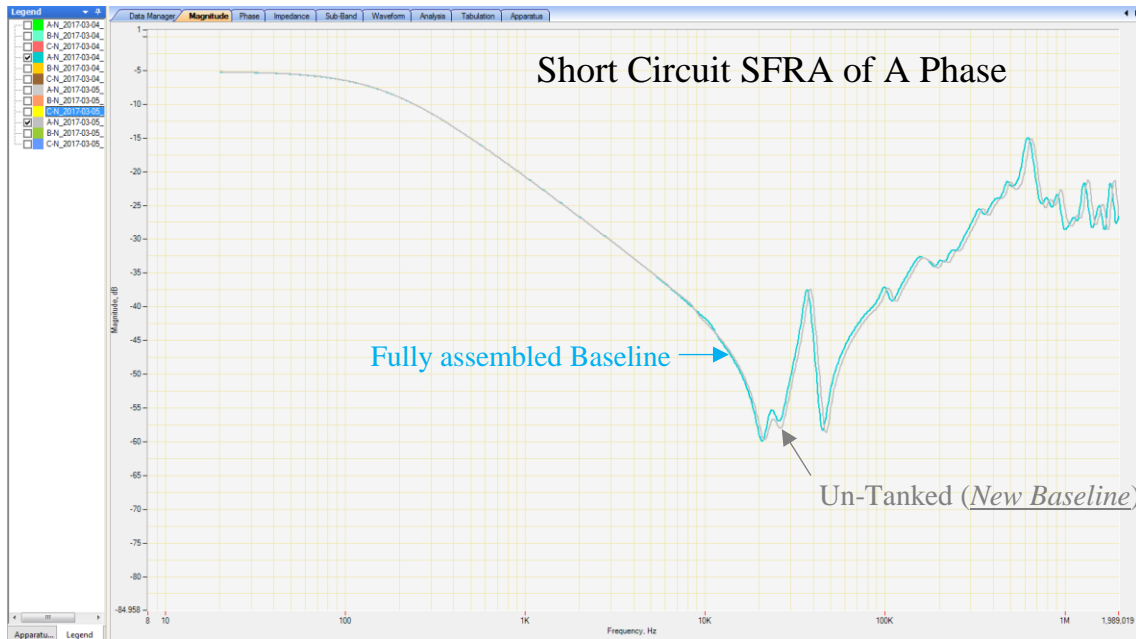
Figure 3.14 – Comparison of 'A phase' short-circuit SFRA trace responses.
Blue Line – Fully assembled 'A phase' SFRA Benchmark
Grey Line – Transformer 'A phase' SFRA trace result after core and coils un-tanking.

Un-tanking of the core and coils removes the capacitive coupling effect between the signal induced windings' and the metal frame tank structure when conducting an SFRA test. The effects of changing the transformers dielectric insulation from oil to air potentially becomes more apparent as the insulation dries. It is likely a combination between un-tanking and drying insulation that creates the uniform offset seen in both Figure 3.13 and Figure 3.14 above. The grey "Un-tanked" line in both Figure 3.13 and Figure 3.14 has been noted as "New Baseline" as all traces from section 3.3.4 onwards will be using this as the comparison baseline. Equivalent B and 'C phase' comparison results were found to have less prominent or very similar deviation to the 'A phase' SFRA trace comparisons presented above. To mitigate repetitive results entries, the B and 'C phase' comparisons for both open and short circuit testing can be found in appendix D.3 below.

3.3.4   Comparative SFRA test with bulk windings movement

Comparative SFRA tests with bulk movement of the A4 to A3 and C1 to C2 phase windings to the bottom of the core window with the un-tanked (new baseline) can be found in Figure 3.15 below. The lower frequency region (20Hz to 2kHz) of the SFRA comparison trace below present's slight deviation from an otherwise very closely matched set of open circuit SFRA traces.
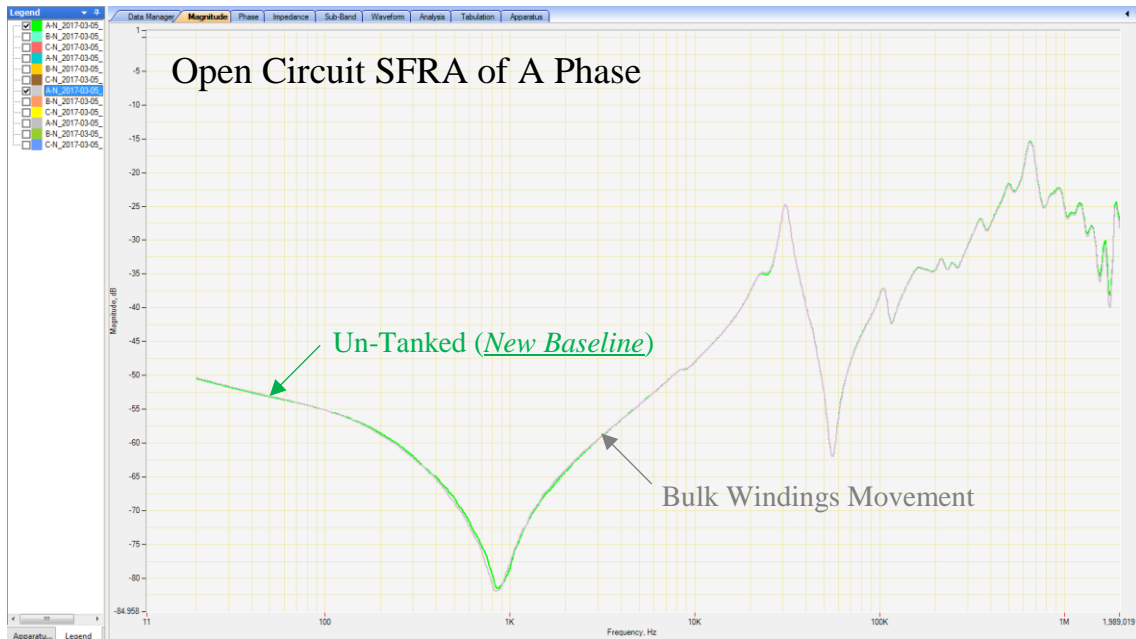
Figure 3.15 – Comparison of 'A phase' open-circuit SFRA trace responses.
Green Line – Un-tanked 'A phase' SFRA Benchmark
Grey Line – Transformer 'A phase' SFRA trace result after bulk windings movement.

The short circuit SFRA trace comparison equivalent of Figure 3.15 can be seen below in Figure 3.16. In the SFRA comparison trace below, both the benchmark and the bulk windings movement SFRA traces have very close alignment for the entire spectrum.
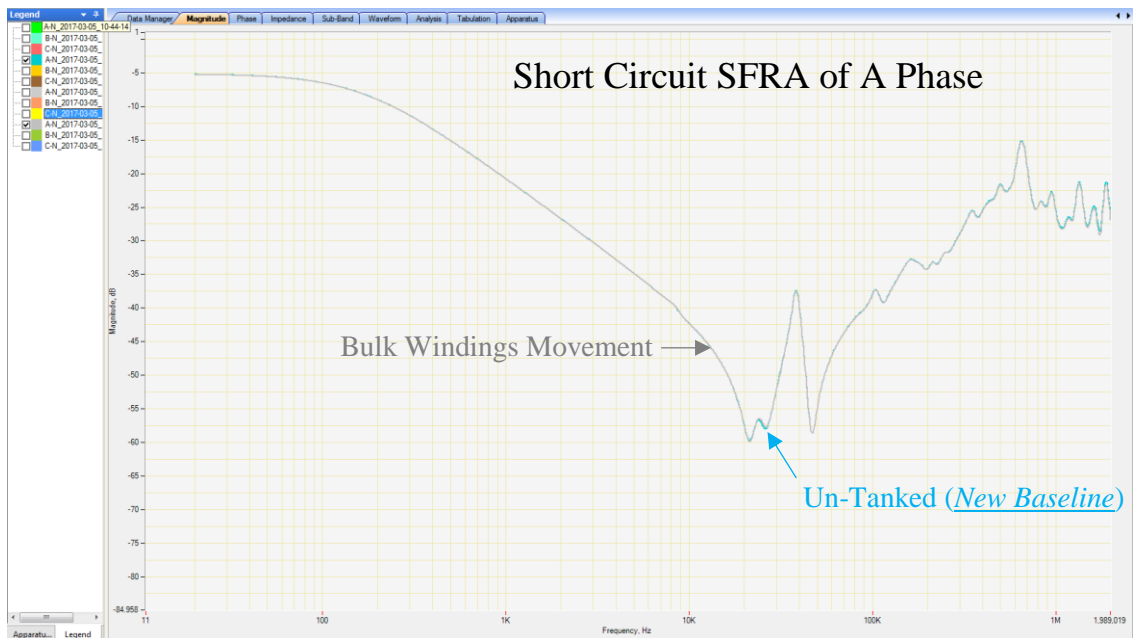
Figure 3.16 – Comparison of 'A phase' short-circuit SFRA trace responses.
Blue Line – Un-tanked 'A phase' SFRA Benchmark
Grey Line – Transformer 'A phase' SFRA trace result after bulk windings movement.

Slight deviations in the SFRA open circuit trace at lower frequencies would most likely be because of the windings capacitive interaction with the transformers core as conceptually introduced in section 2.2.1 above. IEEE's standard 57.149 also discusses the use of short circuit SFRA testing to remove the capacitive coupling effect between the core and injected windings. The open circuit iteration of the bulk windings movement suit of SFRA tests showed only low frequency variation. Isolated low frequency variations confirm that the windings to core capacitive relationship is the only one that changed within the test subject.

The results from bulk windings movement of the test subject do not appear to align with those presented in Figure 2.13 of section 2.3.1.3 above. This could partially be because the transformer was un-tanked, removing the potential coupling effect of the tank structure itself. The test subject for this report has a physically smaller construction and vastly different specifications from the comparison case in Figure 2.13. The most obvious source of deviation could be from model inaccuracy as the comparative case discussed in section 2.3.1.3 was created using finite element modelling software.

Figure 2.14, introduced in section 2.3.1.3, appears to align with the practical simulation results of this section for short circuit testing, however not open circuit testing. The table from IEEE's standard C57.149 notes that the greatest affected area is likely between 5kHz and 100kHz though deviation for the open circuit test instance is greatest between 20Hz and 3kHz.

3.3.5 Axial Windings shift of the inner core towards the top of the core window at 45% and 90%

SFRA results from the simulation of two axial windings displacement faults, each varying in severity, can be found in Figure 3.17 and Figure 3.18 below. Method sections 3.2.2.5 and 3.2.2.6 above along with photos from appendix D.5 of the process provide a step by step breakdown of how the tests were performed. Figure 3.17 is a zoomed open circuit 'A phase' comparison plot between the un-tanked baseline SFRA trace, a 45% windings displacement SFRA trace and a 90% windings displacement SFRA trace. The full frequency sweep results can be found in D.5 below for all test connections defined in the respective method section. The main resonance point of deviation occurs at approximately 20kHz with another point of deviation at the resonance and anti-resonance located around 110kHz. Axial windings displacement appears to have a smoothing effect on the resonant peaks around this frequency point. The first resonance of Figure 3.15 shifts to a lower frequency point with a slightly larger magnitude, proportional to the extent of windings displacement.
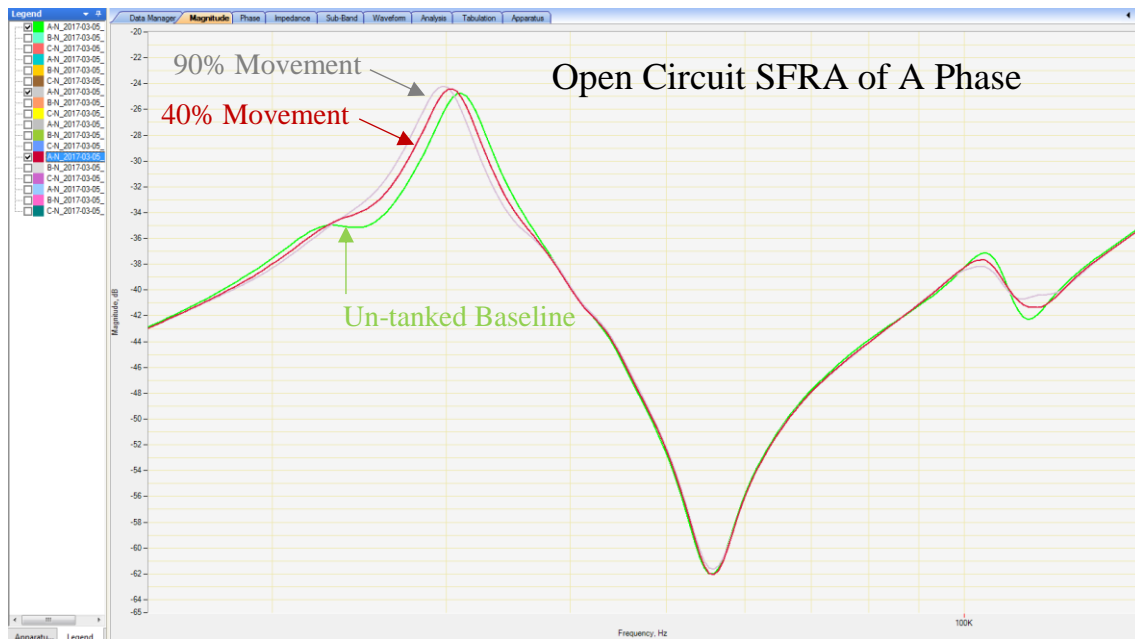
Figure 3.17 – Comparison of 'A phase' open-circuit SFRA trace responses.
Green Line – Un-tanked 'A phase' SFRA Benchmark
Red line – 45% Axial windings displacement proportional to the permissible movement.
Grey Line – 90% Axial windings displacement proportional to the permissible movement.

The equivalent short circuit 'A phase' axial windings displacement comparative plot can be seen below in Figure 3.18. Much like Figure 3.17 above, the plot below is of a zoomed reference to focus on the areas of trace deviation. This has been done because the trace alignment of the three conditions was very consistent for the rest of the frequency sweep. Once again, a full suite of the SFRA trace outputs from this test series can be found in appendix D.5 below. Consistent inductive roll-off frequency offsets for each case in Figure 3.18 appear proportional to the amount of axial winding displacement from approximately 9kHz through to 25kHz. This consistent offset leads to the main resonant point of interest around 25kHz where a large change in magnitude occurs from the windings axial displacement. The large change once again appears to be proportional in nature to the simulated fault severity. As with the open circuit trace, another resonant point of deviation occurs around 110kHz, however, in the 90% axially displaced SFRA trace, a new resonance has formed.
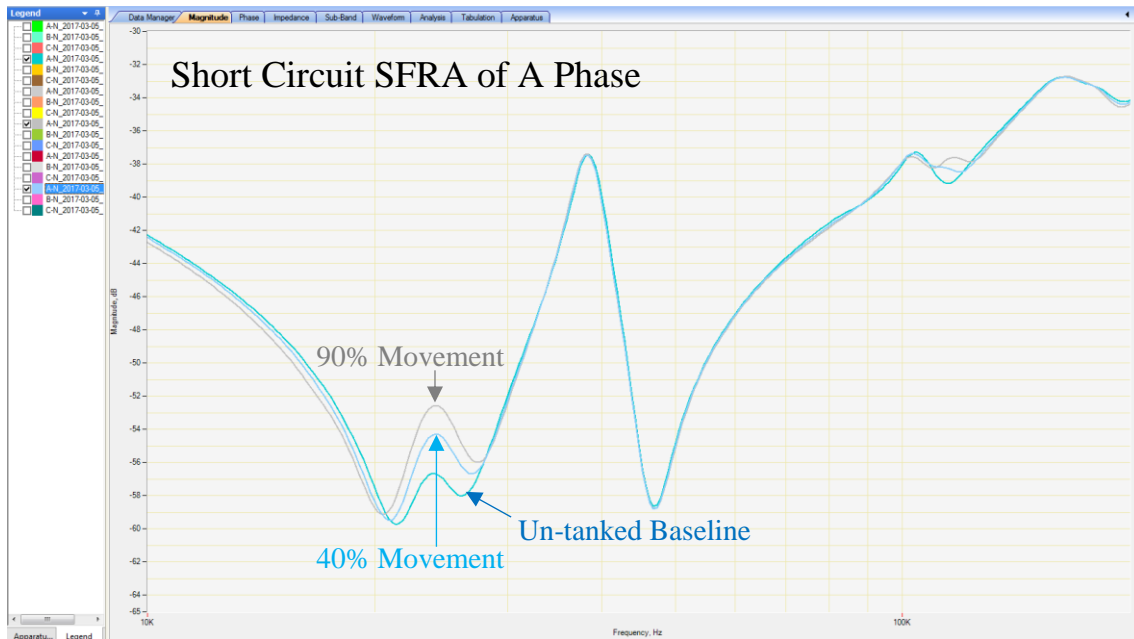
Figure 3.18 – Comparison of 'A phase' short-circuit SFRA trace responses.
Dark blue Line – Un-tanked 'A phase' SFRA Benchmark
Red line – 45% Axial windings displacement proportional to the permissible movement.
Grey Line – 90% Axial windings displacement proportional to the permissible movement.

It is interesting to note that deviation at the primary resonant point in Figure 3.18 is far greater than the open circuit testing instance seen in Figure 3.17 above for each fault case. This could possibly be because the inter-windings capacitive coupling effects have been removed by short circuiting all other bushing connections to the SFRA measurement terminal.

Short circuit testing results presented in Figure 3.18 above, show comparable spectral deviations at similar resonant points to the expected results introduced in Figure 2.12 of section 2.3.1.2 above. The primary resonant peek, seen in Figure 3.18, appears to have a positive magnitude shift as a result of the characteristic extra resonance point.

When compared with the equivalent expected SFRA trace response introduced in Figure 2.11 of section 2.3.1.2 above, Figure 3.17 appears to have a vastly different SFRA open circuit axial winding fault response. This is likely because the comparative fault case from IEEE's standard C57.149 is for a large 3 winding power transformer. This once again solidifies the necessity for the simulated faults specific to earthing transformers conducted throughout this chapter.

44

3.4   Further Discussion

The results presented above satisfy the intended goal to determine if it is possible to diagnose a fault in an earthing transformer using SFRA alone while identifying critical points of deviation. Comparisons with existing research in SFRA testing confirmed the value of simulating faults, specifically in earthing transformers to gain an intimate understanding of the resultant spectrum changes.

The open circuit SFRA benchmark trace result from Figure 3.10 has been added to the twenty randomly selected 'A phase' APU SFRA traces from Figure 3. above to create Figure 3.19 below. Figure 3.19 has been included as it provides an initial understanding of the test subjects characteristic spectral similarities and deviations when compared with other earthing transformers. It is interesting to note that the test subject has an a-typical response for most of the spectrum.
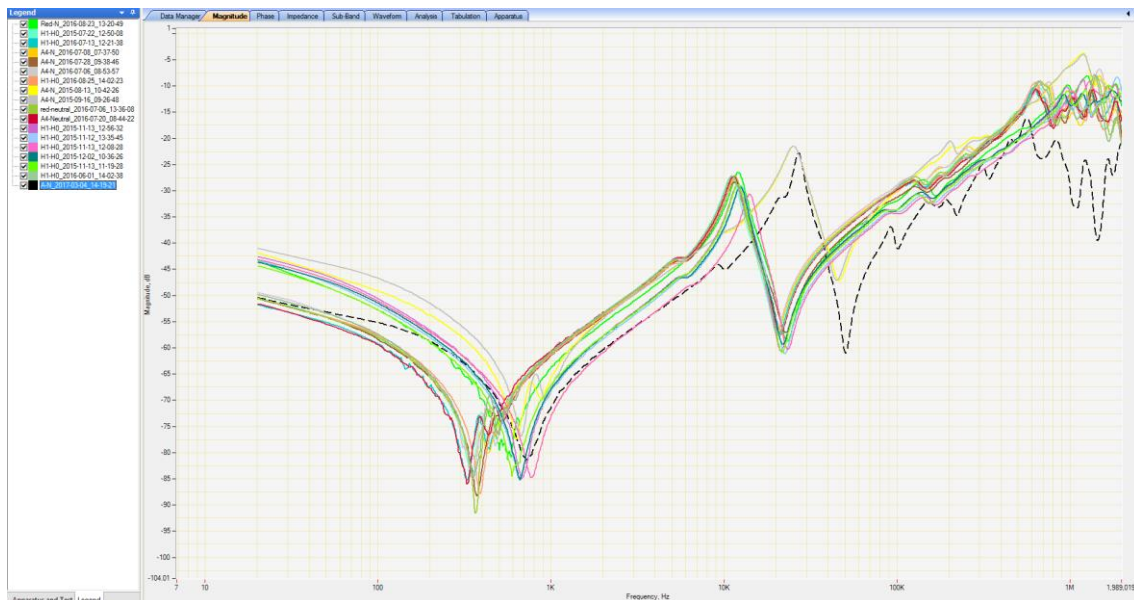
Figure 3.19 – Same plot introduced in Figure 3. above with the 'A phase' Open Circuit transformer SFRA result from section 3.3.1 above, overlayed as the dashed bold black line.

The a-typical nature of the test subject is most likely because of differing design and manufacturing process along with voltage and current rating. All comparisons and analysis from this point of the report forward will be made from an open circuit connection standpoint. This decision was made, based on The Australian power utility's available data to ensure that comparisons could be used at a later point to quantify any results. One suggestion for APU's could be to incorporate short circuit SFRA testing into their conditional monitoring of earthing transformers rather than phase to phase testing.

Having attained the results presented throughout this chapter, the next step was to begin developing a tool to assist in detecting axial windings displacement in earthing transformers.

Chapter 4 Development of a tool for assistive fault diagnosis in earthing transformers

The results from section 3.3 will be used throughout this chapter to justify some design decisions in the development of the proposed assistive fault diagnostic tool for earthing transformers.

As first introduced in section 2.4.1.3 and subsequently in section 2.4.2 earlier in this report, the use of an adapted MFCC process stood out as a possible feature extraction technique for SFRA trace data analysis. This unique approach to SFRA trace analysis provides a method basis for the creation of the proposed analysis tool.

The main design requirements were defined in the introduction as follows:

- Simple interface,
- Automatic data management & simple intuitive data acquisition,
- Multiple trace entry and processing capability,
- Automated processing with minimal user variable inputs,
- Refinable process,
- Simple output display,
- Meaningful output to assist with fault diagnosis.

The first main step of the development process was to choose a platform for the proposed analysis tool.

4.1 Planning and Justification

MathWorks MATLAB [34] was proposed for the implementation of a method to analyse SFRA trace data. MATLAB's coding terminal and suite of predefined functions make it an ideal interface for large data management and processing.

Given the adaptive limitations that LPC and PLP have, as discussed in sections Appendix B below, it was proposed that a customised variation of MFCC could be used to extract the important features of an SFRA trace. Customisations would need to be made in the computational process to tailor the analysis for fault detection. Section 2.4.1.3 discussed the reasoning behind each step of the MFCC feature extraction process, highlighting specific elements that were included for human speech and hearing characteristics;

- Sampling/sampling frequency,
- Pre-emphasis,
- Windowing,
- Logarithm Function application,
- Mel-scale filter wrapping.

Proposed adaptations of each for improved SFRA feature extraction are detailed in sections 4.1.2, 4.1.3, 4.1.4 and 4.1.5 below.

4.1.1   Sampling

Most SFRA software interfaces provide output data in the frequency domain as discussed in section 2.2.1 above. Sampling of an SFRA spectrum is therefore not required given the process of sampling is used for discretising data in the time domain (introduced in section 2.4.1 above).

4.1.2   Pre-emphasis

Pre-emphasis of an SFRA spectrum is not required as correct data acquisition process, proposed in section 2.2.1, captures enough spectral information for analysis purposes.

4.1.3   Windowing

Section 2.3 introduces the concept of SFRA frequency range addressing to physical components within a transformers construction. Faults affecting specific components of the transformers construction (such as axial windings displacement, discussed in section 2.3.1.2 and presented in section 3.3 above), could be isolated through windowing of the transformers SFRA trace. A windowed SFRA trace would provide higher resolution feature extraction for fault detection purposes. The results from axial windings displacement simulations presented in section 3.3 above show the greatest fault variation at the resonant peaks between 10kHz and 200kHz. For this reason, while allowing for some level of tolerance for different transformer designs, the SFRA trace window was proposed to start at 5 kHz and finish at 200 kHz.

4.1.4　　Logarithm function

The purpose of applying a logarithm function to the filtered spectrum as discussed in section 2.4.1.3 above is to compensate for noise in the input signal and provide some level of smoothing. It turns out that smoothing of input magnitude variation is an undesirable effect for SFRA spectrum analysis. Section 2.3.1 above provides examples of comparative transformer SFRA fault response traces, introducing the idea that changes in spectrum magnitude can be indicative of a fault. Results from section 3.3 above solidify the concept that an axial windings displacement fault will change the transformers SFRA resonant peak magnitudes along with frequency location. Discussions from section 2.4.1.3 above introduce the idea that the resulting coefficients from the application of an IDCT are uncorrelated when the input has had a log function applied prior. Uncorrelated coefficients are required analysis and distillation of the spectrum data to encapsulate the important trace information.

Due to contradicting the arguments defined in the paragraph above, it was proposed that as an initial test phase, the logarithm function be included in the feature extraction process to maintain flexibility and robustness. If the resultant distilled data vectors were seen to have little deviation in magnitude between input fault test samples, the logarithm function was proposed to be removed.

4.1.5　　Mel-scale filter application

As introduced in section 2.4.1.3 above, Mel scale filter allocation is used to interoperate an input speech signal in a similar way to human hearing. Most SFRA testers acquire data in a logarithmic fashion with a higher data resolution at lower frequencies [17]. High frequency information would be lost using Mel scale filtering given its logarithmic nature (above 1 kHz), essentially resulting in 'double log' filtering of the spectral information. The idea of customised filter placement for feature extraction of any given spectrum, was however, proposed to be substitutionally implemented for fault identification.

Results from the practical fault simulation presented in section 3.3 of this report identified that the most prominent deviation on the SFRA trace occurred at select resonant peaks. Based on the known points of greater deviation, a suitable filter placement convention to focus on the respective resonant peaks was proposed. The filter placement convention used would need to be adaptable for all earthing transformers given the expected SFRA trace variances, discussed in section 2.2.1 and presented in Figure 3..

Enabling the placement of filters to be adaptable for variances between earthing transformer SFRA traces requires the transient identification of resonant peaks in any given dataset. As discussed in section 2.2 above, most SFRA traces have many resonant points along the frequency axis at different frequency locations. The inclusion of resonant points that do not contain useful information for the detection of a fault in an SFRA transformer trace is not desirable. Zero-point derivative location methods for detecting relative minima and maxima along a given trace would be susceptible misalignment due to noise. Filtering could be applied with discretion to smooth noisy SFRA signals, however, doing do would risk removing useful points of information. Due to the risk of removing useful trace information, selection of an appropriate filter algorithm was seen to be very difficult for various transformer SFRA trace applications.

Section 2.2 above, introduced the relationship between phase angle and the location of resonant peaks in the corresponding magnitude plot of an SFRA trace. The dramatic phase change that occurs around magnitude peak locations was proposed to be exploited for a filter placement convention. Figure 4.1 below is plot of data attained in section 3.3.1 above (fully assembled benchmark test iteration), with the addition of resonance point comparison lines. Figure 4.1 provides a direct comparison for the test subjects open circuit magnitude trace response and phase trace response, mapped on a data-point axis, confirming the proposed interrelationship.
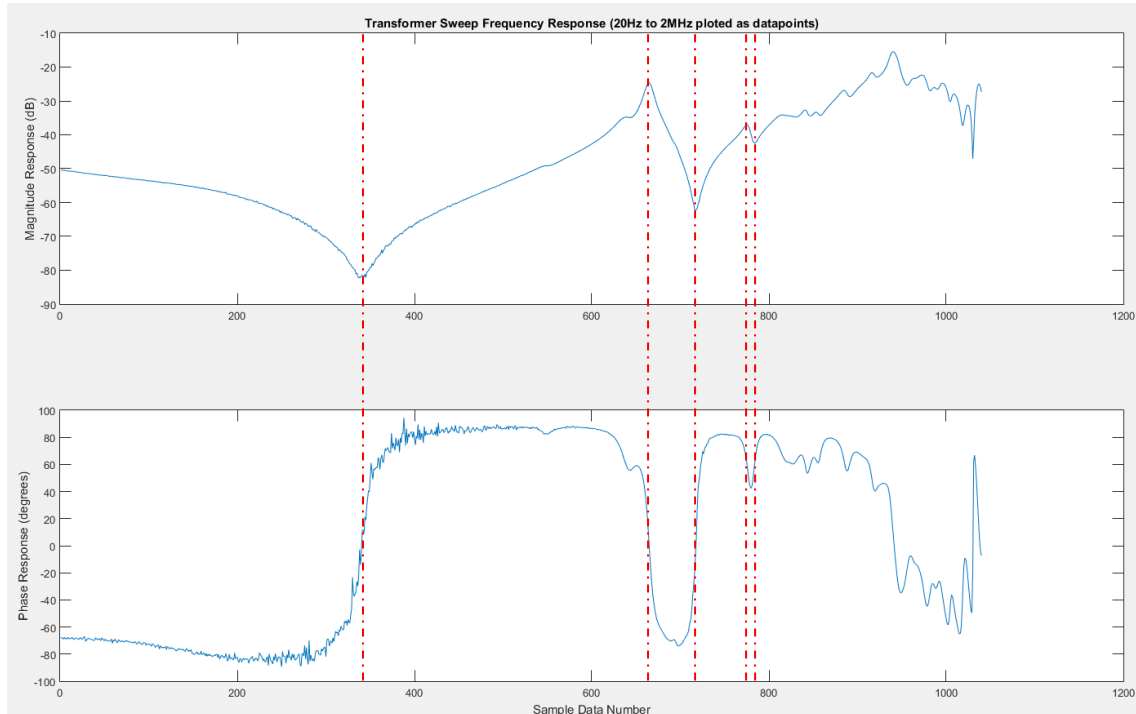
Figure 4.1 – 'A phase' benchmark SFRA open circuit transformer response using MATLAB to plot raw data for comparison. Raw data attained from testing method, defined in section 3.2.2.1 above.

The use of a sweeping two-line window function across an SFRA trace while an algorithm looks for a predefined phase magnitude difference was proposed as first step of the filter placement convention. A function of this nature would be easily tune-able for optimisation of the filter placement convention for application flexibility, sensitivity and robustness.

4.1.6 Additional points of consideration

The application of filters in the MFCC process, defined by section 2.4.1.3 above, occurs at the step before a logarithm function is applied to the spectrum. For this reason, it was proposed that the SFRA input be subjected to exponentiation of the log spectrum data. From this point, it would be possible to apply the predefined (by location) filter bank to the dataset before re-applying the logarithm function as per the MFCC process.

Finally, an Inverse Discrete Cosine Transform (IDCT) would need to be applied to convert the filtered log-spectrum data into cepstrum vectors on a pseudo-frequency axis.

Once the spectrum data has been distilled down to a simple vector representation on the pseudo-frequency axis, analysis of the results would be required. Results analysis would need to include a comparison of the transformers baseline SFRA cepstrum coefficients with the equivalent axial windings displacement fault simulation SFRA cepstrum coefficients. A comparison of this nature would identify the pseudo-frequency 'bins' that show the greatest deviation, unique to the simulated axial winding displacement fault. The magnitude of the two frequency bins that show the greatest deviation between baseline and fault simulation data, were proposed to be plotted against each other on separate axis. The resultant would therefore be a single point on a two-dimensional plot, encoding the important SFRA trace data for the detection of an axial windings displacement fault.

To check that this data distillation method is effective for fault identification, comparison of the baseline and fault simulation processed SFRA data was proposed. Subsequently, it was proposed that all Australian power utility supplied Earthing transformer SFRA trace data be processed using this distillation method for trend identification and analysis between transformers.

4.2 Development

MathWorks' MATLAB was used for the implementation of the proposed SFRA analysis tool. MATLAB's interface enabled the creation of an algorithm that automatically sorts, analyses and process raw csv converted SFRA trace data from Doble's SFRA 5.3 software. A high level representation of the method chosen to create the automated SFRA analysis tool for fault identification in earthing transformers can be seen graphically in Figure 4.2 below (based on discussions from section 4.1 above).
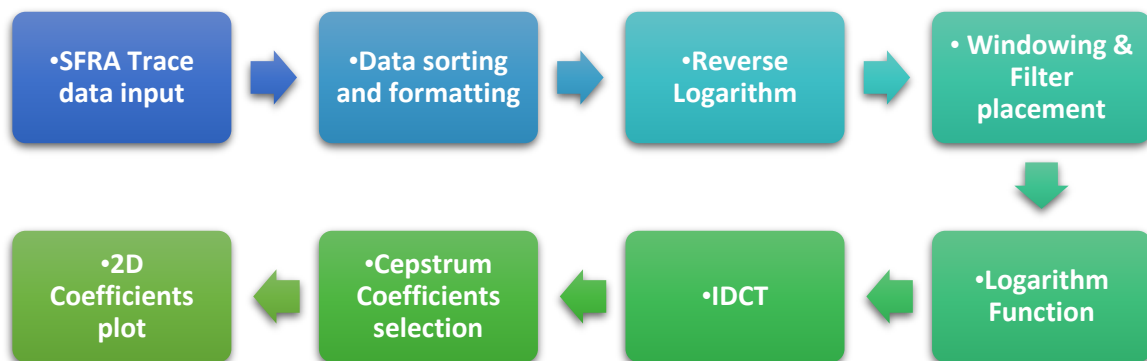
Figure 4.2 – High level breakdown of the computational steps taken in the creation of an automated SFRA analysis tool for assisted fault detection.

Each step in Figure 4.2 has been defined as a sub-section of this chapter. Each sub-section elaborates on the relevant steps taken in the creation of the automated SFRA analysis tool for assisted fault detection. The full code used for each section is available on request from the author.

4.2.1 SFRA Trace data input

The first step was to develop code that can request that the user select a folder path that contains the data that needed to be analyzed in a simple, robust and intuitive way. MATLAB's 'uigetdir' function was used as a part of a script named 'load_datam' to request a user path file location that contained all the respective .csv SFRA files to be analyzed. The code for this component was designed to store the script folder path and returns the user once the data had been imported. Figure 4.3 below is a snipping of the 'load_datam' script once executed, requesting a file path containing the .csv formatted SFRA data to be analyzed.

Careful consideration was given to the code's input data management to ensure that intuitive application did not compromise stability. If the user selects a folder that does not contain valid .csv format files, an error message will appear indicating that "only files of a .csv format can be selected, please run the script again and select a folder with only the .csv format files to be analyzed".
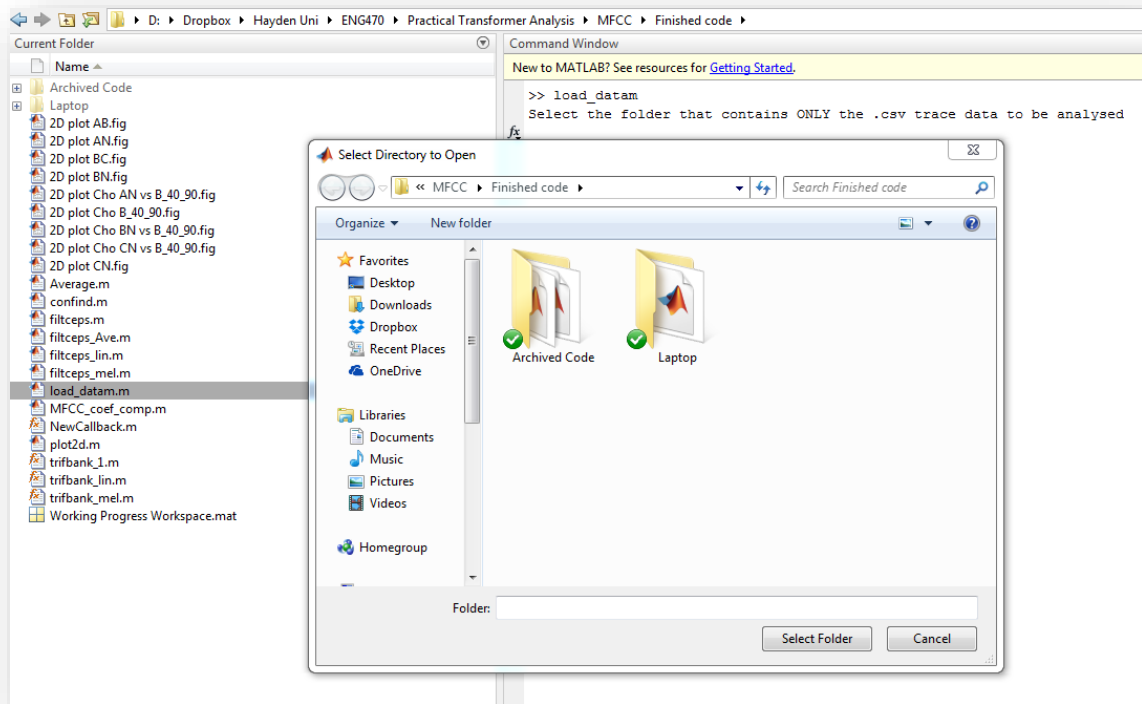
Figure 4.3 – Snipping of MATLAB interface after excitation of data load script. Popup window requests the user to locate the file that contains only the SFRA csv files required for analysis.

Figure 4.4 below is an interface snipping example of the output text once a valid folder path has been selected. The code was designed to restate the folder path selected to provide visual confirmation to the user of the path selected and indication that the task had correctly executed. After execution, the code was designed to return the MATLAB user to the original folder path that contained the 'load_datam' script for the next step of the analysis process.
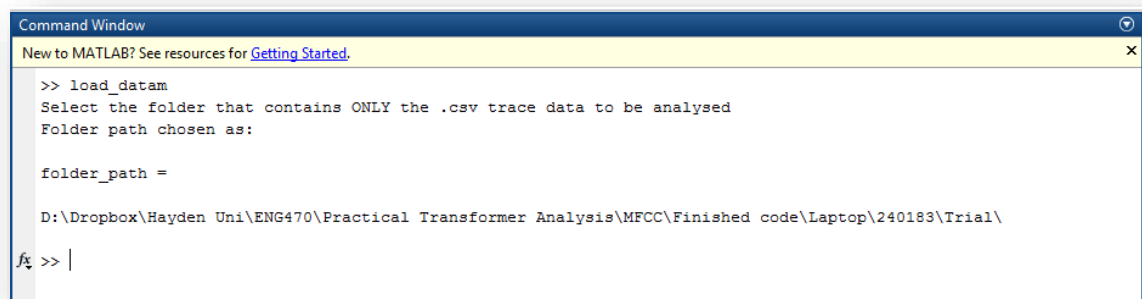
Figure 4.4 - Snipping of MATLAB command window and workspace once folder path has been selected.

4.2.2 Data sorting

Once the folder path has been selected, 'load_datam' automatically detects the number of .csv file, contained within the folder and initialises the matrices 'data_freq', 'data_phase', 'data_mag' and 'nameplates' for the respective number of entries. 'load_datam' was then designed to sweep through every relevant column of the Doble SFRA 5.3 converted .csv data within the containing folder and import all data into the respective matrices. An example snipping of some imported data (separated and formatted into the respective matrices) can be found in Figure 4.5 below.
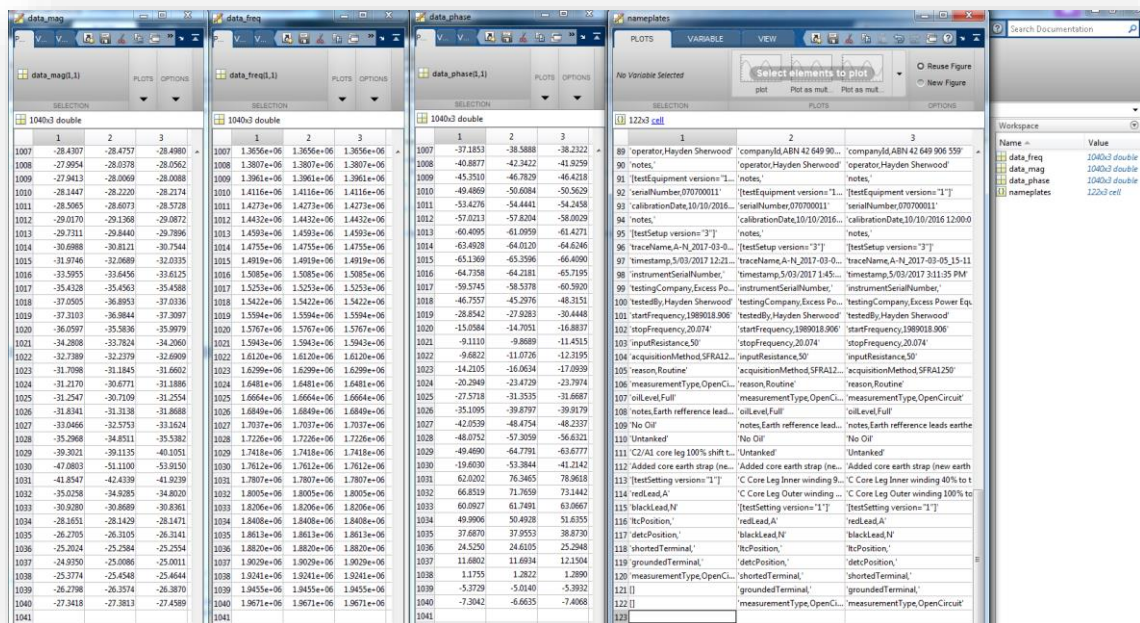
Figure 4.5 – Snipping example of the data once imported and sorted into the respective initialised matrices.

The next step in sorting entry data was to create a way of filtering out specific SFRA lead configuration results for comparison purposes, introduced in section 2.2.2 above. Allowance was made for several different naming conventions of the bushing lead connections to compensate for the SFRA 5.3 software's user input requirements [17]. A sample of the code used to make the appropriate allowances for six different naming conventions has been included in Figure 6.86 of Appendix E below.

Figure 4.6 below is a snipping of the command window and 'SearchResults' Matrix output from running the 'confind' script. In this example, the 'confind' script has been asked to look for any SFRA traces amongst the input data that have the 'Red' test set lead connected to 'A' phase and the 'Black' test set lead connected to the transformers 'N'. The 'SearchResults" cell matrix stores the corresponding row number of any nameplate column that contains the specified lead configuration for automated analysis of comparable data.
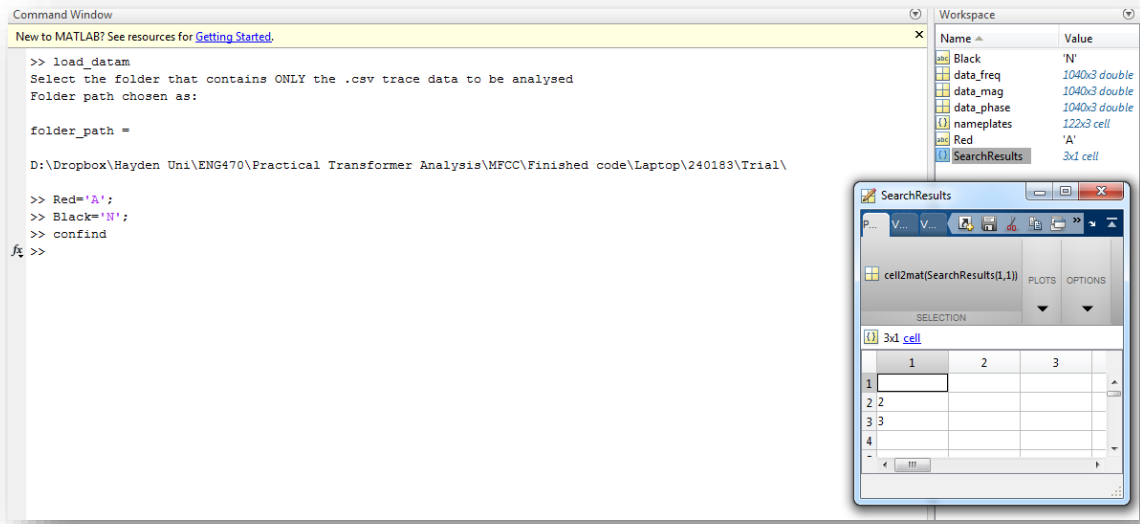
Figure 4.6 – Snipping of the test set connection configuration search script

Once the scripts introduced above were completed and iteratively tested using a multitude of different data entry configurations, the next step was computational data processing.

4.2.3 Reverse Logarithm

The first stage of the computational data processing phase was to apply an inverse logarithm to all data points in the respective 'SearchResults' filtered data sets. The justification behind performing this operation was discussed in section 4.1.6 above. The function applied was as per Equation 4.1 below:

Equation 4.1 – Inverse logarithm function applied to all the SFRA magnitude data points under analysis

$$Inverse\ Logarithm\ of\ SFRA\ data\ \mathrm{X_{InvLogMag}} = 10^{\left(\frac{SFRA\ output\ Spectrum\ data}{20}\right)} \quad (4.1)$$

$$Where:\ X_{InvLogMag}\ is\ a\ matrix\ variable\ for\ storing\ the\ inverse\ Log\ spectrum\ data$$

Equation 4.1 essentially provides the direct ratio of the output voltage over input voltage, measured by the SFRA tester for the pre-operation of windowing and filter placement.

54

4.2.4　　　Windowing & Filter placement

Windowing of the raw SFRA data, discussed in section 4.1.3 above, was used to isolate the frequency region of the trace that had the greatest deviation from fault simulations. To encapsulate the most prominent points of interest for fault diagnosis, 'f_min' was defined to be equal to magnitude plot data point 600 and 'f_max' was defined as data point 875 (15.140kHz to 317.103kHz respectively). Defined data window constraints enabled more relevant filter placement along the ratio data plot.

The filter placement step involved a few separable sub routines of code that have been partially included as snipping's in section E.1.1 of Appendix E below. The first subroutine is an extract of code, to create a sweeping function across the windowed SFRA phase data, presented as Figure 6.87. Section 4.1.5 above introduced the relationship between resonant points of the magnitude plot and sharp changes in the corresponding SFRA phase angle. To exploit this relationship, a sweeping gradient difference function was used to locate points along the given phase trace with pre-set values that could be adjusted for refinement.

The code in Figure 6.87 stores a single row matrix of values (Referred to as a 'double' in MATLAB) in the variable 'Z1' to be used for filter placement. All entries of Z1 were increased by a value of 0.01 to raise all data points off the 0 axis. This has been done to distribute some of the area under the curve for the next sub-routine of the filter placement script.
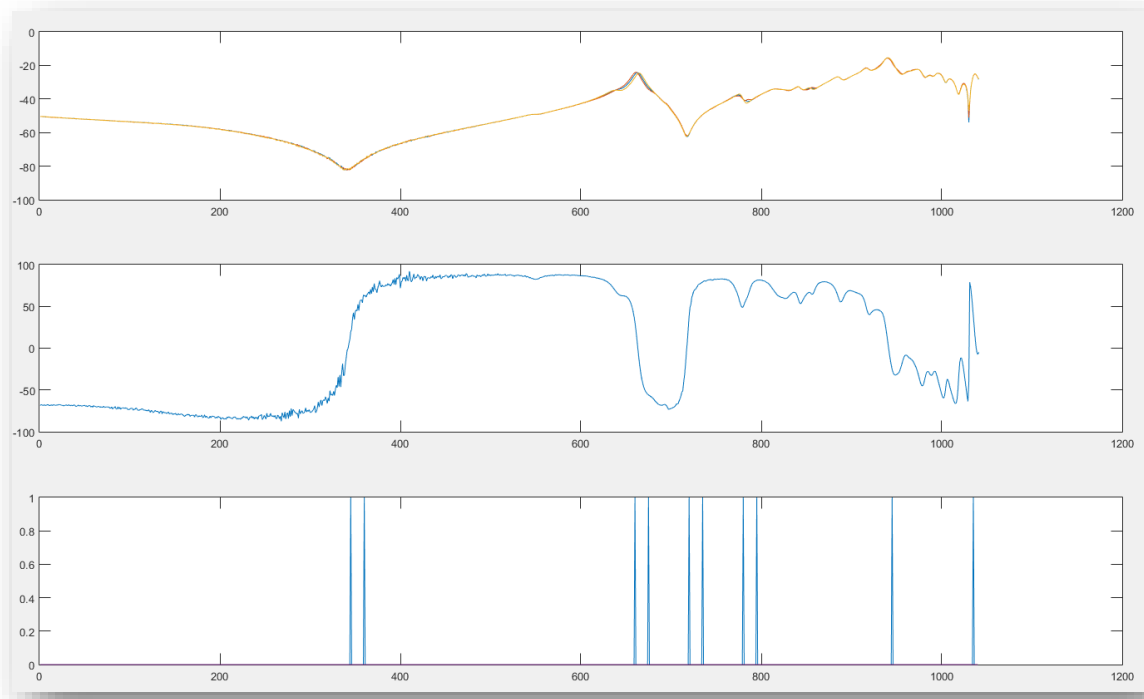
Figure 4.7 – Three tier plot of a sample earthing transformers SFRA Magnitude and Phase traces along with the filter addressing alignment trace, all mapped on the same x axis for comparison.

The bottom graph of Figure 4.7 has been automatically generated from script processing of the SFTA phase response, seen in the middle graph. The top graph is the corresponding magnitude plot to the middle plot phase data on a common data-point axis. This plot format was used for iterative tuning of the first stage filter placement script. The main aim of the tuning process was to ensure that the filters were placed at the appropriate locations for the intended resonant peaks of interest. By fine tuning the sweeping window function size and sensitivity variables, the plot at the bottom of Figure 4.7 was achieved as a first refinement step.
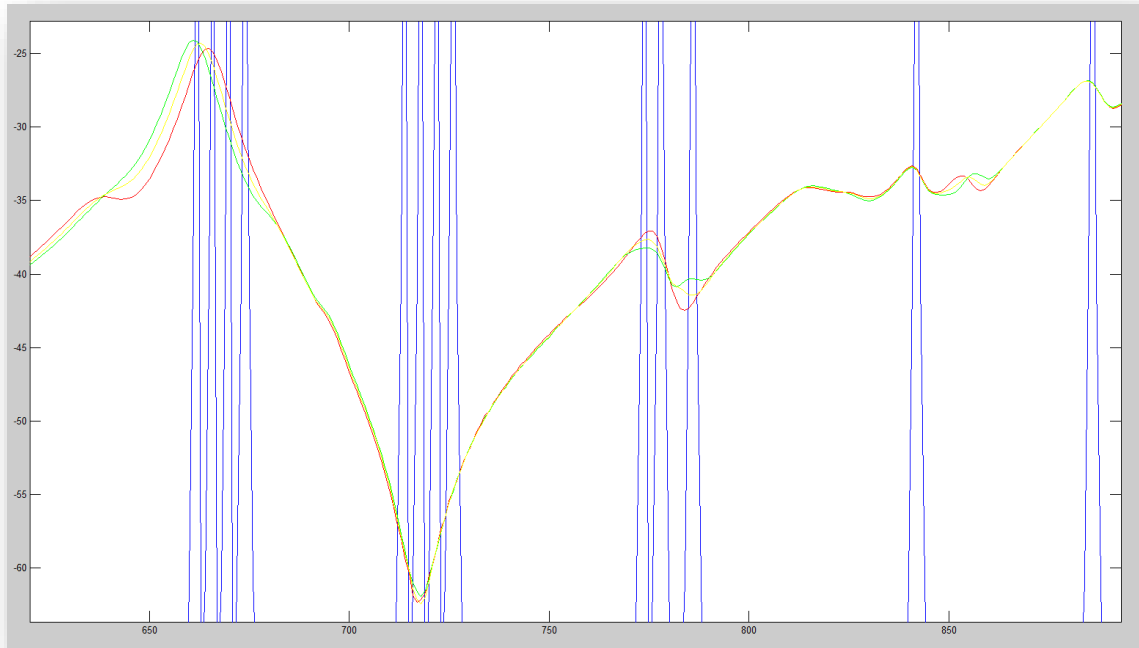
Figure 4.8 - Filter addressing alignment trace, normalised to the axis of a zoomed fault simulation open circuit 'A phase' SFRA test results (*Settings -> 'inc'=4, 'Delta'=10*).

The second refinement stage involved applying global window constraints (samples 600 - 900) to the fault magnitude plot data, followed by further refining of the filter placement variables. Figure 4.8 above is an example of the zoomed filter alignment trace used for refining of the filter placement script variables further. Code was adapted to superimpose the filter placement plot over the top of the fault magnitude plot to facilitate easier visual alignment. Once the variables were fixed, the next stage was to create a way of using the resultant filter alignment trace to create an array that defines values along the x axis that the filters will be centred on.

The next step in creating the filter placement script was to determine the area under the new filter location plot that was generated in the previous step. Figure 6.88 of Appendix E below is the corresponding code extract that exploits MATLAB's 'trapz' function to estimate the area under the curve. The area under the curve is required to be used as a devisable 'total' by the respective number of filters (pre-set to 15) for the creation of a new variable, 'a_space' (summed area between filters).

56

Figure 6.89 of Appendix E provides a sub routine that was designed to output the array that containing values along the x axis that the filters will be centred on. This sub routine code sweeps across the 'Z1' dataset, summing each value with the previous loop iteration, stored in the variable 'Q1' until the pre-defined constraint 'a_space' is less than 'Q1'. With each inner loop, the temporary variable 'i' increases by a value of 1, where 'i' indicates the data point along the c axis of the SFRA trace that the 'Z1(i)' value is referring to. The corresponding phase-plot data-point is then stored in a pre-initialised matrix 'E1' before the inner loop finishes. Each time the inner 'for loop' is satisfied, the temporary variable 'a' takes on the 'E1(b)' value to allow the continuation of the sweep from that point. The temporary variable 'b' also increases by a value of 1 each loop as this defines the cell in 'E1' that the next data point number 'i' will be stored into.

Once the complete row vector 'E1' was attained, the code was tested by successfully processing a random selection of 20 of the Australian power utility supplied SFRA earthing transformer datasets. No anomalies or errors were found from the testing process.

The next step was to create a function that can generate hamming filter windows, wrapped to various x axis scales as introduced in section 2.4.1.3 above. The function utilised to create the continuous filter windows has been defined in Equation 4.2 below and was named 'hummfbank.m' for MATLAB scrip execution.

Equation 4.2 – The hamming window function [26]

$$H_1[n] = \begin{cases} 0.54 - 0.46\cos\left(\dfrac{2\pi n}{L}\right) & 0 \leq n \leq L - 1 \\ 0 & otherwise \end{cases} \tag{4.2}$$

$$Where: \ H_1 \ is \ an \ \text{arbitrary} \ variable \ for \ storing \ the \ filter \ bank \ Matrix$$
$$L \ is \ the \ number \ of \ samples \ per \ hamming \ window$$

The filters created using the Equation 4.2 were then wrapped to a Mel-scale axis and then subsequently a linear scale axis to prove that the function was working correctly. Figure 6.90 of Appendix E below is a plot of the resultant Mel-scale filter bank, consisting of 15 Hamming filters spaced with unit area normalisation. The applied function required normalisation of the filter unit area because it ensures that the data captured reflects an even sampling method and is more sensitive to data around an area of concentrated filter placement. For this test iteration of the hamming function code, all filters were found to be spaced correctly.

Figure 6.91 of Appendix E below provides a sample of the test iteration for linear scale wrapping of the hamming window function. In this case, the filter bank consisted of 15 hamming filters spaced evenly between window constraints of data points 500 to 750 along the x axis. Once again, a variety of different parameters were tested to ensure that the code was stable for the application and adaptation purposes.

Parameter testing confirmed that the maximum number of filters that can be used is 30 before the script provides an error message. The filter limitation is because of the initialisation method used for some variables within the code. Background presented in section 2.4 above supported the decision to initialise variables for a maximum of 30 filters to avoid results distortion.

The filter placement script was then adapted to enable the values of row vector 'E1' to define each filter centre points along the x axis. Figure 4.9 below is a comparative plot of a sample SFRA magnitude trace along with the corresponding filter bank that resulted from processing the samples phase trace data using the filter placement scripts. In this case, the clusters of hamming filters align well with the SFRA magnitude trace resonance points of known fault deviation. A larger sample plot of a resonant point focused, windowed filter bank has been included in Appendix E as Figure 6.92 below.
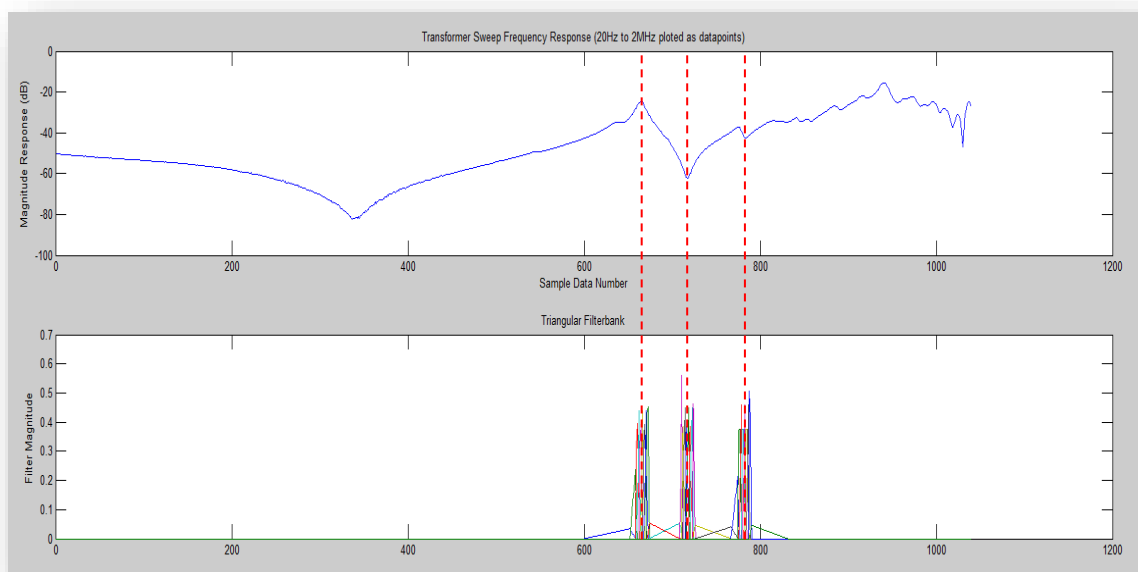
Figure 4.9 – Comparative plot of a sample SFRA magnitude trace along with the resulting filter bank from processing of the SFRA phase trace data using the filter placement script discussed above. The Filter bank includes 30 filters, all normalised with the same unit area.

A random sample of 20 SFRA trace results from The Australian power utility's earthing transformer dataset were processed in the same way as Figure 4.9. Each output filter bank was compared with the equivalent SFRA magnitude trace as a qualitative matrix for success, concluding that the filter placement script worked well for filter alignment with resonant peaks.

58

Application of the filter placement script required a simple multiplication between each point of each filter and the inverse-log, SFRA magnitude spectrum data as seen in Equation 4.3 below.

Equation 4.3 – Equation used to apply the filter bank H1 to the inverse Log spectrum data

$$Filtered\ log\ spectrum\ data\ H_2 = [H_1] .* [X_{mag}]$$

(4.3)

$Where$: H_2 $is\ an$ arbitrary $variable\ for\ storing\ the\ filtered\ spectrum\ data$
H_1 $is\ the\ output\ matrix\ from\ the\ 'hammfbank.m'\ function\ defined\ above$
$X_{InvLogMag}$ $is\ the\ matrix\ of\ inverse\ Log\ spectrum\ dat$a from section 4.2.3 above

4.2.5   Logarithm Function

The next step of the development process was to code in the re-application of the logarithm function to the filtered spectrum data. MATLAB's 'LOG' function was used to perform the task as per Equation 4.4 below.

Equation 4.4 – Mathematical expression for the operation used to re-apply a logarithm function.

$$Log\ filtred\ spectrum\ data\ H_3 = 20LOG(H_2)$$

$Where$: H_3 $is\ an$ arbitrary $variable\ for\ storing\ the$ log $filtered\ spectrum\ data$
H_2 $is\ the\ filtred\ spectrum\ data\ attained\ from\ the\ previous\ subsection$

Once the logarithm function had been applied, the next step of the modified MFCC process was the convert the spectrum data into a cepstrum on a pseudo-frequency axis.

4.2.6   IDCT

Conversion of the log spectrum data into cepstrum coefficients on a pseudo-frequency axis, discussed in section 2.4.1.3 was achieved by applying an Inverse Cosine transform to the data. MATLAB's 'idct' function made this operation simple, converting all log filtered spectrum values into cepstrum coefficients.

Additional coding was then applied to automatically output the test subject SFRA magnitude plot, filter bank and cepstrum coefficients in one 'figure' as seen in Figure 4.10 below. Figure 4.10 provides a snipping of the output interface resulting from running the 'filtceps' script for a random sample SFRA trace dataset with the following settings:

- SFRA test set red lead connected to the earthing transformer's 'A' phase bushing,
- SFRA test set black lead connected to the earthing transformers 'N' bushing,
- Windowing of data points 500 to 875

- 15 hamming window filters
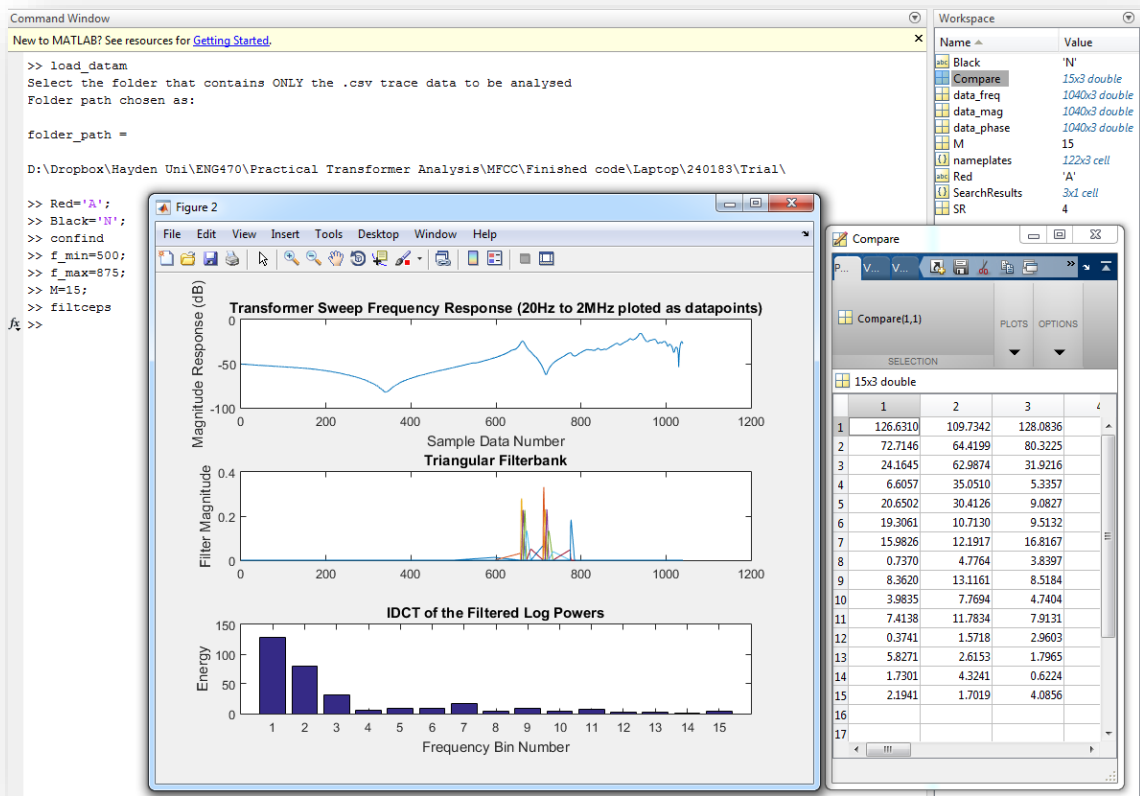
Figure 4.10 – Sample snipping of MATLAB's command window and workspace with the 'filtceps' script output figure and 'compare' matrix displayed in the foreground.

The 'compare' matrix, also seen in Figure 4.10 stores all the resultant cepstrum coefficients from the 'filtceps' script for comparative plotting purposes.

4.3   Cepstrum Coefficients

The next step of the process was to compare the resultant cepstrum coefficients from baseline and fault simulated SFRA results presented in section 3.3 above of this report. It was found that the magnitude of the cepstrum coefficients for the 45% and 90% axial windings displacement fault cases deviated in specific 'filter bins' from the baseline magnitude cepstrum coefficients.

To test the effect that changing the number of filters had on the resulting cepstrum coefficients, a series of test iterations were conducted. Test iterations spanned from 10 to 30 hamming filters (10:5:30 in 5 filter increments) contained within the filter bank with a frequency window spanning from 15.140 kHz to 240.494 kHz (data points 600 to 850).

The next phase of testing involved shifting the 'frequency window' to a lower frequency region of 5.009 kHz to 79.564 kHz (data points 500 to 750) to assess if this affected the cepstrum coefficient magnitude and addressing. Figure 3.19 of section 3.4 above, reinforced the various earthing transformer SFRA trace responses that can be expected, with the greatest deviation being along the frequency axis. Shifting the frequency window, tests to see if the same filter bank magnitudes will deviate when processing the fault simulation data.

Table 4 – 4.3   Cepstrum Coefficient tune-able code test iteration reference table

Frequency Window (data-points)	'*M*' Number of Filters	'*M*' Number of Filters	'*M*' Number of Filters	'*M*' Number of Filters	'*M*' Number of Filters
600-850 15kHz-240kHz	10	15	20	25	30
500-750 *5kHz – 79kHz*	10	15	20	25	30

For both the 15.140 kHz to 240.494 kHz window and the 15.140 kHz to 240.494 kHz window test iterations, filter bins 2 and 3 were found to consistently have the greatest deviation. The results from all of the respective test iterations outlined in Table 4 above can be found in section E.1.3 of Appendix E with an example coefficient comparison plot shown below in Figure 4.11.
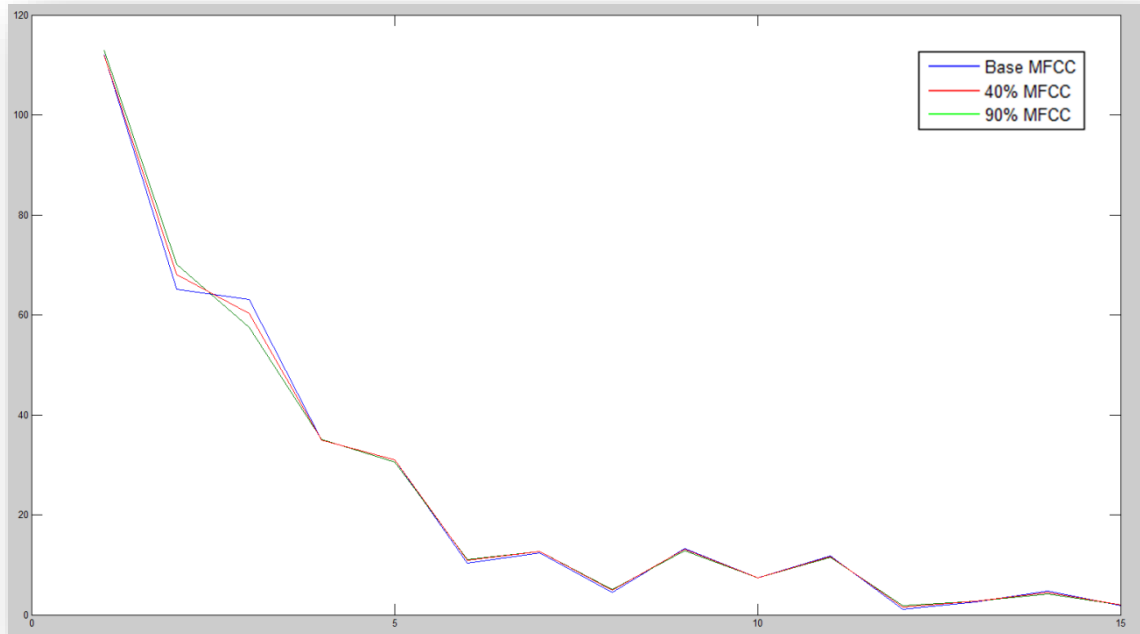
Figure 4.11 - Comparison plot of the cepstrum coefficients resulting from processing baseline, 45% and 90% fault simulation data (from section 3.2.2) using the method detailed in section 4.2 above. *Settings -> 'f_min'=500 (5.009 kHz), 'f_max'=750 (79.564 kHz), 'M'=15*

Discussions in section 2.4.1.3 introduced the concept that each subsequent cepstrum coefficient represents a higher frequency order component of the spectrum under analysis. This theory was supported by the results from iterative testing discussed in the paragraphs above. The iterative input data results from section 3.3.5 show spectral deviance of a low order oscillating frequency nature, resulting in deviation, consistently addressed to the lower number frequency bins.

The test iteration from Figure 4.11 was qualitatively found to have the consistent cepstrum coefficient deviation and quantitatively one of the largest magnitude deviation results for windows 2 and 3. For these reasons, standardization on the code's refine-able parameters were solidified for further testing as defined in Table 5 below.

Table 5 – Analysis script code refinable parameters

'*Delta*' Required difference between front and rear sweeping window	'*inc*' Sweeping phase trace window size (x axis)	'*M*' Number of filters	'*f_min – f_max*' Frequency window in terms of data points
10	4	15	500 - 750

4.4   2D Plotting Results and Discussion

Discussions from section 2.4.1.3 introduced the idea that for speech recognition, most of the useful spectral content can be found within a select number of filter bins. Cepstrum coefficient comparison results, discussed in section 4.3 above agreed with the concept that particular filter bins contain the 'important' spectral information for detecting faults.

In an effort to satisfy the "Simple output display" and "Meaningful output to assist with fault diagnosis" design criteria defined at the start of Chapter 4, 2D plotting was proposed. The proposed 2D plot was designed to incorporate only the filter bins that were the most critical for fault detection while plotting the magnitude of each on the x and y axis respectively. Filter bins 2 and 3 of the 15 cepstrum coefficients were selected as a result of justifications presented in section 4.3 above.

From this point, a script was written to automate the two-dimensional plotting of the filter bin 2 and 3 cepstrum coefficients against each other. The script code was designed to automatically plot each SFRA trace within the selected folder (with the pre-specified test set lead connection configuration). An example 2D plot of the resultant cepstrum coefficients has been provided in Figure 4.12 below. In the case of Figure 4.12, the 'A' to 'N', Baseline, 45% and 90% axial windings displacement SFRA data from section 3.3 of the report has been processed and plotted in the single point, 2D representation proposed.
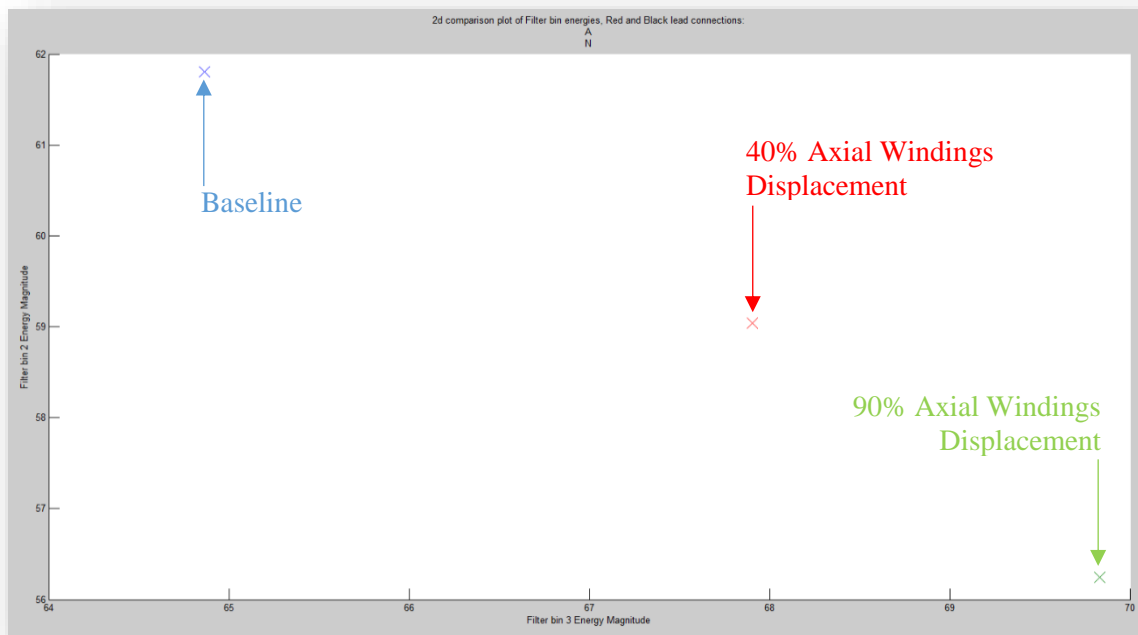
Figure 4.12 – A sample two dimensional plot of the resultant cepstrum coefficients from filter bin 2 providing a y axis value while the corresponding cepstrum coefficients from filter bin 3 in each case provides the x axis value. Cases processed using baseline, 45% and 90% SFRA data from section 3.3 above. Filter bank used to calculate each value is based on the baseline case only, using dynamic filter placement presented in section 4.2 above.

It is clear to see that each coefficient comparison point deviates substantially as a result of the simulated windings axial displacement fault. It is interesting to note that in this case, the displacement magnitude and direction appear to be somewhat proportional to the severity of the simulated fault. An index of the different comparison plots that were used as a matrix to measure success of the analysis tool can be found in Table 6 below.

Table 6 – Index for the 2D comparison plot test iterations

Test Description	Test set lead connections	Reference plot
1. Simulated SFRA fault data	A-N	Figure 6.103
2. Simulated SFRA fault data and APU full data	A-N	Figure 6.104
3. Simulated SFRA fault data	B-N	Figure 6.105
4. Simulated SFRA fault data and APU full data	B-N	Figure 6.106
5. Simulated SFRA fault data	C-N	Figure 6.107
6. Simulated SFRA fault data and APU full data	C-N	Figure 6.108
7. APU Data	A-B	Figure 6.109
8. APU Data	B-C	Figure 6.110
9. APU Data	C-A	Figure 6.111
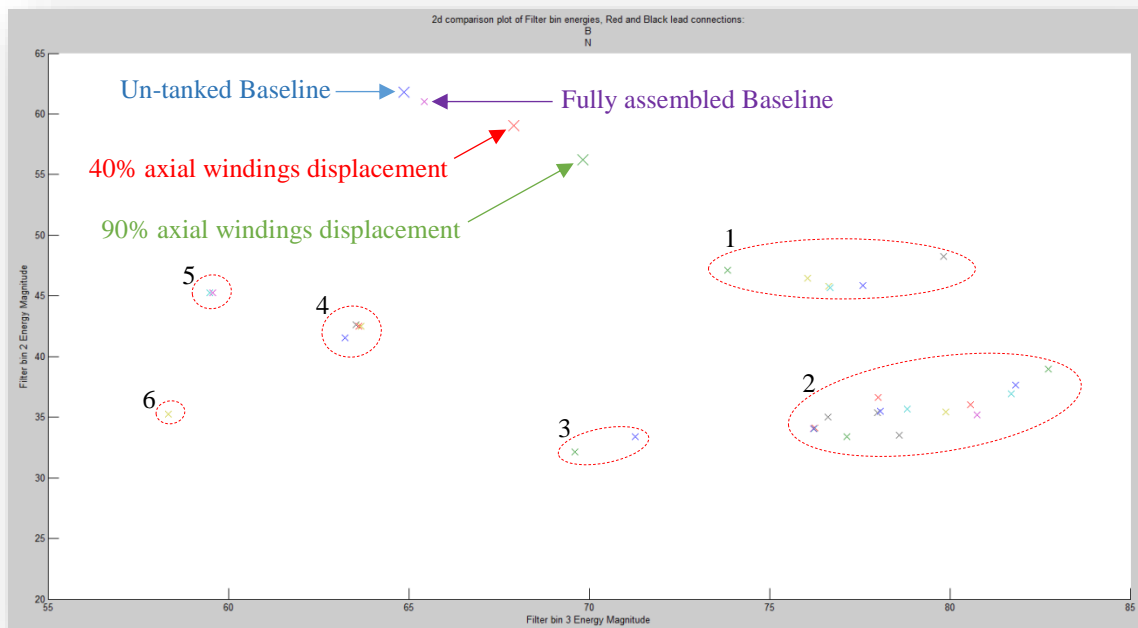
Figure 4.13 – Data points from Figure 4.12 plotted with the fully assembled test subject OC baseline and all of the available APU earthing transformer A-N phase connection SFRA trace data in the distilled, single point, filter bin 2 and 3 representation. All APU data generated using dynamic filter placement presented in section 4.2 above.

Figure 4.13 has been used to compare all of the distilled APU earthing transformer data against the test subject of this report. The purpose of this comparison is to determine if a cluster relationship exists between the transformers. It was hypothesised that if clustering existed between all distilled earthing transformer data, it may be possible to determine if a transformer is showing symptoms of a fault if the data-point were to shift away from the cluster.

It is clear to see that some clustering exists between different transformers as highlighted and numbered in Figure 2.1. Table 7 below outlines the main characteristics of each transformer within each of the numbered clusters to determine if any trends exist. The Doble SFRA 5.3 software requires the operator to populate the transformers nameplate data manually. As a result, some data entries were missing for the corresponding SFRA traces analysed.

The transformer characteristics defined in Table 7 were those described in section 2.2 above to have the greatest impact on a transformer's SFRA output trace. Once again, a lack of user defined information made current rating addressing impossible with the dataset provided. Comparison of the transformer's year of manufacture could also be advantageous for cluster identification, however, due to confidentiality requirements; specific year grouping has been omitted from this report.

It can be noted that the author observed that the transformer's year of manufacture affected the relative position of the respective data point within the cluster, although, the difference observed was far less than the clustering effects seen from manufacturer and voltage ratings. Variations in current rating could have a substantial effect of the relative single point position of each transformer. This could assist in explaining why some of the know manufacturer 'Type B' transformers of the same voltage rating are split between different clusters seen in Table 7. An example of this can be seen in a comparison between 'cluster 2' and 'cluster 3' of Figure 4.13 above.

Table 7 – Reference table for cluster data characteristics highlighted in Figure 4.13 above

Cluster Reference Number	*1*	*2*	*3*	*4*	*5*	*6*
Manufacturer	2 x Type A 4 x Type B	6 x Type A 9 x Type B	2 x Type B	5 x Type B	2 x Type B	1 x Type C
Voltage Rating	1 x 11kV 3 x 22kV 2 x unknown	10 x 22kV 5 x Unknown	2 x 22kV	2 x 11kV 3 x Unknown	2 x Unknown	1 x 22kV

It is interesting to note that the test subject's atypical SFRA response, seen in Figure 3.19 of section 3.4 above, has been carried through to the distilled coefficient data point seen in Figure 4.13. This is an important characteristic as it proves (for the test subject) that even characteristic spectral differences (between compared earthing transformers) have been retained throughout the data distillation process.

Fortunately, earthing transformers used in distribution systems are often larger in both rating and physical size, proven from APUs sample data. Consequently, it is very likely that the concepts and results discussed throughout this report could become characteristically more prominent for larger transformers.

Results from comparisons, analysing the A-N connections only, were deemed adequate for explanation of the underlying relationships between the data. Results attained from the other test set connections listed in Table 6 have been included in Appendix E for interested readers.

Chapter 5   Conclusion

Throughout this report, the importance of earthing transformers for the power and distribution industry has been highlighted. The basic concepts of SFRA testing have been outlined and presented as being fundamentally important to conditional monitoring of Zn wound earthing transformers.

The type of fault that a Zn wound earthing transformers is most susceptible to was found to be an axial displacement between the inner and outer windings. Practical simulation of an axial windings displacement fault proved that (for the test subject), it was possible to detect and isolate changes in the transformers SFRA spectrum as a result. The resultant changes were presented in full for all test iterations to aid with communal understanding of a Zn wound earthing transformers SFRA characteristics.

A tool was developed with the intention of assisting the user to decide if an earthing transformer needs to be serviced, refurbished or replaced. Preliminary tests of the tool proved that positive fault identification was possible for the test subject. An adapted feature extraction technique, common to human speech recognition and known as MFCC, formed the foundation for the assistive decision making tool. Adaptions were based on fault simulation results to make the process sensitive to fault identification.

Script created for the assistive decision making tool automatically managed the imported data from a familiar browser interface. The corresponding interface script allowed the entry of as many SFRA .csv datasets as desired. User input requirements were minimised to simplify the process and reduce the analysis application time. Each step of the code development process isolated variables that could be used to refine the respective computational iteration for future adaptations. The resultant output, per transformer, was shown to be a single point on a two-dimensional plot, encapsulating the important spectral information to fault identification.

The simple, single point representation of the transformers spectral shape showed notable deviation as a result of fault simulation comparisons. Notable deviation confirmed that the simple output provided a meaningful representation of trace data for fault identification analysis.

Providing power utilities with the ability to confidently detect developing faults, prior to catastrophic failure of an earthing transformer and subsequently the primary power transformer holds great value. Value can be seen not only in monetary form but also in grid stability and improved safety. Although future testing and development is required, the main project goal to highlight the value of monitoring and maintenance strategies for earthing transformers has been achieved.

Chapter 6   Future Work

The results attained throughout this project were based on a select Zn wound earthing transformer and as such, further analysis would be required. A future project goal could be to develop a large sample of earthing transformer SFRA results for identification and analysis purposes; however, this would likely require industry cooperation.

It would be advantageous if specific Earthing transformer failure case studies were available to solidify conceptual understanding of the most common failure mode. As a future consideration, a survey of known Zn wound earthing transformer failure cases could be conducted.

Chapter 3 presented the method used during this thesis project to simulate an axial windings displacement fault on the test subject earthing transformer. Given that the testing conducted was non-destructive, it may be possible to convince suppliers to temporarily donate Zn wound earthing transformers for fault simulation analysis. Further fault simulation analysis using a common methodology would assist to further validate the results discussed throughout this report.

Adaptations to the method presented in Chapter 3 could further investigate the apparent proportional relationship between the SFRA trace and the magnitude of axial windings displacement. The author suggests conducting fault simulations with a greater number of test iterations.

From a data analysis standpoint, it would be well worth investigating the performance of another feature extraction method such as LPC (presented in Appendix B below) against the adapted MFCC process. Implementation of the LPC was found to be more difficult than MFCC, however, for speech recognition LPC has been found to be one of the most powerful feature extraction techniques [29].

Optimisation of select variables for the given test subjects SFRA fault deviation results were used when creating the assistive analysis tool presented in Chapter 4 above. Given a sample of different transformers having faults simulated in a similar manor, as suggested in the paragraphs above, variables could require refinement to make the tool more versatile and robust.

Another possible area for future work would be to develop a spectral filter to remove the high frequency component of an SFRA trace where unavoidable noise is present. The feature extraction process could be utilised to separate the respective high frequency components in the persuado-frequency domain. This would serve to make the assistive analysis tool discussed in Chapter 4 more robust for high distortion applications where unavoidable interference is prevalent.

The analysis of a greater sample of earthing transformer SFRA trace results could aid to develop a classifier by transformer manufacturer and rating for type based comparisons. The single point representation of each transformer makes cluster identification easy when mapped on the same plot; however, a greater number of samples are required to solidify the validity of this type of analysis. As an extension, it may be possible to develop a repository of reference transformer fault cases for automated identification purposes. Such a system could be based on pre-existing 'phone' identification systems, typically used for automated speech processing [28].

The concept of transformer clarification could potentially be opened to use on all transformer types through further research, testing and development. The tool presented in Chapter 4 was specifically designed for assistive fault detection in Zn Earthing transformers. An adapted assistive decision making tool could theoretically, make fault detection in any type of transformer achievable. The author suggests that the best approach for this would likely be software that has customised variables for each type of transformer that is under analysis.

Limitations of sister transformer comparisons by direct spectrum analysis as discussed in section 2.2.2.2 above could become less subjective and prone to miss-diagnosis with a larger data sample. Clustering of transformer by type in a single point representation as seen in section 4.4 above provides comparisons with tolerance to manufacturer inconsistencies. For this reason, further research is the area of clustering analysis is required to prove if this type of comparison can be used for real world decision making.

Appendix A   Other Researched Transformer Failure Modes

A.1   Core Defects

For earthing transformers, Core defects are seldom an issue given correct design and manufacturing process. IEEE's standard C57.149, section 6.5.3 outlines most common core defects seen in oil filled transformers.

A.2   Contact resistance

Contact resistance failure within a transformer is an inherent issue with poor manufacturing process and quality control. Although SFRA is also capable of detecting faults of this variety, live transformer infrared heat camera tests and windings resistance tests are more often used for diagnosis. The effect of high contact resistance on a transformers SFRA is specifically presented in Ryder's 2003 conference paper for a multitude of different resistance test iterations [9]. Ryder's results support and extrapolate theory presented in section 2.2 of this report suggesting that a large enough resistance will shift the SFRA to a larger magnitude basis. For this reason, contact resistance faults will not be investigated further for earthing transformers in this report.

A.3   Winding Turn-to-Turn Short Circuit

Due to the robust nature of the windings construction as discussed above in section 2.3.1.1, turn to turn short circuit failures were found to be rare amongst earthing transformers. The voltage potential across an earthing transformers windings' is seldom greater than the transformers basic impulse level (BIL) rating resulting in relatively unstressed insulation.

A.4   Open Circuited Winding

Other tests such as transformer ratio and windings resistance tests are more commonly used to detect open circuit windings faults. Given limited background information on the trace data supplied, typical open circuit windings responses as detailed in section 6.5.7 of IEEE's Standard C57.14, were used for data analytics in the sections below.

A.5   Winding Looseness due to Transportation

As with many smaller transformers, earthing transformers seldom suffer from windings looseness as a result of transportation. The respective windings and interconnection leads do not weigh much resulting in strong support, bracing and clamping insulation that seldom moves from transport. Once again, the lack of inter-winding layer oil ports allows for simple robust construction.

A.6   Residual Magnetization

Residual magnetism affects SFRA trace results as displayed graphically in section 6.5.9 of IEEE's Standard C57.14, however, is not a 'failure mode' for earthing transformers.

A.7   Floating Shield

Earthing transformers do not require an inter-winding shield given by design; they have only a single winding per phase wound on multiple legs of the transformer core.

Appendix B Other Researched Feature Extraction Techniques

B.1   Linear predictive coding analysis (LPC)

Linear predictive coding analysis (LPC) relies on a large database of predictor coefficients for accurate speech analysis. LPC utilises a linear combination of known samples to approximate an unknown speech sample. LPC aims to minimise the sum of the square error between the approximated model and the unidentified speech sample. The predictor coefficients are often Cepstrum values of the original known sample to minimise variation predominantly due to pitch and gain [28].

B.2   Perceptual linear predictive coefficients (PLP)

Perceptual linear predictive coefficients (PLP) is a short-term spectrum feature extraction technique that exploits the psychophysics of human sound perception. Mathematical transforms based on three psychophysics of hearing (Critical-band spectral resolution, equal-loudness curve and the Intensity-loudness power law [35]) are used to approximate a model of the speech signal. The spectrum is wrapped to a 'Bark scale' using an 'all-pole' model to smooth the power spectrum [28]. Although PLP is a well proven technique, its psychophysics dependency and above average implementation complexity makes it difficult to adapt for different applications.

B.3   Linear-frequency cepstral coefficients (LFCC)

As the name suggests, Linear-frequency cepstral coefficients (LFCC) is a feature extraction technique that only deviates from MFCC at the stage of filter wrapping. Rather than plotting the Hamming window filter bank on a Mel-scale axis, the filters are spaced evenly from 133Hz through to 6857Hz along the spectrum. Typically, 40 filters are used with a pre-defined bandwidth of 164Hz. The main advantage of using LFCC over MFCC is its simplicity yielding a slightly faster computational output, however for speech processing, the result is less accurate.

Appendix C Earthing Transformer Test Subject for Fault Simulation

Appendix A contains the transformer specifications along with some photos and test results, prior to modification of the transformer for SFRA fault simulation testing.

C.1   Transformer specifications

Silvergate Holdings Pty Ltd AFT The Power Equipment Unit Trust T/as

EXCESS POWER EQUIPMENT

Refurbished Transformer Data Sheet

Make: Cho-Il		*Serial No:*	240183
KVA/MVA: Earthing		*Year:*	2004
Prim Volts 1: 11000		*Prim Volts 2:*	
Prim Amps 1: 75A, 10 SEC		*Prim Amps 2:*	
Sec Volts 1:		*Sec Volts 2:*	
Sec Amps 1:		*Sec Amps 2:*	
Impedence:		*Imp 2nd:*	
Vector: ZN		*Tap Change:*	
Temp Rise: 55		*Max Winding Temp:*	
Mounting: Ground		*Cooling:*	ONAN
Connections HV:		*Connections LV:*	
Weight: 600		*Oil Qty:*	166L
Size - H: 1010		*Tag Number:*	1622
Size - W: 1150		*EPE Sector:*	21
Size - L: 1110			

Data Sheet Notes: 75A, 10 SEC
NEEDS NER TO WORK WITH IT

*This transformer is sold under **EPE's** Terms and Conditions, being fully refurbished, repainted and warranted for 12 months.*

Figure 6.1 – Datasheet for an EPE stock Zig-Zag wound earthing transformer donated for destructive testing purposes.
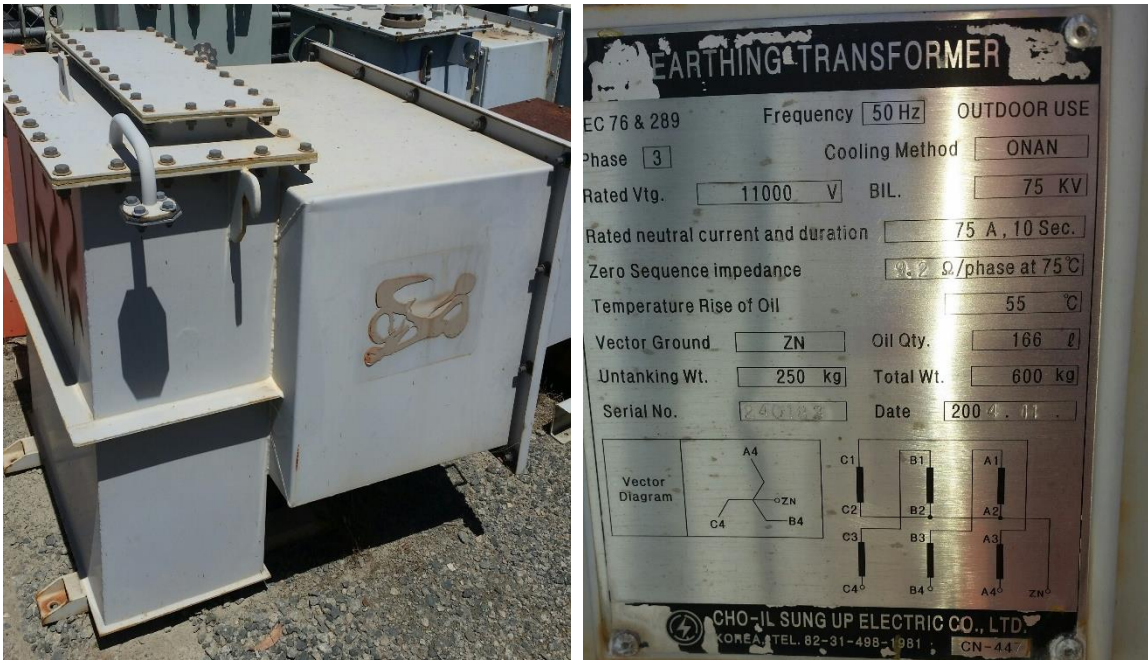
Figure 6.2 – Photos of an EPE stock Zig-Zag wound earthing transformer donated for destructive testing purposes. External transformer (Left) Transformer Nameplate (Right).

C.2   Condition Assessment Method

C.2.1   Oil dielectric test

An oil sample was taken from the bottom of the transformer tank for the purpose of testing its dielectric strength. The test equipment used was a Foster Megger, OTS/60SX with a 2.5mm electrode gap, testing at up to 60kV. 6 tests were taken with a minimum 5-minute break between tests while a magnetic stirrer circulated the oil sample after each test for approximately 30 seconds. The results from all 6 tests were averaged as per the requirements of AS 1767.2.1-1999 Section 10 [36].

Testing of the dielectric strength of the insulating fluid within the transformer was used to indicate if the transformer oil had any foreign contaminants present. Foreign contaminants in the oil such as water or small semi-conductive particles can contribute to the internal flash-over of a transformer winding during or upon energisation. This test was performed to ensure the integrity of the insulating fluid within the transformer prior to SFRA testing.

C.2.2   Dissolved gas analysis (DGA) test

An Oil sample from the bottom of the transformer tank was also taken for the purpose of testing for dissolved fault gasses within the oil. A GE Energy Kelman Transport X was used to analyse the sample. The sample was tested for Hydrogen, Carbon Monoxide, Carbon Dioxide, Methane, Acetylene, Ethane, Ethylene and Water content.

Testing of the insulating fluid using a DGA provided an indication of the transformer's health. The DGA results were used to concurrently confirm that no fault had previously occurred within the transformer.

C.2.3   Insulation resistance test

An insulation resistance test of the fully assembled transformer was conducted using a Fluke 1550B by injecting HVDC with the connections and potentials detailed in Table 6.1 below.

Table 6.1 – Insulation resistance test lead connections

Positive Lead (Red)	High Voltage Neutral bushing
Negative Lead (Black)	Transformer Tank (Ground)
Voltage potential	2.5kV DC

Insulation resistance testing was conducted to ensure that the electrical components of the transformer were insulated adequately from the transformers tank at ground potential. Separation of the phase and ground potential components was important to ensure that conclusive and repeatable SFRA test results could be achieved.

C.2.4 Windings Resistance test

A windings resistance test was conducted using a Sivananda, TWRM10A with the test set connections and settings seen in Table 6.2 below. The test subject was left for 24 hours with a shorting lead connected to all the transformers bushing terminals to the tank earth following the windings resistance test.

Table 6.2 – Windings resistance test lead connections and settings

Connection	A-N	B-N	C-N
Injected current	5A	5A	5A

A windings resistance test was conducted on the Earthing transformer to ensure the following:

- All windings had the same number of turns
- No resistive connections were present
- Interconnecting wires were evenly measured and solidly connected
- No short-circuited turns existed
- No open-circuited turns existed
- No resistive connections were present

The Transformers terminals were shorted to earth following the windings resistance test to demagnetise the transformers core, prior to SFRA testing as is recommended by CIGRE's technical brochure 342, section 3.4.7 [15].

C.3   Condition Assessment Test Results

Silvergate Holdings Pty Ltd ATF The Power Equipment Unit Trust (ABN: 42 649 906 559) Trading as

Excess Power Equipment

Office: +61 8 9493 3077
Fax: +61 8 9493 2336
Address: 27-29 Mandarin Road, Maddington WA 6109

Email: info@epe.com.au
Website: www.epe.com.au
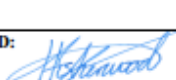
Transformer Test Certificate and Refurbish Procedure

Job No.   **Client:**   **Contact:**

NAME PLATE DATA			
Manufacturer	Cho-Il Sung	Stock No	-
Year Made	2011	Cooling	ONAN
Serial No.	240184	HV Connections	Cable Box
KVA Rating	300A @ 10 Sec	LV Connections	N/A
Vector Group	ZN	Total Weight	590kg
Impedance %	12.1Ω/Phase @ 75°C	Oil QTY	175L
High Voltage	3300	Height (mm)	
Low Voltage		Width (mm)	
Mounting	Ground	Length (mm)	

PROCEDURE (WHERE APPLICABLE)			
No.	Item	Criteria	Result
1	Oil Sample for PCB Test	None Detectable	N/A
2	Ratio Test	+/- 0.5 % x HV	N/A
3	Insulation Res. Test	Min.300M Ω @ 20°C	OK
4	Induced Overvoltage Withstand Test	AS 2374 pt3 cl 12. (450Hz @ 760v for min 15s)	N/A
5	Oil Dielectric Test	Method AS 1767 App.C (Average of 6 tests)	OK
6	Oil Drain Valve	Leak Proof / Stop Plug Fitted	OK
7	Remove Core	Inspection / Clean / Oven Dry	N/A
8	Tank Lid & Inspection Cover Gaskets	Inspect / Replace / Tighten	OK
9	Bushings / Gaskets	Inspect / Clean / Replace	OK
10	Cable Boxes / Fittings / Extension Bars	Inspect / Clean / Repair	OK
11	Gland Plates	Inspect / Replace	OK
12	Pressure Test Tank to 5 PSI	Inspect / Repair / Retest	N/A
13	Sight Glass	Readable / Oil Tight / Oil Level	OK
14	Breathers and Vents	Inspect/Clean/Replace NOT FITTED	OK
15	Bucholz G.R. Temp. Gauge	Functional / Readable	N/A
16	Paint Finish	Primer / Topcoats	OK
17	Name Plate	Check / Replace	OK
18	Identification Labels	Voltage Warning / Company	OK
19	Tap Changer	Lock Bolt fitted and correct sequence rotation	N/A
20	Vector Check	Determined with Ratio Meter	N/A
21	Instructions Sheet	Affix or in Cable Box	OK
22	Test Certificate	Complete	OK
PROCEDURE COMPLETE	NAME: Hayden Sherwood	SIGNED:	DATE: 3.3.17

Page 1 of 2

Excess Power Equipment

Office: +61 8 9493 3077
Fax: +61 8 9493 2336
Address: 27-29 Mandarin Road, Maddington WA 6109

Email: info@epe.com.au
Website: www.epe.com.au

Transformer Test Certificate and Refurbish Procedure

Job Number: 12847   Serial Number: 240184

WINDING RESISTANCE

	Tap Position	Nominal Volts	Tested Ratio	Volts Diff.	Tap Position	Nominal Volts	Tested Ratio	Volts Diff.
R	A-N	1.5189Ω						
	B-N	1.5184Ω						
E	C-N	1.5173Ω						
	A-B	3.060Ω						
D	B-C	3.059Ω						
	C-A	3.058Ω						
W								
H								
I								
T								
E								
B								
L								
U								
E								
MAXIMUM ALLOWANCE VOLTS DIFF 0.5% x HV:				MAXIMUM ALLOWANCE VOLTS DIFF:				

OIL TESTS

Dielectric Strength	Test 1	Test 2	Test 3	Test 4	Test 5	Test 6	Average
	43.0	75.0	61.0	67.5	68.0	67.5	63.6

PCB Content:		Acidity:	
IFT:		Moisture:	

INSULATION TESTS

AMB Temp °C	HV-GND @ 2.5 KV	LV-HV @ 2.5 KV	LV-GND @ 1 KV
22	17.5GΩ	N/A	N/A
Induced O/V withstand:	@450Hz	AC Hi-Pot:	

COMMENTS

TEST COMPLETE

NAME: Hayden Sherwood	SIGNED:	DATE: 3.3.17

Transformer Database Updated ☒

Figure 6.3 – Completed transformer test certificate containing the results from windings resistance testing, Oil dielectric strength testing and Insulation resistance testing of the earthing transformer test subject, serial number-420184

TRANSFORMER DGA OIL TEST CERTIFICATE

Distribution Transformer

Job: **Customer:** **Contact:**

TX Serial #: 240183 **Date:** 03/03/2017

Method: GE Energy Kelman Transport X: 80-2621
Sampling Point: Main Tank/bottom

Gases:	Results:	Ranges of 90% typical gas concentrations for distribution transformers according to IEC60599
Hydrogen H2:	< 5	100
Carbon Dioxide CO2:	315	5000
Carbon Monoxide CO:	6	200
Ethylene C2H4:	14	50
Ethane C2H6:	28	50
Methane CH4:	5	50
Acetylene C2H2:	< 0.5	5
Water H2O:	22	
Total Dissolved Combustible Gas:	54	

Caution Gasses: None
Warning Gasses: None
Transformer Condition: Normal

Authorising Officer: Hayden Sherwood   Date: 03/03/2017

Signature:

Figure 6.4 – Completed DGA test certificate for the transformer test subject, serial number-420184

Appendix D SFRA Test Setup Configuration and Full Results

Appendix B contains photos of the transformer and test lead connections along with modifications made to the core/coils/packing insulation subdivided into test iteration sections. All of the corresponding SFRA test results have also been subdivided into test iteration topic headings below.

D.1 Fully assembled benchmark testing

D.1.1 Photos of the test connections for open circuit SFRA testing

Figure 6.5 – Open circuit SFRA test set connection

The figure above shows the red lead of the SFRA tester connected to 'A phase', the black lead connected to the Neutral bushing and the reference leads connected to the common earth.

Figure 6.6 - Open circuit SFRA test set connection

The figure above shows the red lead of the SFRA tester connected to 'B phase', the black lead connected to the Neutral bushing and the reference leads connected to the common earth.

Figure 6.7 - Open circuit SFRA test set connection

The figure above shows the red lead of the SFRA tester connected to 'C phase', the black lead connected to the Neutral bushing and the reference leads connected to the common earth.

D.1.2 SFRA phase comparison results for open circuit testing

Figure 6.8 - SFRA phase comparison results for open circuit testing – Fully assembled

The figure above shows the Green line = 'A phase', Blue Line = 'B phase', Red Line = 'C phase'

D.1.3 Photos of the test connections for short circuit SFRA testing

Figure 6.9 - Short circuit SFRA test set connection

The figure above shows the red lead of the SFRA tester connected to 'A phase', the black lead connected to the Neutral bushing and shorted to all other phase bushings. Reference leads connected to the common earth.
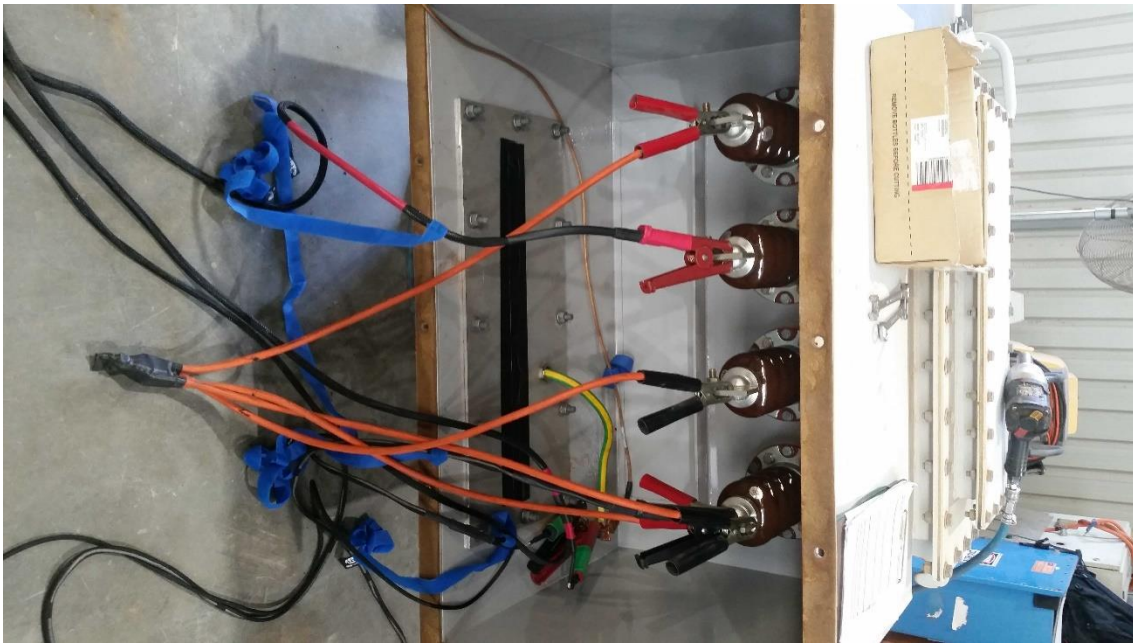
Figure 6.10 - Short circuit SFRA test set connection

The figure above shows the red lead of the SFRA tester connected to 'B phase', the black lead connected to the Neutral bushing and shorted to all other phase bushings. Reference leads connected to the common earth.
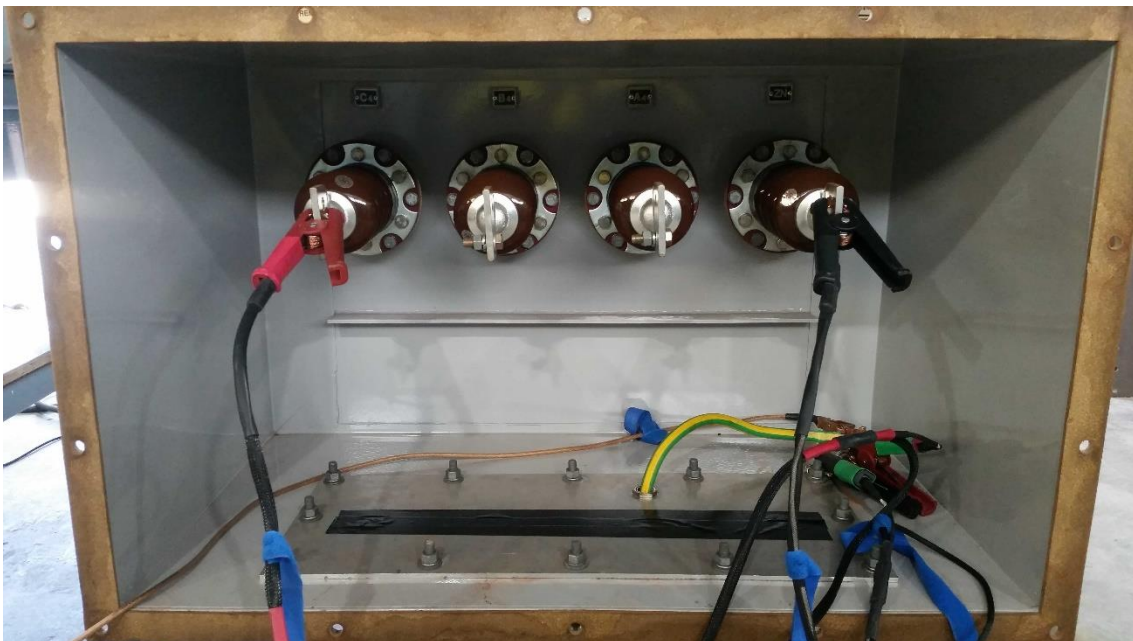

Figure 6.11 - Short circuit SFRA test set connection

The figure above shows the red lead of the SFRA tester connected to 'C phase', the black lead connected to the Neutral bushing and shorted to all other phase bushings. Reference leads connected to the common earth.

D.1.4 SFRA phase comparison results for short circuit testing

Figure 6.12 - SFRA phase comparison results for short circuit testing – Fully assembled

The figure above shows the Blue line = 'A phase', Orange Line = 'B phase', Brown Line = 'C phase'

D.2 Benchmark plotted against oil removed

D.2.1 Photos of the transformer's internals with and without oil

Figure 6.13 – Photo of the test earthing transformer internals with the lid removed and full of oil.

Figure 6.14 - Photo of the test earthing transformer internals with the lid removed and oil removed.

D.2.2 SFRA open circuit results for comparisons between fully constructed and oil removed

Figure 6.15 - SFRA comparison results for open circuit testing

The figure above shows the Green line = 'A phase' before oil removed (Benchmark fully assembled) and the Grey Line = 'A phase' after oil removed.

Figure 6.16 - SFRA comparison results for open circuit testing

The figure above shows the Green line = 'B phase' before oil removed (Benchmark fully assembled) and the Grey Line = 'B phase' after oil removed.

Figure 6.17 - SFRA comparison results for open circuit testing

The figure above shows the Green line = 'C phase' before oil removed (Benchmark fully assembled) and the Grey Line = 'C phase' after oil removed.

D.2.3   SFRA short circuit results for comparisons between fully constructed and oil removed

Figure 6.18 - SFRA comparison results for short circuit testing

The figure above shows the Green line = 'A phase' before oil removed (Benchmark fully assembled) and the Grey Line = 'A phase' after oil removed.
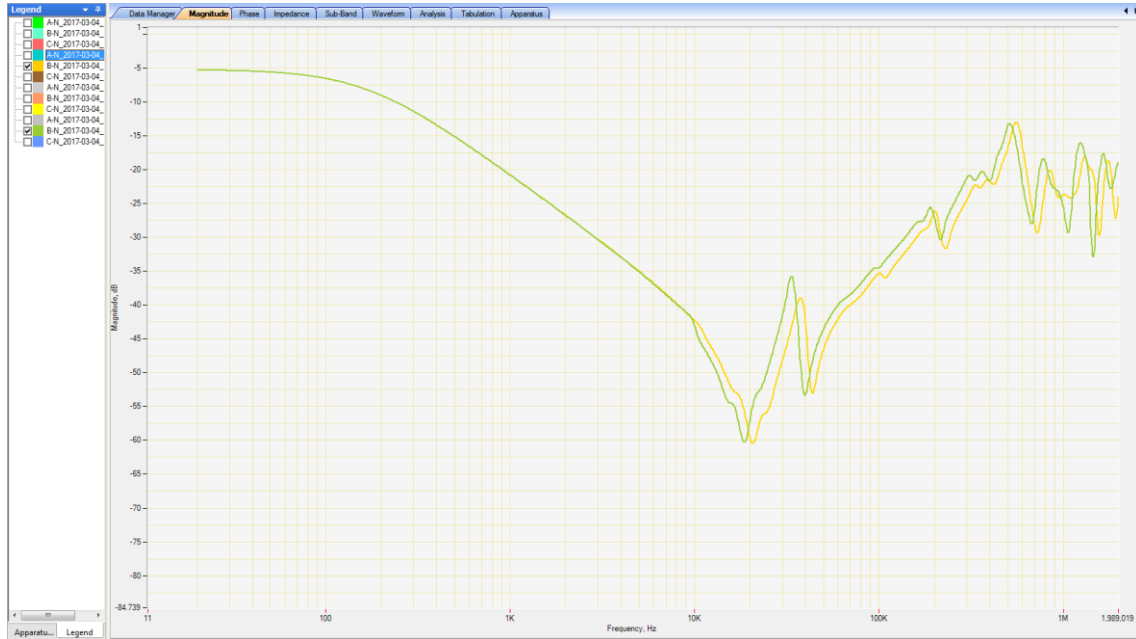
Figure 6.19 - SFRA comparison results for short circuit testing

The figure above shows the Green line = 'B phase' before oil removed (Benchmark fully assembled) and the Grey Line = 'B phase' after oil removed.

Figure 6.20 - SFRA comparison results for short circuit testing

The figure above shows Green line = 'C phase' before oil removed (Benchmark fully assembled) and the Grey Line = 'C phase' after oil removed.

D.3 Benchmark plotted against un-tanked transformer core and coil

D.3.1 Photos of the un-tanking the transformer core and coils

Figure 6.21 - Photo of the test earthing transformers core and coils being removed

Figure 6.22 – North side photo of the test earthing transformers core and coils sitting on top of two large wooden blocks in a metal oil containment tray with connection leads visible.

Figure 6.23 – South side photo of the test earthing transformers core and coils sitting on top of two large wooden blocks in a metal oil containment tray.

Figure 6.24 – West side photo of the test earthing transformers core and coils sitting on top of two large wooden blocks in a metal oil containment tray.

Figure 6.25 - East side photo of the test earthing transformers core and coils sitting on top of two large wooden blocks in a metal oil containment tray.

D.3.1.1 Photos of open circuit SFRA testing lead connections

Figure 6.26 – Un-tanked (New Benchmark) open circuit SFRA test set connection

The figure above shows the red lead of the SFRA tester connected to 'A phase', the black lead connected to the Neutral (Zn) lead and the reference leads connected to the transformers core clamping bolts.

Figure 6.27 - Un-tanked (New Benchmark) open circuit SFRA test set connection

The figure above shows the red lead of the SFRA tester connected to 'B phase', the black lead connected to the Neutral (Zn) lead and the reference leads connected to the transformers core clamping bolts.

Figure 6.28 - Un-tanked (New Benchmark) open circuit SFRA test set connection

The figure above shows the red lead of the SFRA tester connected to 'C phase', the black lead connected to the Neutral (Zn) lead and the reference leads connected to the transformers core clamping bolts.

D.3.2 Open circuit SFRA results from benchmark against un-tanked transformer core and coil comparisons

Figure 6.29 - SFRA comparison results for open circuit testing

The figure above shows the Green line = 'A phase' before oil removed (Benchmark fully assembled) and the Grey Line = 'A phase' after fully un-tanked (New Benchmark).

Figure 6.30 - SFRA comparison results for open circuit testing

The figure above shows the Blue line = 'B phase' before oil removed (Benchmark fully assembled) and the Red Line = 'B phase' after fully un-tanked (New Benchmark).

Figure 6.31 - SFRA comparison results for open circuit testing

The figure above shows Red line = 'C phase' before oil removed (Benchmark fully assembled) and the Yellow Line = 'C phase' after fully un-tanked (New Benchmark).

D.3.3   Photos of short circuit SFRA testing lead connections

Figure 6.32 – Un-tanked (New Benchmark) short circuit SFRA test set connection

The figure above shows the red lead of the SFRA tester connected to 'A phase', the black lead connected to the Neutral (Zn) lead/all other leads and the reference leads connected to the transformers core clamping bolts.

Figure 6.33 - Un-tanked (New Benchmark) short circuit SFRA test set connection

The figure above shows the red lead of the SFRA tester connected to 'B phase', the black lead connected to the Neutral (Zn) lead/all other leads and the reference leads connected to the transformers core clamping bolts.
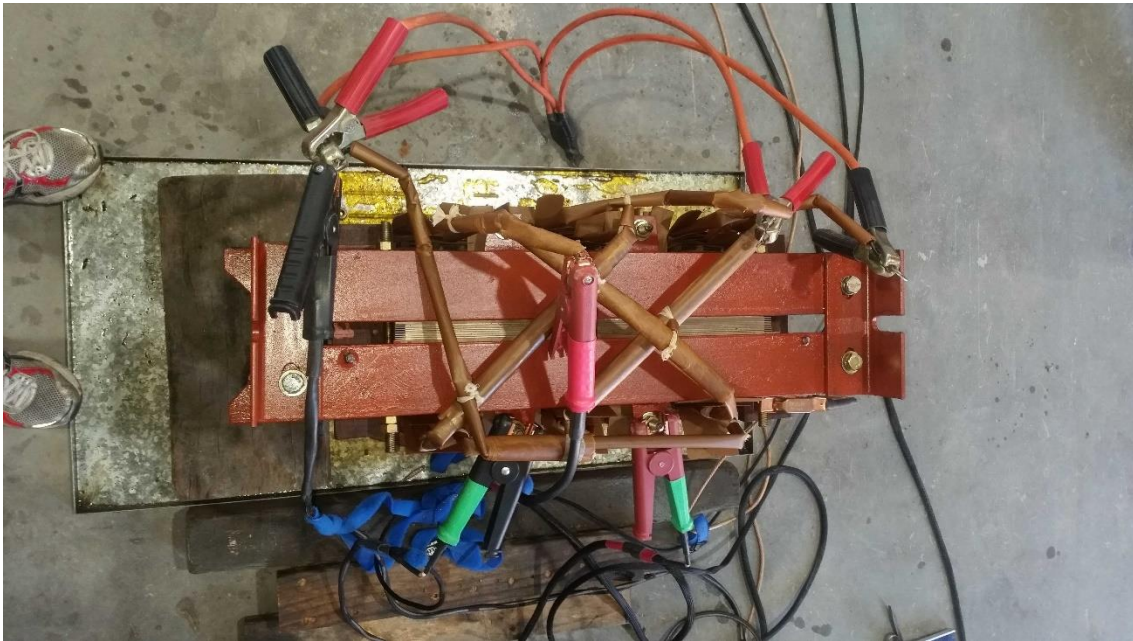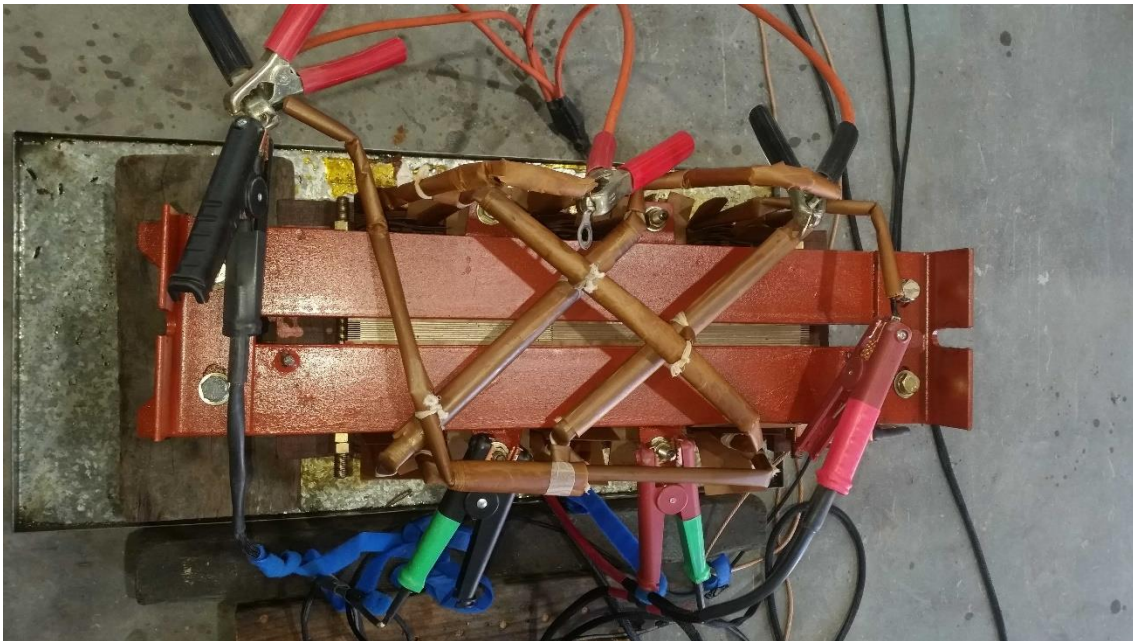

Figure 6.34 - Un-tanked (New Benchmark) short circuit SFRA test set connection

The figure above shows the red lead of the SFRA tester connected to 'C phase', the black lead connected to the Neutral (Zn) lead/all other leads and the reference leads connected to the transformers core clamping bolts.
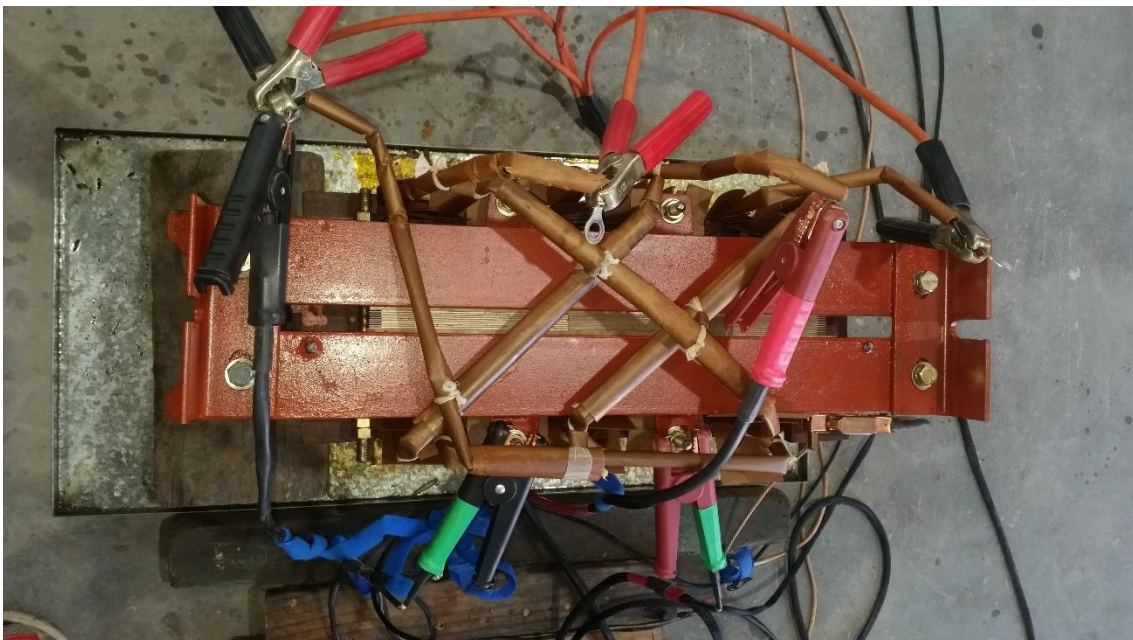
D.3.4 Short circuit SFRA results from benchmark against un-tanked transformer core and coil comparisons

Figure 6.35 - SFRA comparison results for short circuit testing

The figure above shows the Blue line = 'A phase' before oil removed (Benchmark fully assembled) and the Grey Line – 'A phase' after fully un-tanked (New Benchmark).

Figure 6.36 - SFRA comparison results for short circuit testing

The figure above shows the Orange line = 'B phase' before oil removed (Benchmark fully assembled) and the Green Line = 'B phase' after fully un-tanked (New Benchmark).

Figure 6.37 - SFRA comparison results for short circuit testing

The figure above shows the Brown line = 'C phase' before oil removed (Benchmark fully assembled) and the Blue Line = 'C phase' after fully un-tanked (New Benchmark).

D.4   Bulk windings movement

Table 6.3 – Table of the measured parameters for the transformer, prior to fault simulation – All measurements made using a Vernier calliper.

Top of winding to top of core window measurement (mm)	7.35mm
Bottom of winding to bottom of core window measurement (mm)	6.59mm
Total core window permissible windings movement (mm)	13.94mm

D.4.1 Photos of removing transformer windings supports and chocks

Figure 6.38 – Close photo of the inter-winding insulation packer prior to removal.

Figure 6.39 – Un-tanked transformer core and coils

The figure above shows arrows as indication of the procedure conducted to loosen the core clamping structure to enable the removal of packers without damage.

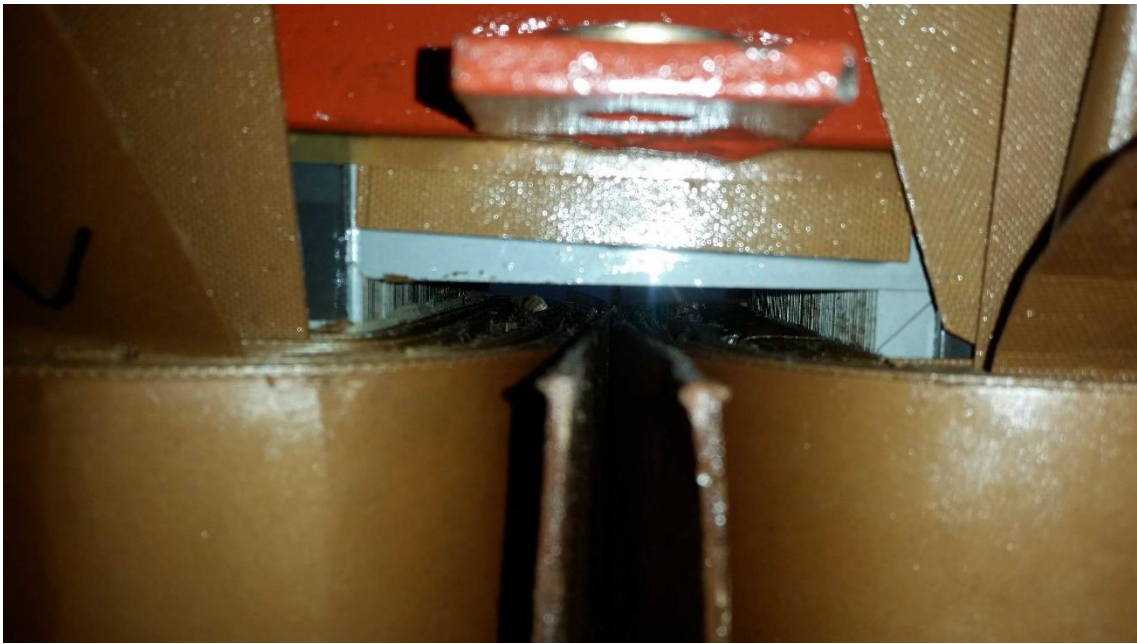Figure 6.40 - Close photo of the inter-winding insulation void after removal.

Figure 6.41 – Inter-winding insulation packer once removed, prior to modification
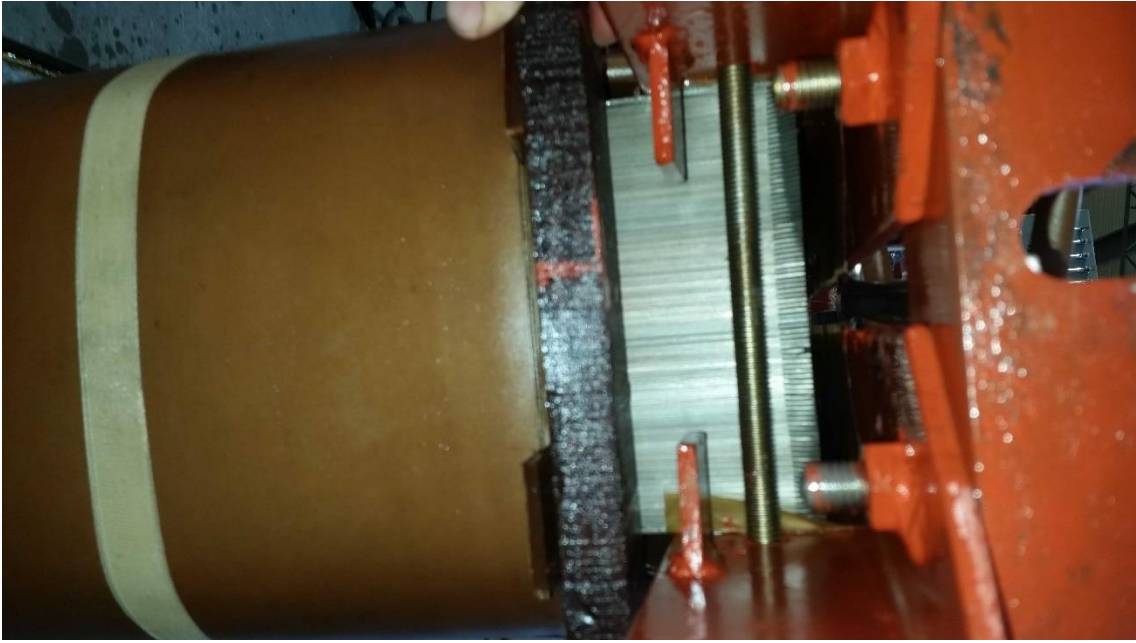
Figure 6.42 – East side windings outer coil packer prior to removal once core clamping structure loosened and shifted upwards.
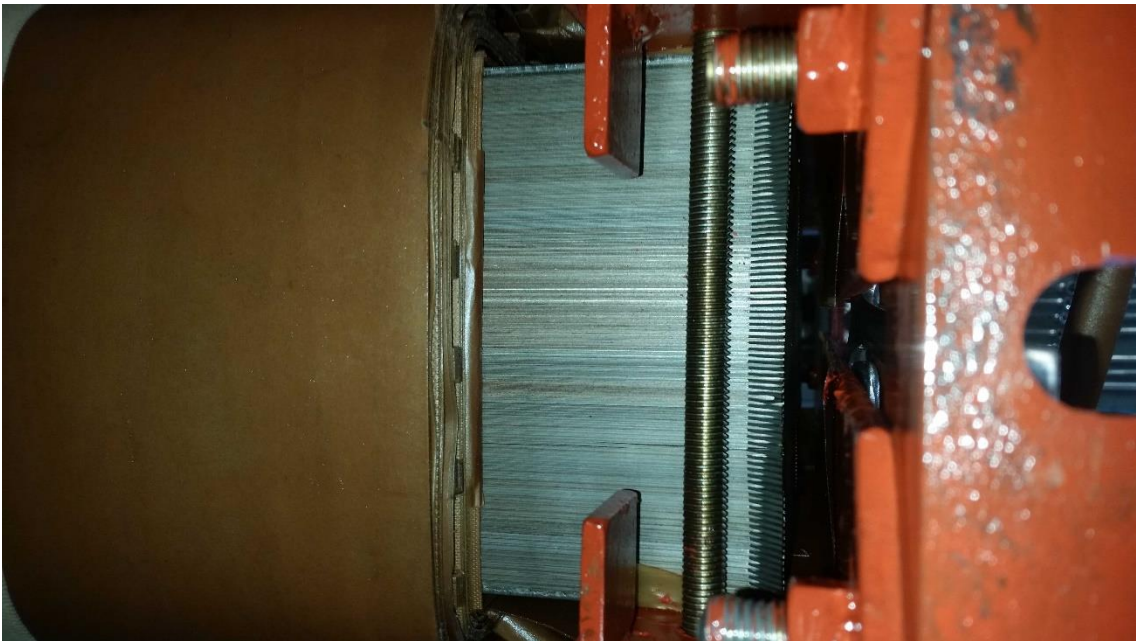
Figure 6.43 - East side windings outer coil packer void after removal. Core clamping structure loosened and shifted upwards.
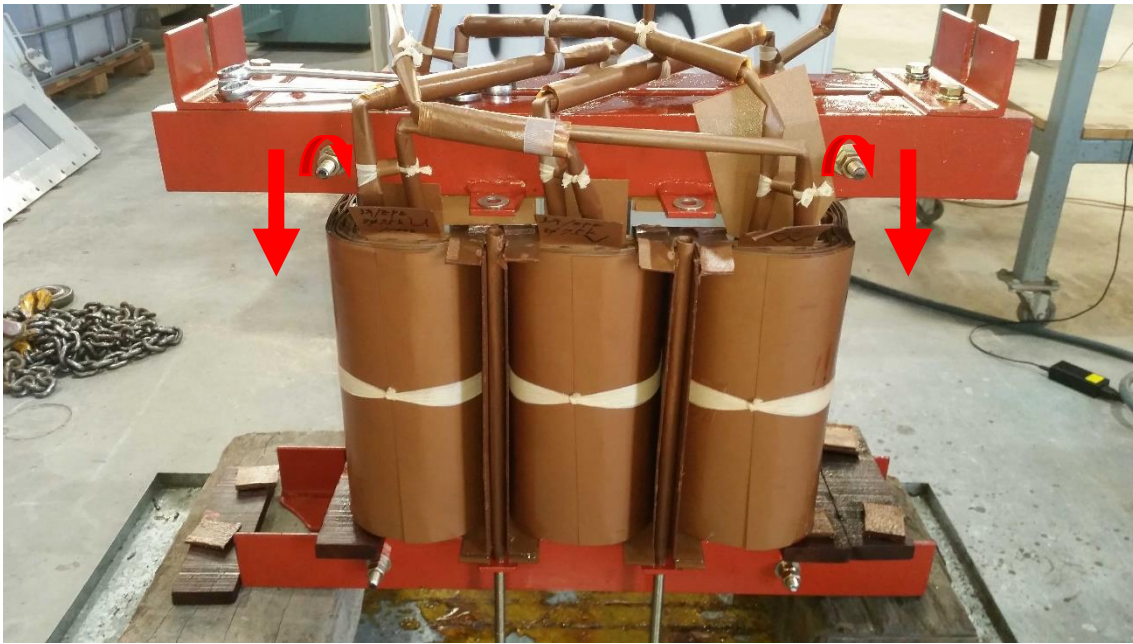
Figure 6.44 - Un-tanked transformer core and coils

The figure above shows arrows as indication of the procedure conducted to re-align core clamping structure once relevant packers removed.

D.4.2   Photos of bulk windings movement

Figure 6.45 – Close north facing view of the top outer C windings core leg (bulk windings movement) – 100% axial shift to the bottom of the core window.
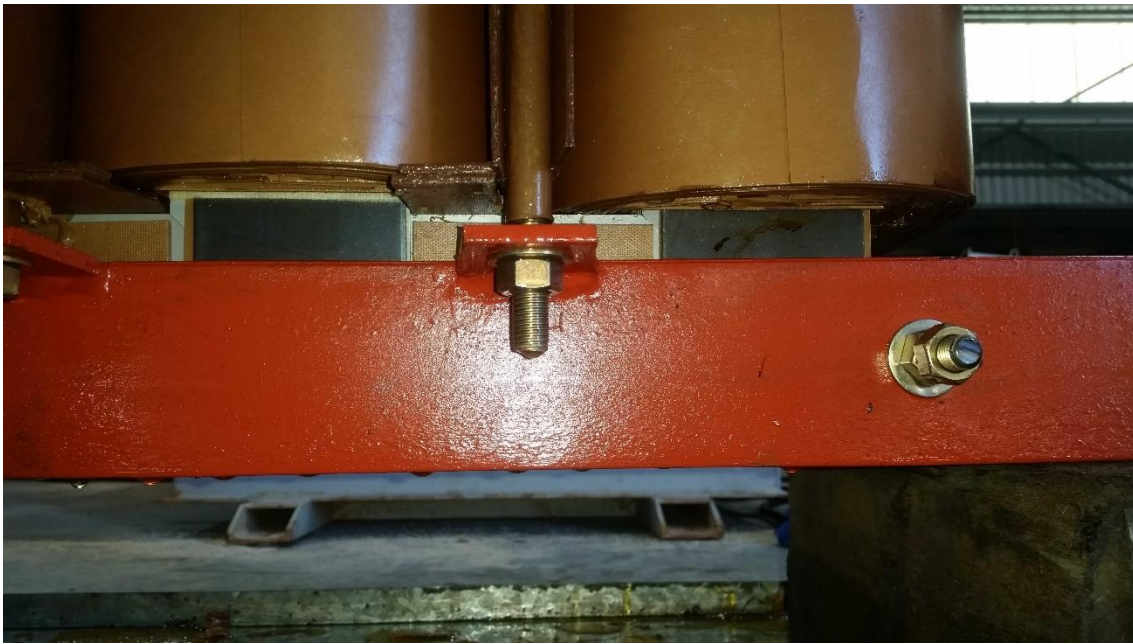
Figure 6.46 - Close north facing view of the bottom outer C windings core leg (bulk windings movement) – 100% axial shift to the bottom of the core window.
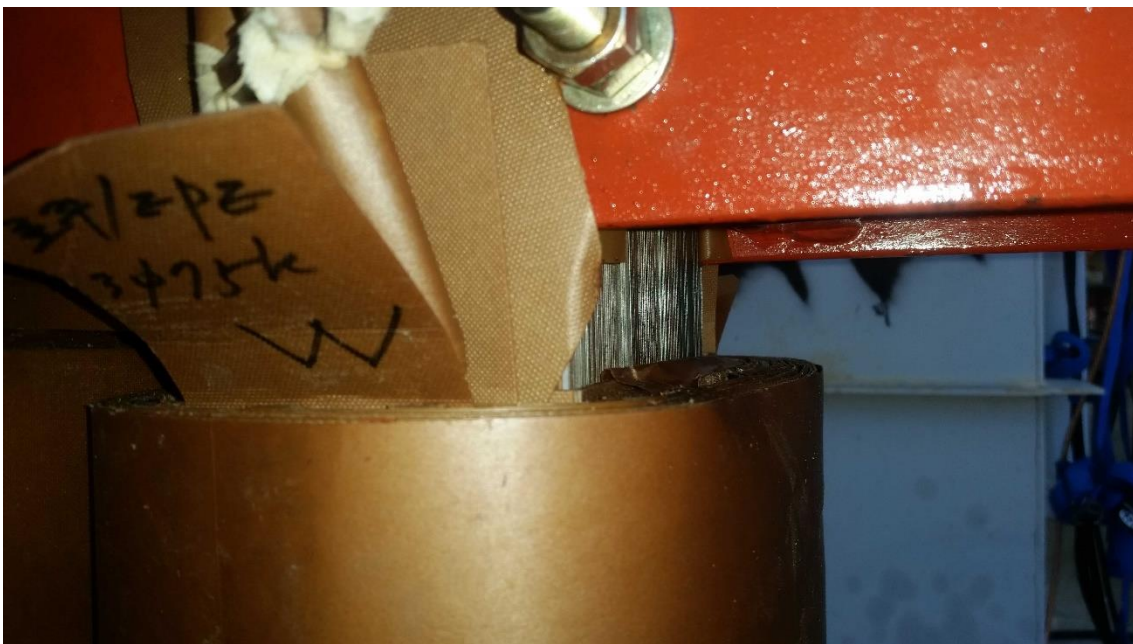
Figure 6.47 – Close north-east facing view of the top outer C windings core leg (bulk windings movement) – 100% axial shift to the bottom of the core window.

Figure 6.48 - Close north-east facing view of the bottom outer C windings core leg (bulk windings movement) – 100% axial shift to the bottom of the core window.

D.4.3 Open circuit SFRA results from bulk windings movement plotted against un-tanked benchmark

Figure 6.49 - SFRA comparison results for open circuit testing

The figure above shows the Green line = 'A phase' after fully un-tanked (New Benchmark) and the Grey Line = 'A phase' after Bulk windings movement 100% to bottom of core window (New Benchmark).

Figure 6.50 - SFRA comparison results for open circuit testing

The figure above shows the Blue line = 'B phase' after fully un-tanked (New Benchmark) and the Red Line = 'B phase' after Bulk windings movement 100% to bottom of core window (New Benchmark).

Figure 6.51 - SFRA comparison results for open circuit testing

The figure above shows the Red line = 'C phase' after fully un-tanked (New Benchmark) and the Yellow Line = 'C phase' after Bulk windings movement 100% to bottom of core window (New Benchmark).

106

D.4.4 Short circuit SFRA results from bulk windings movement plotted against un-tanked benchmark

Figure 6.52 - SFRA comparison results for short circuit testing

The figure above shows the Blue line = 'A phase' after fully un-tanked (New Benchmark) and the Grey Line = 'A phase' after Bulk windings movement 100% to bottom of core window (New Benchmark).

Figure 6.53 - SFRA comparison results for short circuit testing

The figure above shows the Orange line = 'B phase' after fully un-tanked (New Benchmark) and the Green Line = 'B phase' after Bulk windings movement 100% to bottom of core window (New Benchmark).

Figure 6.54 - SFRA comparison results for short circuit testing

The figure above shows the Brown line = 'C phase' after fully un-tanked (New Benchmark) and the Blue Line = 'C phase' after Bulk windings movement 100% to bottom of core window (New Benchmark).

D.5 Windings axial separation

D.5.1 Windings axial spacer specifications

Table 6.4 – Windings spacer measured specifications

	45% windings axial displacement	90% windings axial displacement
Length (mm)	24.13mm	24.13mm
Width (mm)	6.06mm	6.06mm
Height of outer spacer (mm)	21.27mm	27.49mm
Height of inner spacer (mm)	6.22mm	12.44mm

D.5.2   Photos of windings axial spacers

Figure 6.55 – East facing bottom view of the C windings core leg lifted to 100% top of the core window with fabricated inner windings (outer core) spacer in place for 90% bulk windings movement test

Figure 6.56 - Fabricated inner windings (inner core) spacer for 90% bulk windings movement test (Not in place as vantage point makes a photo un-recognisable)

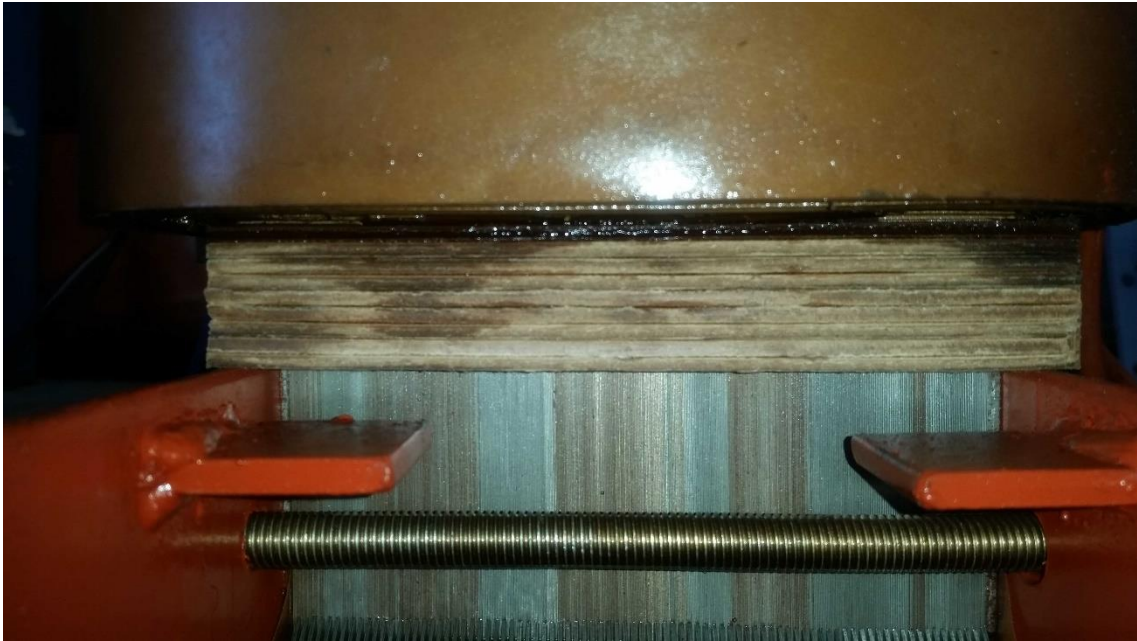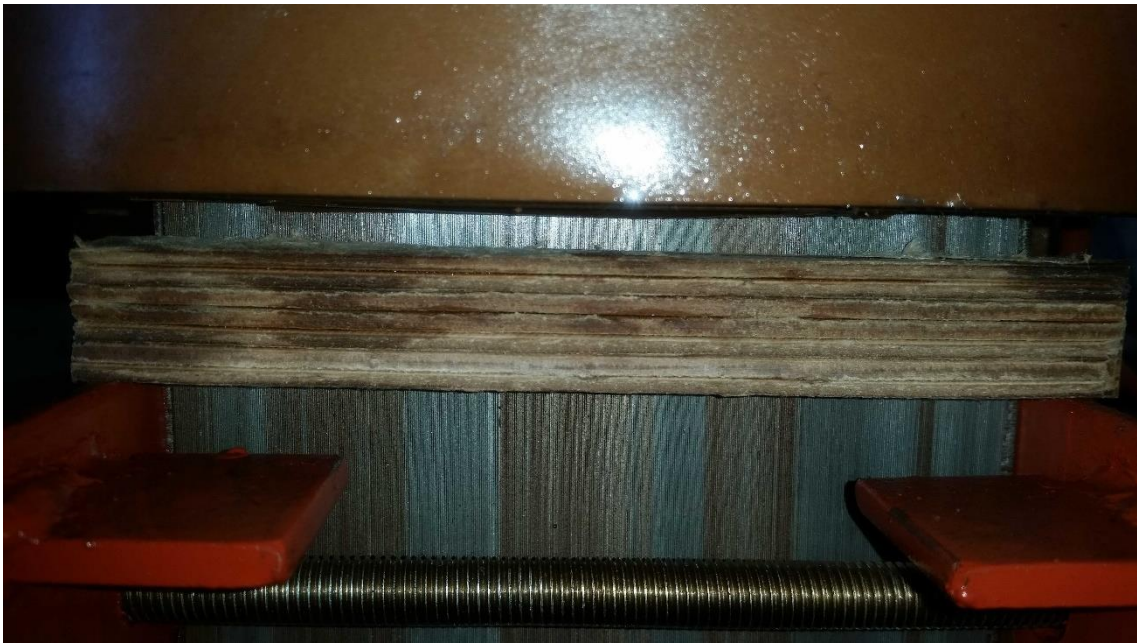Figure 6.57 - East facing bottom view of the C windings core leg lifted to 100% top of the core window with fabricated inner windings (outer core) spacer in place for 45% bulk windings movement test

Figure 6.58 - Fabricated inner windings (inner core) spacer (made by splitting 90% spacer in half) for 45% bulk windings movement test (Not in place as vantage point makes a photo un-recognisable)

D.5.3   Photos of 90% windings axial separation

Figure 6.59 – North-east top view of 90% windings axial displacement test iteration.

The figure above shows the C3 to C4 winding pushed 100% to bottom of core window and C1 to C2 winding spaced 90% towards the top of the windings window.

Figure 6.60 - North top view of 90% windings axial displacement test iteration.

The figure above shows the C3 to C4 winding pushed 100% to bottom of core window and C1 to C2 winding spaced 90% towards the top of the windings window.
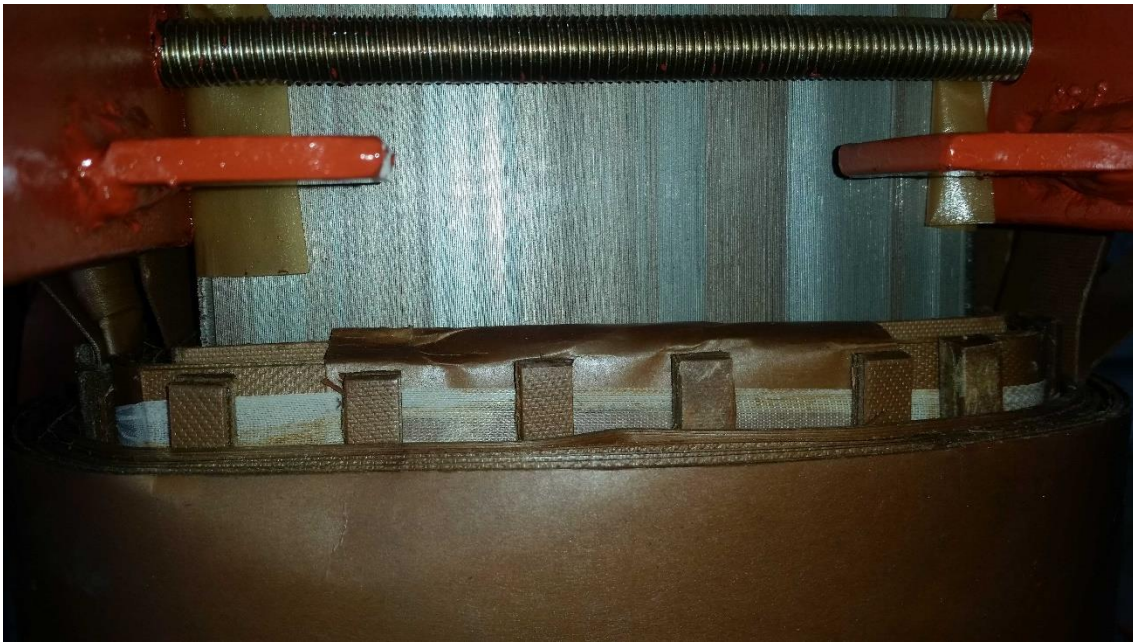
Figure 6.61 - East top view of 90% windings axial displacement test iteration.

The figure above shows the C3 to C4 winding pushed 100% to bottom of core window and C1 to C2 winding spaced 90% towards the top of the windings window.

Figure 6.62 – North bottom view of 90% windings axial displacement test iteration.

The figure above shows the C3 to C4 winding pushed 100% to bottom of core window and C1 to C2 winding spaced 90% towards the top of the windings window.
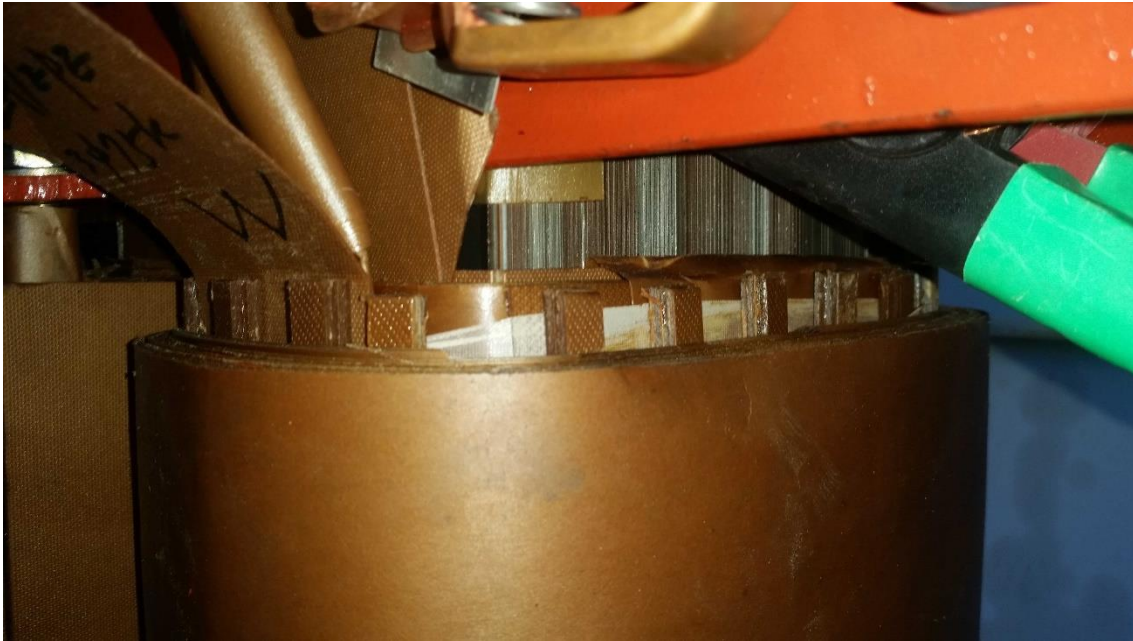
112

Figure 6.63 - East view of 90% windings axial displacement test iteration.

The figure above shows the C3 to C4 winding pushed 100% to bottom of core window and C1 to C2 winding spaced 90% towards the top of the windings window.

D.5.4   SFRA results from 90% windings axial displacement plotted against un-tanked (New benchmark)

Figure 6.64 - SFRA comparison results for open circuit testing

The figure above shows the Green line = 'A phase' after fully un-tanked (New Benchmark)and the Grey Line = 'A phase' after C3 to C4 winding pushed 100% to bottom of core window and C1 to C2 winding spaced 90% towards the top of the windings window.

Figure 6.65 - SFRA comparison results for open circuit testing

The figure above shows the Blue line = 'B phase' after fully un-tanked (New Benchmark) and the Red Line = 'B phase' after C3 to C4 winding pushed 100% to bottom of core window and C1 to C2 winding spaced 90% towards the top of the windings window.

Figure 6.66 - SFRA comparison results for open circuit testing

The figure above shows the Red line = 'C phase' after fully un-tanked (New Benchmark) and the Yellow Line = 'C phase' after C3 to C4 winding pushed 100% to bottom of core window and C1 to C2 winding spaced 90% towards the top of the windings window.
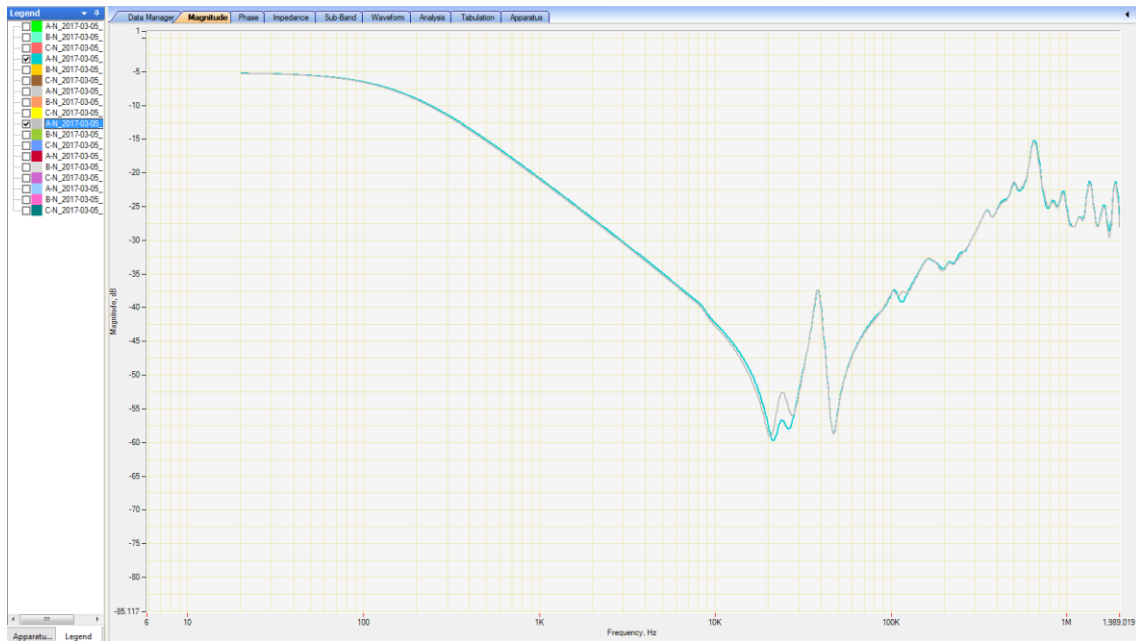
Figure 6.67 - SFRA comparison results for short circuit testing

The figure above shows the Blue line = 'A phase' after fully un-tanked (New Benchmark) and the Grey Line = 'A phase' after C3 to C4 winding pushed 100% to bottom of core window and C1 to C2 winding spaced 90% towards the top of the windings window.

Figure 6.68 - SFRA comparison results for short circuit testing

The figure above shows Orange line = 'B phase' after fully un-tanked (New Benchmark) and the Green Line = 'B phase' after C3 to C4 winding pushed 100% to bottom of core window and C1 to C2 winding spaced 90% towards the top of the windings window.

Figure 6.69 - SFRA comparison results for short circuit testing

The figure above shows the Brown line = 'C phase' after fully un-tanked (New Benchmark) and the Blue Line = 'C phase' after C3 to C4 winding pushed 100% to bottom of core window and C1 to C2 winding spaced 90% towards the top of the windings window.

D.5.5   Photos of 45% windings axial separation

Figure 6.70 - North top view of 45% windings axial displacement test iteration.

The figure above shows the C3 to C4 winding pushed 100% to bottom of core window and C1 to C2 winding spaced 45% towards the top of the windings window.
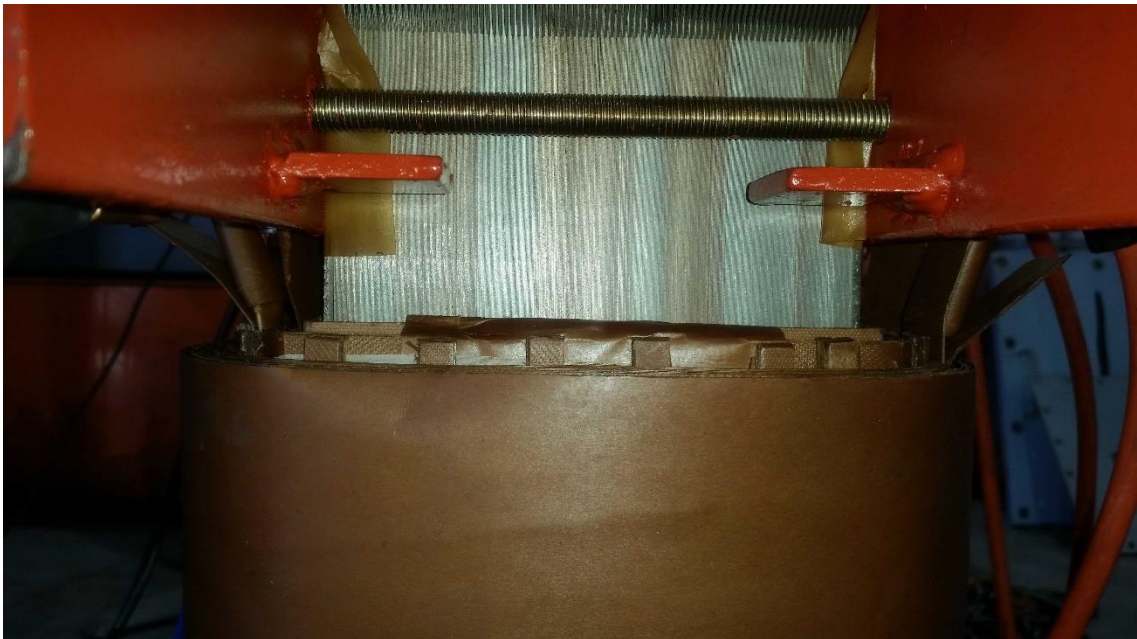
Figure 6.71 - East top view of 45% windings axial displacement test iteration.

The figure above shows the C3 to C4 winding pushed 100% to bottom of core window and C1 to C2 winding spaced 45% towards the top of the windings window.

Figure 6.72 - North bottom view of 45% windings axial displacement test iteration.

The figure above shows the C3 to C4 winding pushed 100% to bottom of core window and C1 to C2 winding spaced 45% towards the top of the windings window.

Figure 6.73 - North view of 45% windings axial displacement test iteration.

The figure above shows the C3 to C4 winding pushed 100% to bottom of core window and C1 to C2 winding spaced 45% towards the top of the windings window.

118

D.5.6 SFRA results from 45% windings axial displacement plotted against un-tanked (New benchmark)

Figure 6.74 - SFRA comparison results for open circuit testing

The figure above shows the Green line = 'A phase' after fully un-tanked (New Benchmark) and the Red Line = 'A phase' after C3 to C4 winding pushed 100% to bottom of core window and C1 to C2 winding spaced 45% towards the top of the windings window.

Figure 6.75 - SFRA comparison results for open circuit testing

The figure above shows the Blue line = 'B phase' after fully un-tanked (New Benchmark) and the Grey Line = 'B phase' after C3 to C4 winding pushed 100% to bottom of core window and C1 to C2 winding spaced 45% towards the top of the windings window.

Figure 6.76 - SFRA comparison results for open circuit testing

The figure above shows the Red line = 'C phase' after fully un-tanked (New Benchmark) and the Purple Line = 'C phase' after C3 to C4 winding pushed 100% to bottom of core window and C1 to C2 winding spaced 45% towards the top of the windings window.

Figure 6.77 - SFRA comparison results for short circuit testing

120

The figure above shows the Blue line = 'A phase' after fully un-tanked (New Benchmark) and the Light Blue Line = 'A phase' after C3 to C4 winding pushed 100% to bottom of core window and C1 to C2 winding spaced 45% towards the top of the windings window.

Figure 6.78 - SFRA comparison results for short circuit testing

The figure above shows the Orange line = 'B phase' after fully un-tanked (New Benchmark) and the Pink Line = 'B phase' after C3 to C4 winding pushed 100% to bottom of core window and C1 to C2 winding spaced 45% towards the top of the windings window.

Figure 6.79 - SFRA comparison results for short circuit testing

The figure above shows the Brown line = 'C phase' after fully un-tanked (New Benchmark) and the Blue Line = 'C phase' after C3 to C4 winding pushed 100% to bottom of core window and C1 to C2 winding spaced 45% towards the top of the windings window.

D.5.7   Zoomed trace comparison between un-tanked (new benchmark), 45% and 90% windings axial displacement (Open circuit tests)

Figure 6.80 – Zoomed SFRA comparison results for open circuit testing

The figure above shows the Green line = 'A phase' after fully un-tanked (New Benchmark), the Grey Line = 'A phase' after C3 to C4 winding pushed 100% to bottom of core window and C1 to C2 winding spaced 90% towards the top of the windings window and the Red Line = 'A phase' after C3 to C4 winding pushed 100% to bottom of core window and C1 to C2 winding spaced 45% towards the top of the windings window.
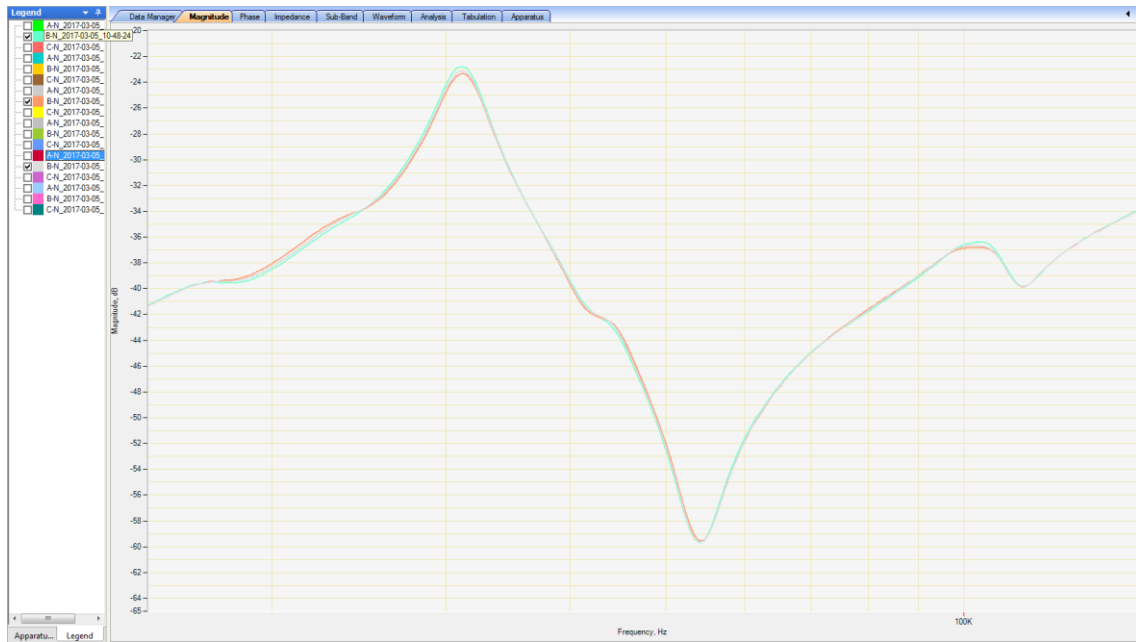
Figure 6.81 - Zoomed SFRA comparison results for open circuit testing

The figure above shows Blue line = 'B phase' after fully un-tanked (New Benchmark), the Orange Line = 'B phase' after C3 to C4 winding pushed 100% to bottom of core window and C1 to C2 winding spaced 90% towards the top of the windings window and the Grey Line = 'B phase' after C3 to C4 winding pushed 100% to bottom of core window and C1 to C2 winding spaced 45% towards the top of the windings window.

Figure 6.82 - Zoomed SFRA comparison results for open circuit testing

The figure above shows the Red line = 'C phase' after fully un-tanked (New Benchmark), the Yellow Line = 'C phase' after C3 to C4 winding pushed 100% to bottom of core window and C1 to C2 winding spaced 90% towards the top of the windings window and the Purple Line = 'C phase' after C3 to C4 winding pushed 100% to bottom of core window and C1 to C2 winding spaced 45% towards the top of the windings window.
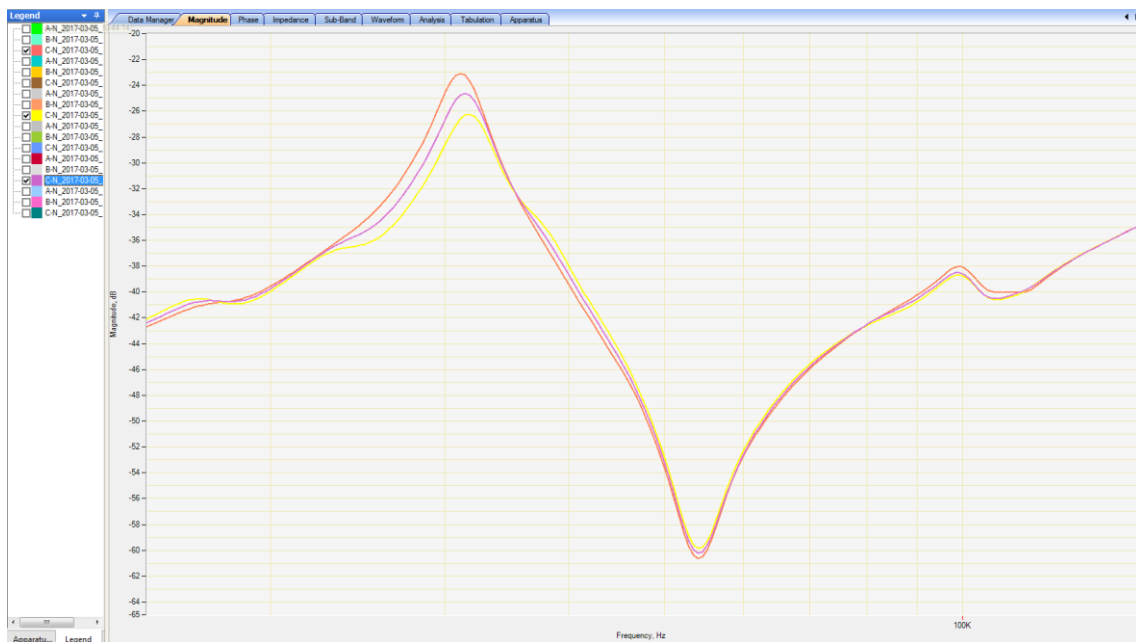
D.5.8   Zoomed trace comparison between un-tanked (new benchmark), 45% and 90% windings axial displacement (Short circuit tests)

Figure 6.83 - Zoomed SFRA comparison results for short circuit testing

The figure above shows the Blue line = 'A phase' after fully un-tanked (New Benchmark), the Grey Line = 'A phase' after C3 to C4 winding pushed 100% to bottom of core window and C1 to C2 winding spaced 90% towards the top of the windings window and the Light Blue Line = 'A phase' after C3 to C4 winding pushed 100% to bottom of core window and C1 to C2 winding spaced 45% towards the top of the windings window.

Figure 6.84 - Zoomed SFRA comparison results for short circuit testing

The figure above shows the Orange line = 'B phase' after fully un-tanked (New Benchmark), the Green Line = 'B phase' after C3 to C4 winding pushed 100% to bottom of core window and C1 to C2 winding spaced 90% towards the top of the windings window and the Pink Line = 'B phase' after C3 to C4 winding pushed 100% to bottom of core window and C1 to C2 winding spaced 45% towards the top of the windings window.
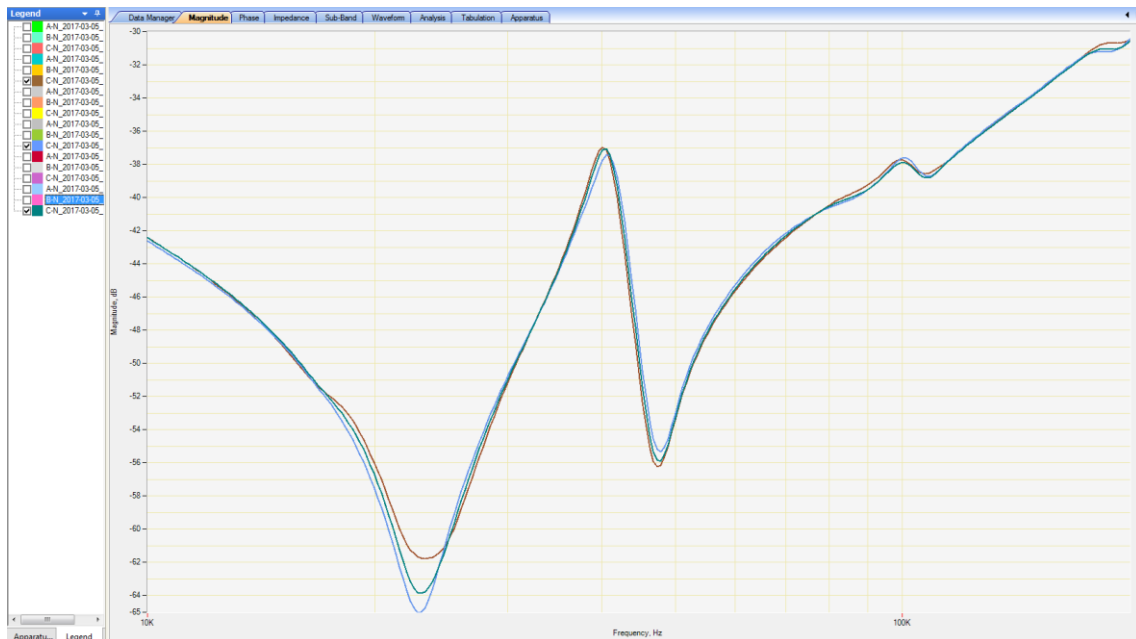

Figure 6.85 - Zoomed SFRA comparison results for short circuit testing

The figure above shows the Brown line = 'C phase' after fully un-tanked (New Benchmark), the Blue Line = 'C phase' after C3 to C4 winding pushed 100% to bottom of core window and C1 to C2 winding spaced 90% towards the top of the windings window and the Dark blue Line = 'C phase' after C3 to C4 winding pushed 100% to bottom of core window and C1 to C2 winding spaced 45% towards the top of the windings window.

Appendix E Development Code and Analysis Results

E.1.1   Specific sub-routines of script code

```
33 -    if Red=='A';
34 -        red{1,1}='A';
35 -        red{2,1}='A4';
36 -        red{3,1}='H1';
37 -        red{4,1}='red';
38 -        red{5,1}='Red';
39 -    elseif Red=='B';
40 -        red{1,1}='B';
41 -        red{2,1}='B4';
42 -        red{3,1}='H2';
43 -        red{4,1}='white';
44 -        red{5,1}='White';
45 -    elseif Red=='C';
46 -        red{1,1}='C';
47 -        red{2,1}='C4';
48 -        red{3,1}='H3';
49 -        red{4,1}='blue';
50 -        red{5,1}='Blue';
51 -    elseif Red=='N';
52 -        red{1,1}='N';
53 -        red{2,1}='n';
54 -        red{3,1}='H0';
55 -        red{4,1}='neutral';
56 -        red{5,1}='Neutral';
57 -    end
58
59 -    if Black=='A';
60 -        black{1,1}='A';
61 -        black{2,1}='A4';
62 -        black{3,1}='H1';
63 -        black{4,1}='red';
64 -        black{5,1}='Red';
65 -    elseif Black=='B';
66 -        black{1,1}='B';
67 -        black{2,1}='B4';
```

Figure 6.86 – Extract code

The code above is from the 'confind' script that creates a list of all the data column numbers that contain a pre-defined SFRA test set lead connection configuration. The purpose of this code is to allow for six different known naming conventions for a transformer's bushing phases.

```
58 -    inc=4;
59 -    delta=10;
60 -    Z1=zeros(1,length(DataP));
61
62      % This code sweeps the 'data_phase' trace data-points from 'f_min' to
63      % 'f_max' (area of trace that we are most interested in) and creates a new
64      % data set that has positive peeks around a magnitude response's resonant
65      % points (positive or negative)
66 -    for i=f_min:inc:f_max;
67 -        if abs(DataP(i)-DataP(i-inc))>delta;
68 -            Z1(i-3)=.125;
69 -            Z1(i-2)=.25;
70 -            Z1(i-1)=.5;
71 -            Z1(i)=1;
72 -            Z1(i+1)=.5;
73 -            Z1(i+2)=.25;
74 -            Z1(i+3)=.125;
75 -        else
76 -            Z1(i)=0;
77 -        end
78 -    end
79      % Can tune the filter placement by increasing or decreasing the value of
80      % Z=Z+... term as the smaller this value, the more focused the filterbank
81      % will be on the resonant points
82 -    Z1=Z1+0.01;
```

Figure 6.87 – Extract code

The code above was created as a sweeping function across the windowed SFRA phase data to locate the points along a given phase trace where the phase angle change occurs abruptly (around the respective resonant points). This code stores a single row matrix of values (Referred to as a 'double' in MATLAB) in the variable 'Z1' to be used for filter placement. In this code, all values of Z1 have been increased by a value of 0.01 to raise all data points off the 0 axis. This has been done to distribute some of the area under the curve as will be computed in the next step. This factor was included after the main loop for tuning purposes.

```
104     % Calculating the total area under the curve using the trapazoidal method
105     % as we have data points, not a 'function'
106 -   int_Z1=trapz(Z1);
```

Figure 6.88 - Extract code

The code above exploits MATLAB's 'trapz' function to estimate the area under the curve to be used as a devisable 'total' by the respective number of filters (pre-set to 15) for the creation of a new variable, 'a_space' (summed area between filters).

```
118        % Calculating the filter placement vector E
119        % Q is the sumed area at the corrasponding point of vector E from the
120        % previous point
121 -      a=f_min;
122 -      b=2;
123        %Used 50 as an arbatary number as it must be greater than the possible
124        %number of entries (dose not affect result)
125 -      Q1=zeros(1,50);
126 -      Q1(1)=0;
127        % Must be M+2 because of the number of entries required by the filter
128        % generator code
129 -      E1=zeros(1,M+2);
130 -      E1(1)=f_min;
131        %This code creates a vector E of length M+2 for the filter placement
132        %focused around the trace resonant peaks as determined (location wise) by
133        %Z above
134 -    ┌ for z=2:M+2
135 -    ┌     for i=a:1:f_max;
136 -              if Q1(z)<a_space;
137 -              Q1(z)=Q1(z)+Z1(i);
138 -              E1(b)=i;
139 -              end
140 -    └     end
141 -          a=E1(b)+1;
142 -          b=b+1;
143 -    └ end
144        % reseting the respective variables
145 -      a=1;
146 -      b=1;
147 -      z=1;
148
149 -      clearvars Z1 Z2 Q1 a b z inc delta %DataM DataP
```

Figure 6.89 – Extract code

The code above sweeps across the 'Z1' dataset, summing each value with the previous loop iteration, stored in the variable 'Q1' until the pre-defined constraint 'a_space' is less than 'Q1'. With each inner loop, the temporary variable 'i' increases by a value of 1, indicating the data point along the SFRA trace that the 'Z1(i)' value is referring to. The corresponding phase-plot data-point is then stored in the pre-initialised matrix 'E1' before the inner loop finishes. Each time the inner 'for loop' is satisfied, the temporary variable 'a' takes on the 'E1(b)' value to allow the continuation of the sweep from that point and the temporary variable 'b' increases by a value of 1 each loop as this defines the cell in 'E1' that the next data point number 'i' will be stored.

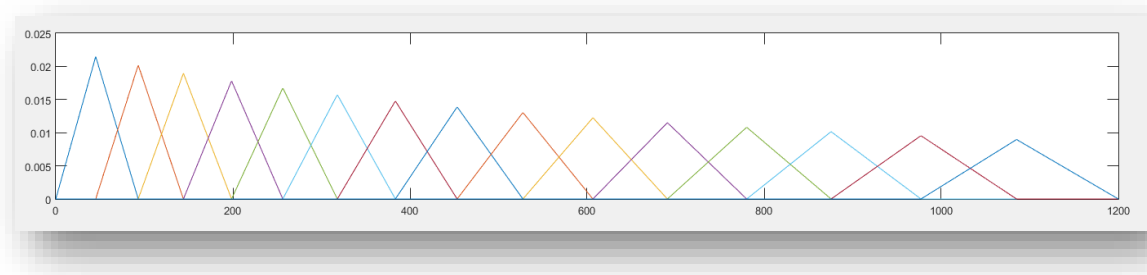# E.1.2   Filter Bank testing

Figure 6.90 – Filter bank consisting of 15 Hamming filters spaced using a Mel-scale axis with unit area normalisation.
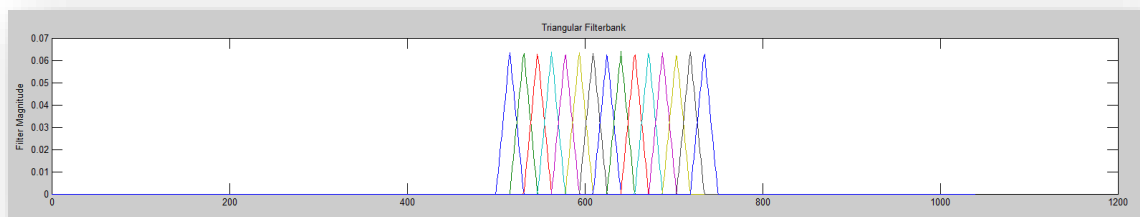

Figure 6.91 – Filter bank consisting of 15 hamming filters spaced using a linear scale axis between a window constraints of 500 to 750.
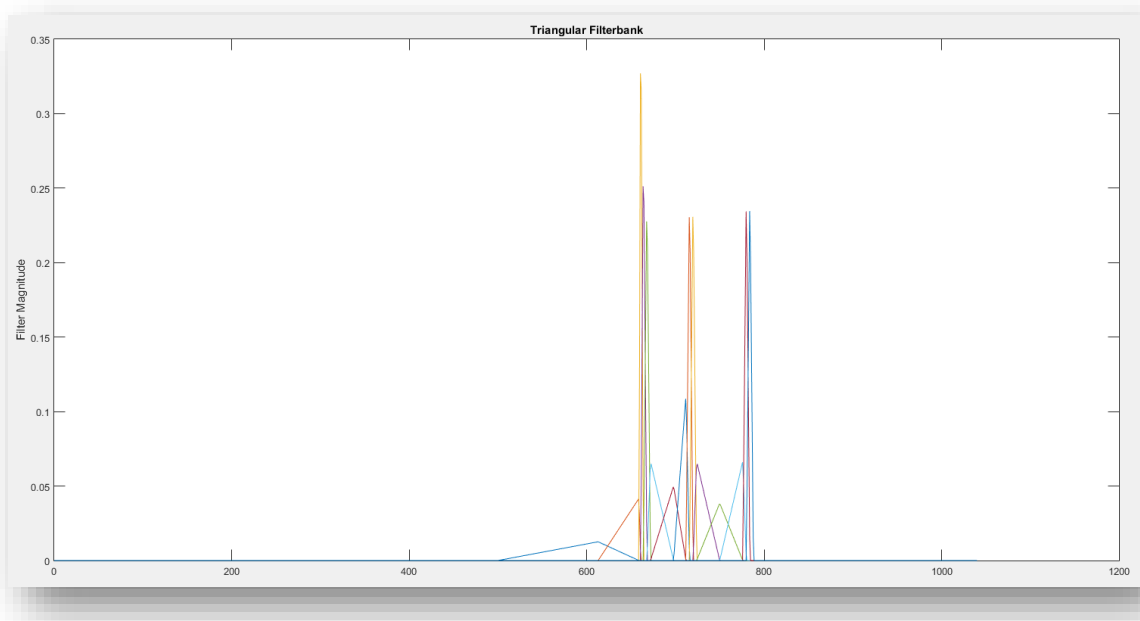

Figure 6.92 – Plot of a sample hamming filter bank containing 15 filters.

The plot above was created by analysing a sample SFRA phase trace to determine the resonant peak locations along the corresponding magnitude plot, focusing filters around these points. Normalisation of the unit area for all filters in this plot has been applied.
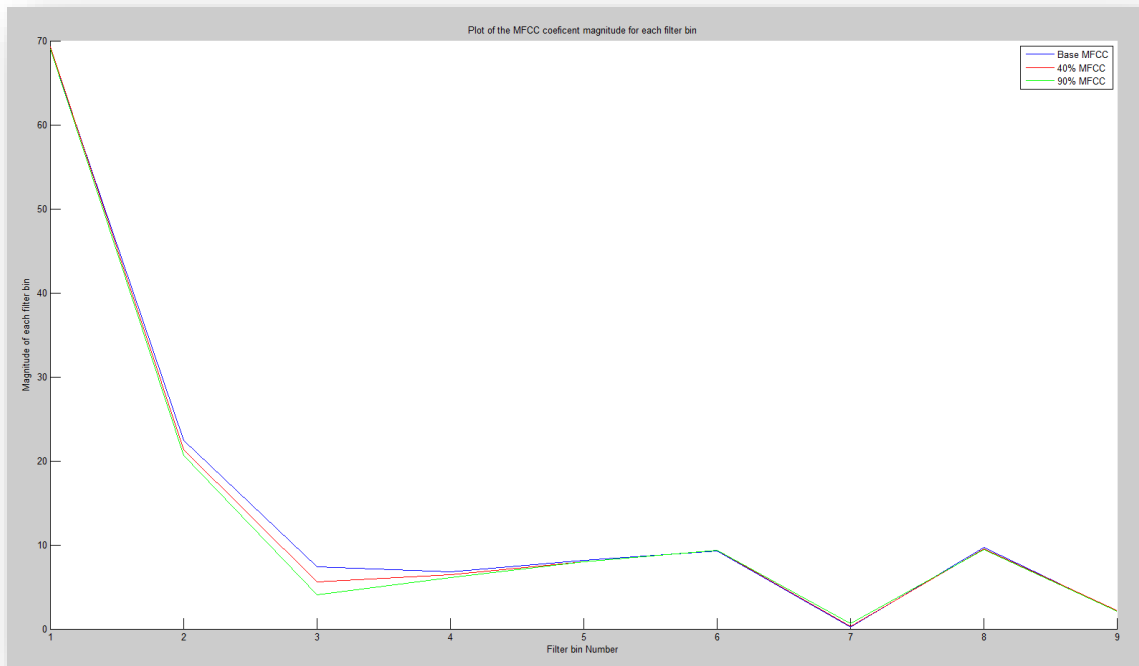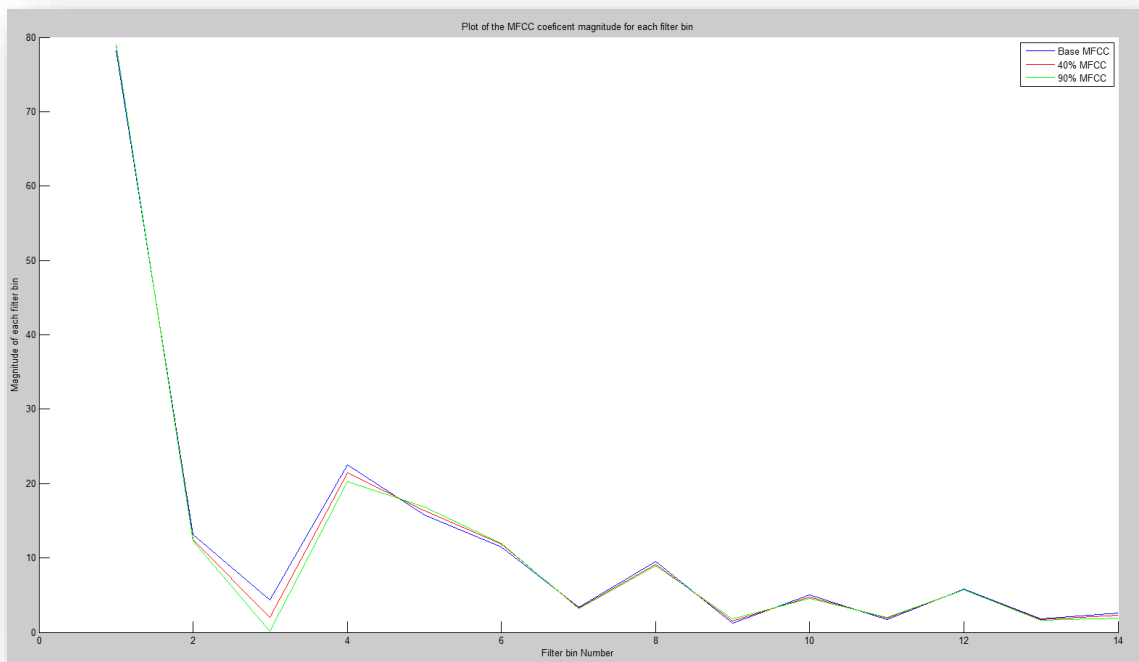
E.1.3 Cepstrum coefficient comparisons

Figure 6.93 - Comparison plot 1 of the cepstrum coefficients

The figure above is the resulting output from processing baseline, 45% and 90% fault simulation data (from section 3.2.2) using the method detailed in section 4.2 above. *Settings -> 'f_min'=600, 'f_max'=850, 'M'=10.*
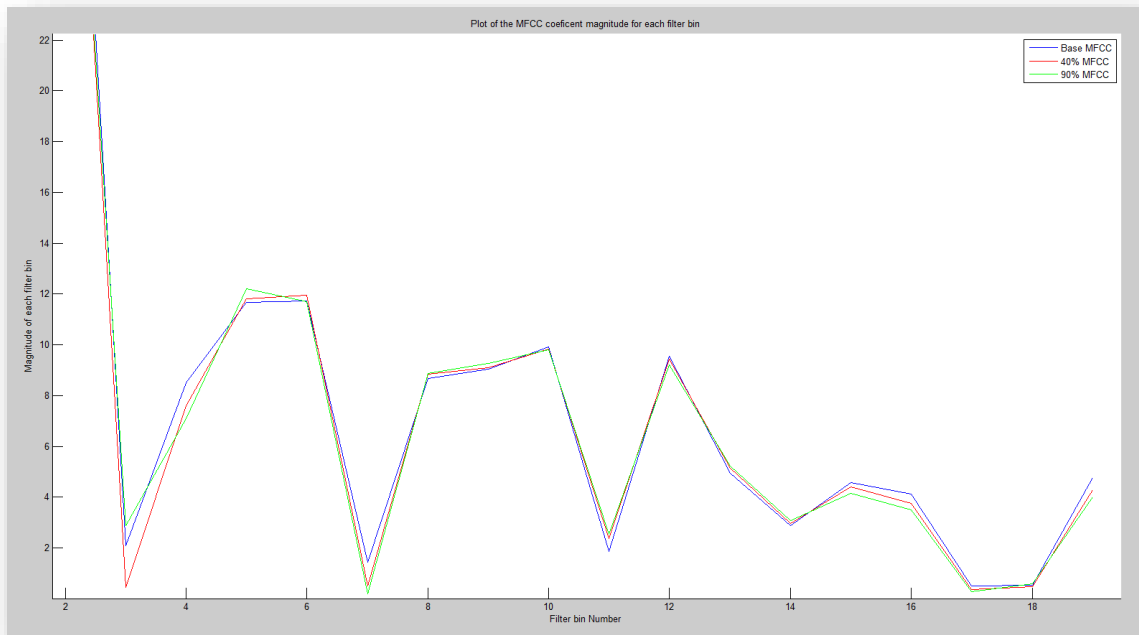

Figure 6.94 – Comparison plot 2 of the cepstrum coefficients

The figure above is the resulting output from processing baseline, 45% and 90% fault simulation data (from section 3.2.2) using the method detailed in section 4.2 above. *Settings -> 'f_min'=600, 'f_max'=850, 'M'=15*
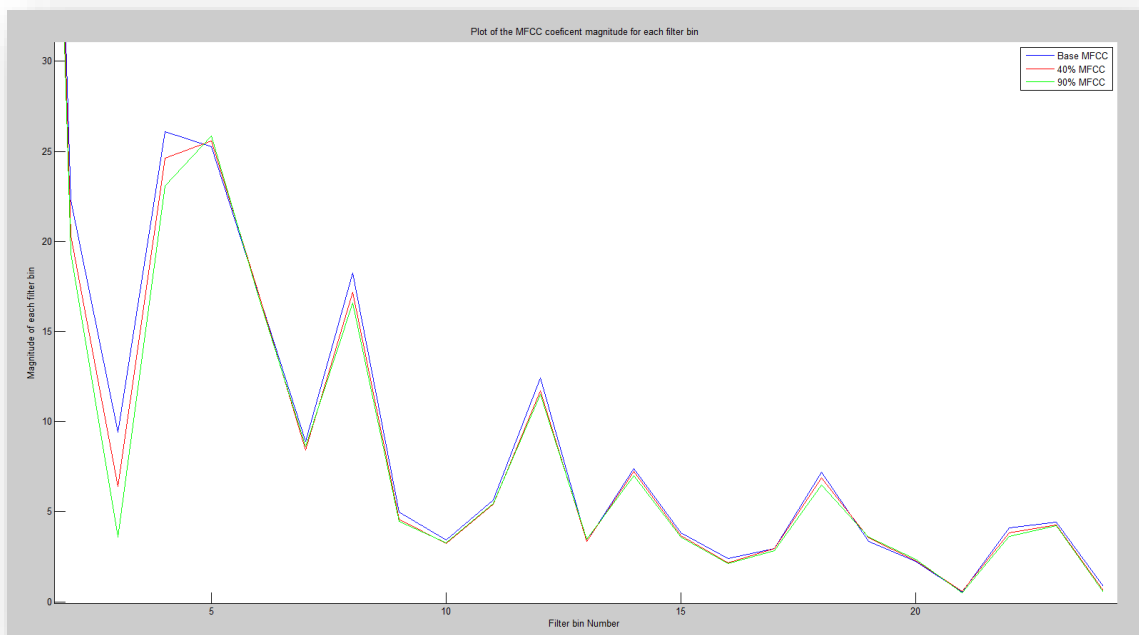

Figure 6.95 - Comparison plot 3 of the cepstrum coefficients

The figure above is the resulting output from processing baseline, 45% and 90% fault simulation data (from section 3.2.2) using the method detailed in section 4.2 above. *Settings -> 'f_min'=600, 'f_max'=850, 'M'=20.*
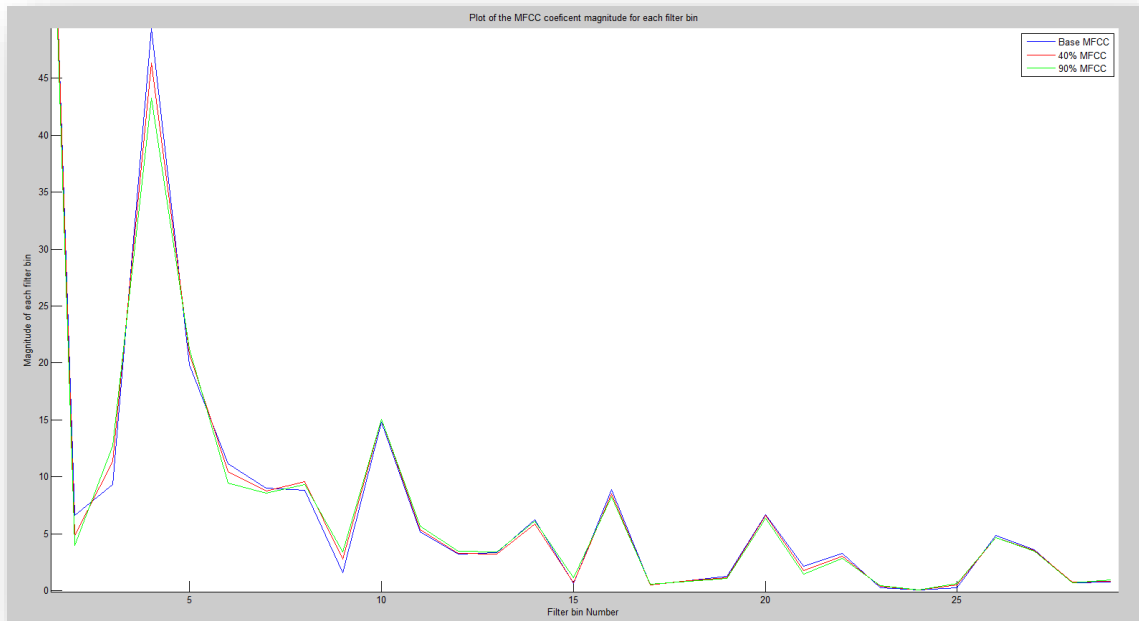
Figure 6.96 - Comparison plot 4 of the cepstrum coefficients

The figure above is the resulting output from processing baseline, 45% and 90% fault simulation data (from section 3.2.2) using the method detailed in section 4.2 above. *Settings -> 'f_min'=600, 'f_max'=850, 'M'=25.*

Figure 6.97 - Comparison plot 5 of the cepstrum coefficients

The figure above is the resulting output from processing baseline, 45% and 90% fault simulation data (from section 3.2.2) using the method detailed in section 4.2 above. *Settings -> 'f_min'=600, 'f_max'=850, 'M'=30.*
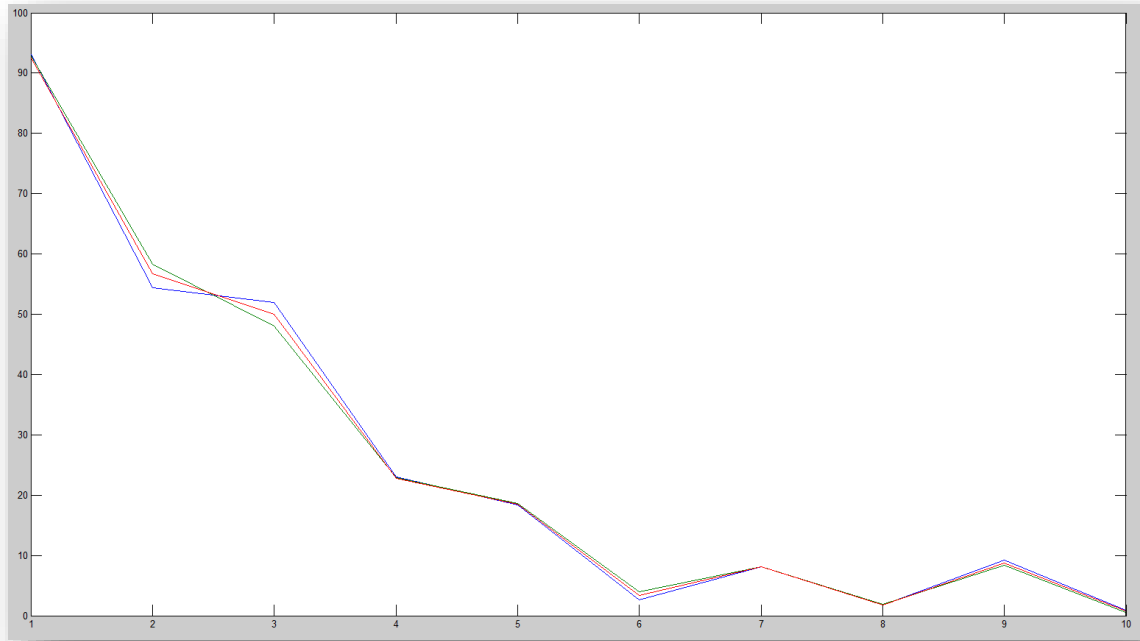
Figure 6.98 - Comparison plot 6 of the cepstrum coefficients

The figure above is the resulting output from processing baseline, 45% and 90% fault simulation data (from section 3.2.2) using the method detailed in section 4.2 above. *Settings -> 'f_min'=500, 'f_max'=750, 'M'=10.*
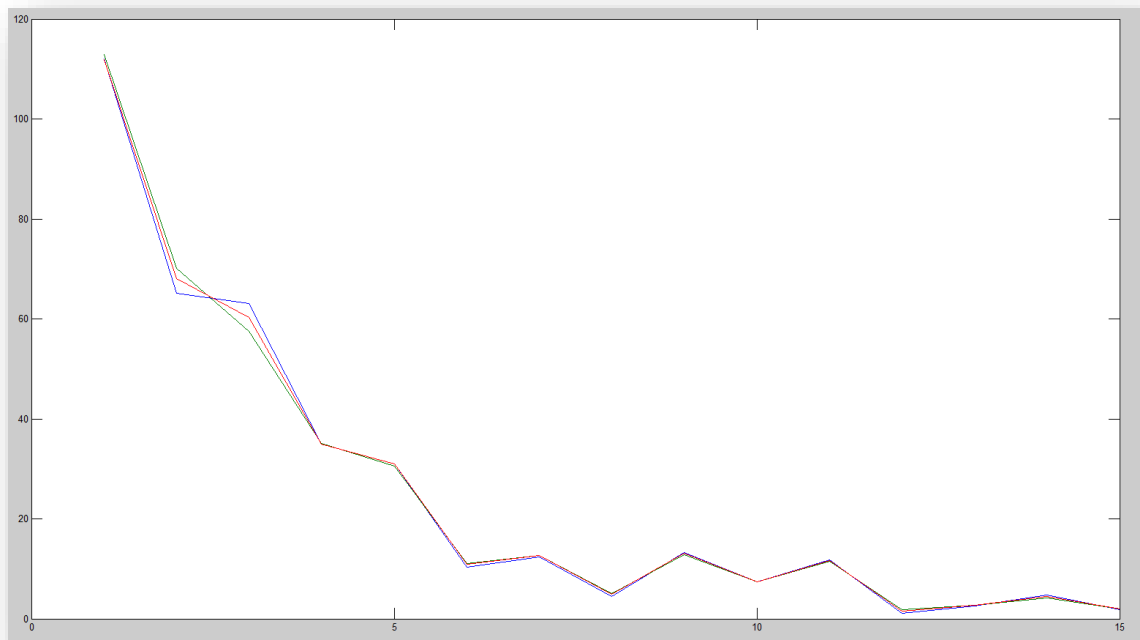

Figure 6.99 - Comparison plot 7 of the cepstrum coefficients

134

The figure above is the resulting output from processing baseline, 45% and 90% fault simulation data (from section 3.2.2) using the method detailed in section 4.2 above. *Settings -> 'f_min'=500, 'f_max'=750, 'M'=15.*
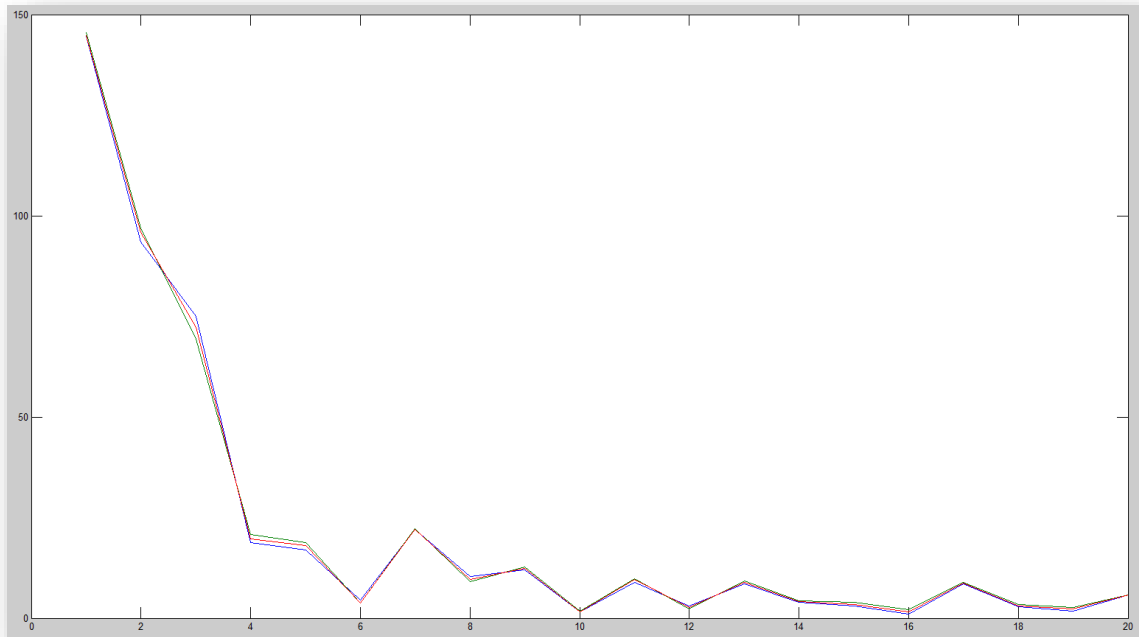

Figure 6.100 - Comparison plot 8 of the cepstrum coefficients

The figure above is the resulting output from processing baseline, 45% and 90% fault simulation data (from section 3.2.2) using the method detailed in section 4.2 above. *Settings -> 'f_min'=500, 'f_max'=750, 'M'=20.*

Figure 6.101 - Comparison plot 9 of the cepstrum coefficients

The figure above is the resulting output from processing baseline, 45% and 90% fault simulation data (from section 3.2.2) using the method detailed in section 4.2 above. *Settings -> 'f_min'=500, 'f_max'=750, 'M'=25*
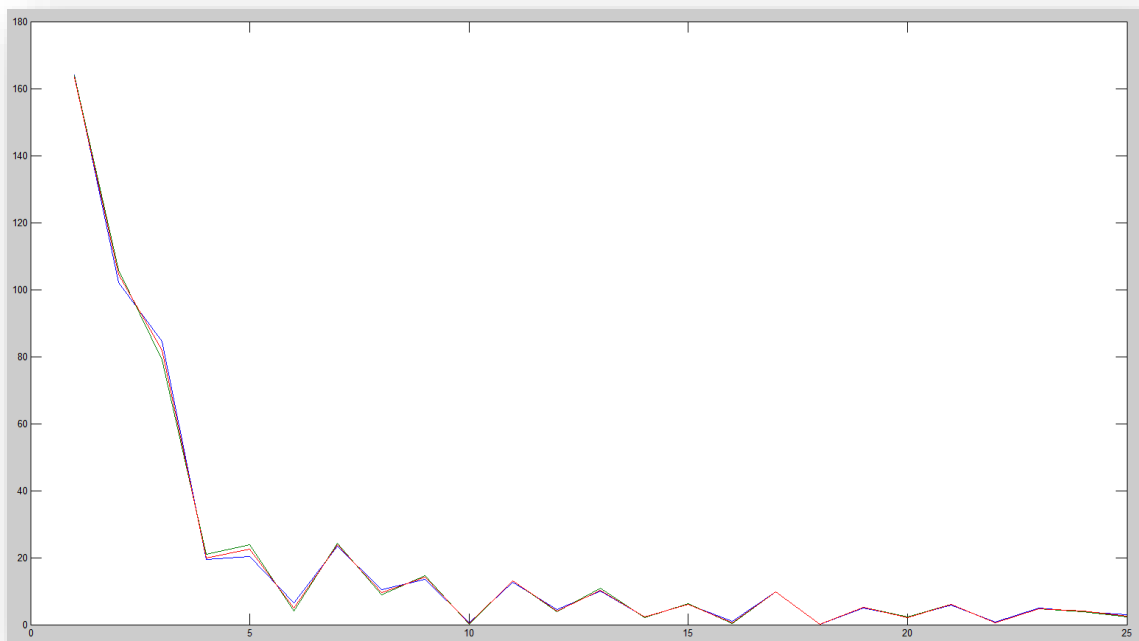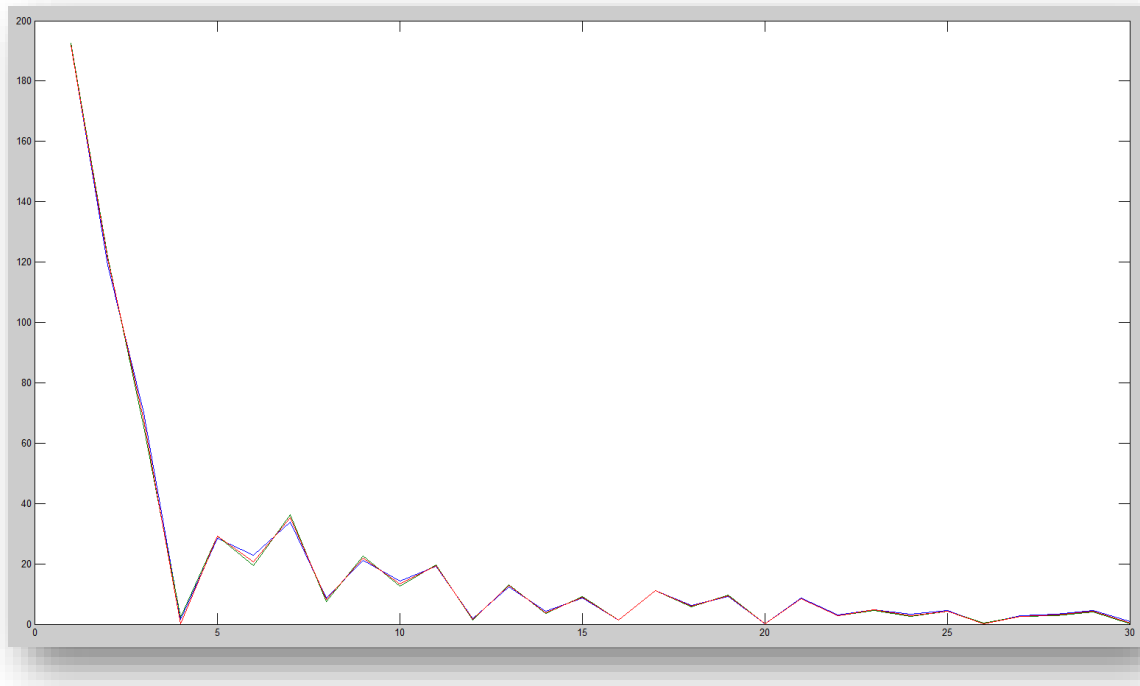

Figure 6.102 - Comparison plot 10 of the cepstrum coefficients

The figure above is the resulting output from processing baseline, 45% and 90% fault simulation data (from section 3.2.2) using the method detailed in section 4.2 above. *Settings -> 'f_min'=500, 'f_max'=750, 'M'=30.*

E.1.4 Full Two-Dimensional Plot Comparison Results

Figure 6.103 - Comparison plot 1 of the cepstrum coefficient 2 plotted against cepstrum coefficient 3

The figure above is the resulting output from the test subject, resulting from processing baseline, 45% and 90% fault simulation data (from section 3.2.2) using the method detailed in section 4.4 above. *Settings -> 'f_min'=500, 'f_max'=750, 'M'=30, A-N phase test.*
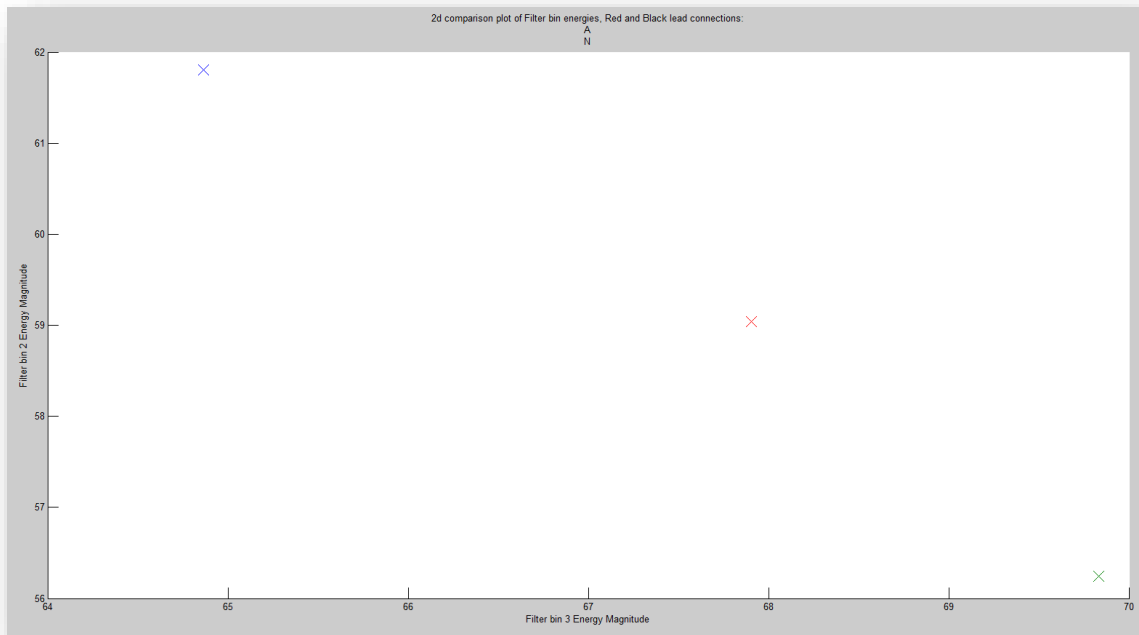

Figure 6.104 - Comparison plot 2 of the cepstrum coefficient 2 plotted against cepstrum coefficient 3

The figure above is the resulting output from the test subject and all APU transformers, resulting from processing baseline, 45% and 90% fault simulation data (from section 3.2.2) using the method detailed in section 4.4 above. *Settings -> 'f_min'=500, 'f_max'=750, 'M'=30, A-N phase test.*
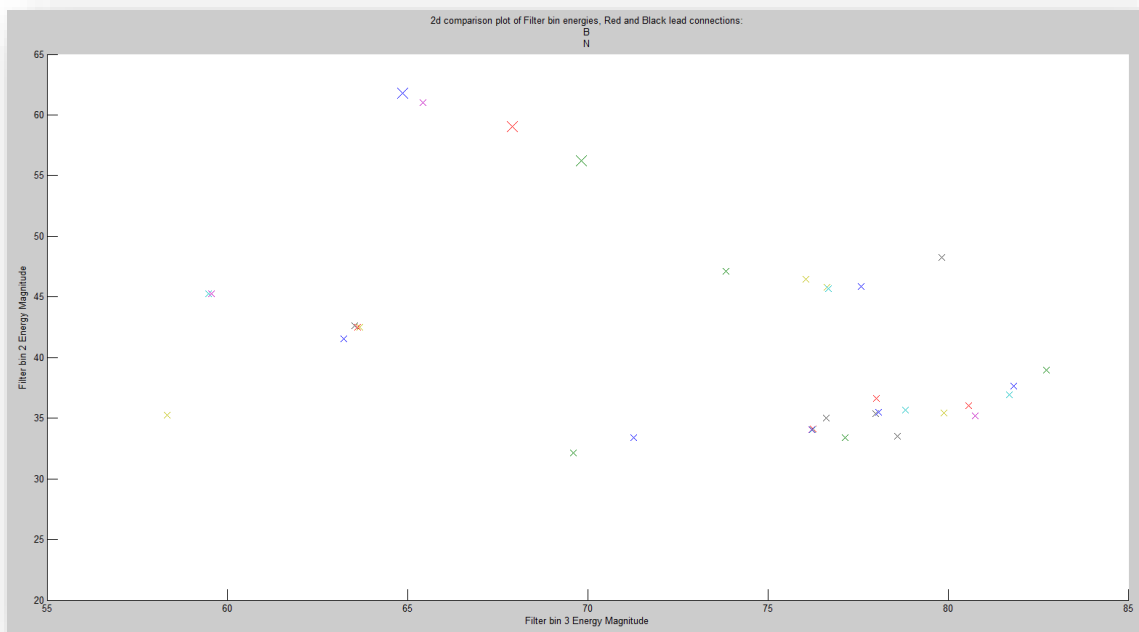

Figure 6.105 - Comparison plot 3 of the cepstrum coefficient 2 plotted against cepstrum coefficient 3

The figure above is the resulting output from the test subject, resulting from processing baseline, 45% and 90% fault simulation data (from section 3.2.2) using the method detailed in section 4.4 above. *Settings -> 'f_min'=500, 'f_max'=750, 'M'=30, B-N phase test.*

Figure 6.106 - Comparison plot 4 of the cepstrum coefficient 2 plotted against cepstrum coefficient 3

The figure above is the resulting output from the test subject and all APU transformers, resulting from processing baseline, 45% and 90% fault simulation data (from section 3.2.2) using the method detailed in section 4.4 above. *Settings -> 'f_min'=500, 'f_max'=750, 'M'=30, B-N phase test.*
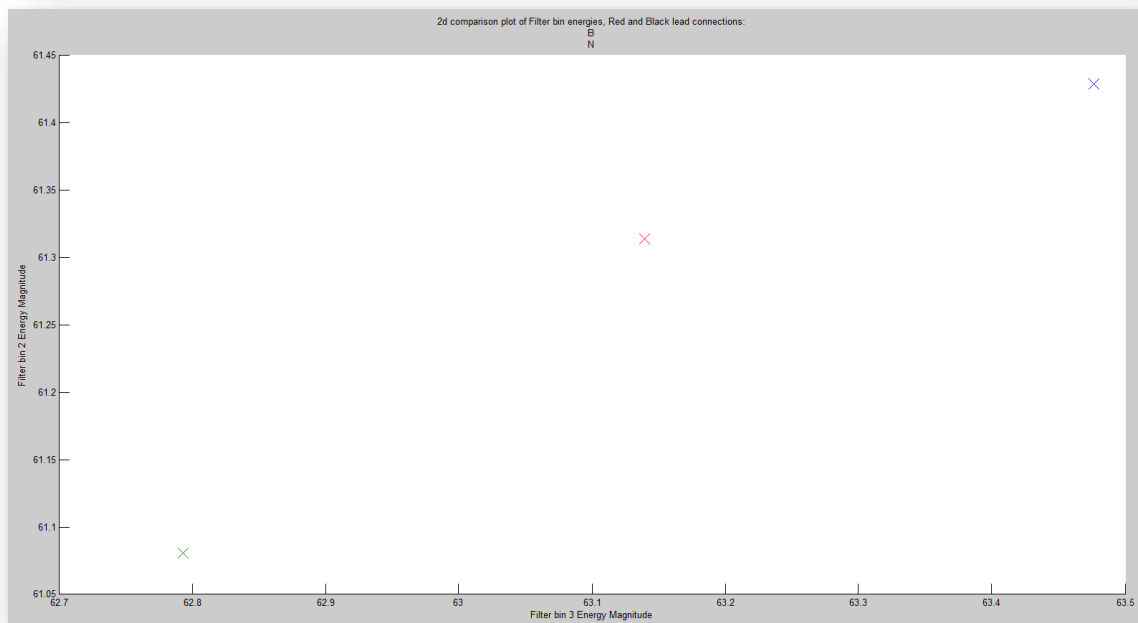

Figure 6.107 - Comparison plot 5 of the cepstrum coefficient 2 plotted against cepstrum coefficient 3

The figure above is the resulting output from the test subject, resulting from processing baseline, 45% and 90% fault simulation data (from section 3.2.2) using the method detailed in section 4.4 above. *Settings -> 'f_min'=500, 'f_max'=750, 'M'=30, C-N phase test.*
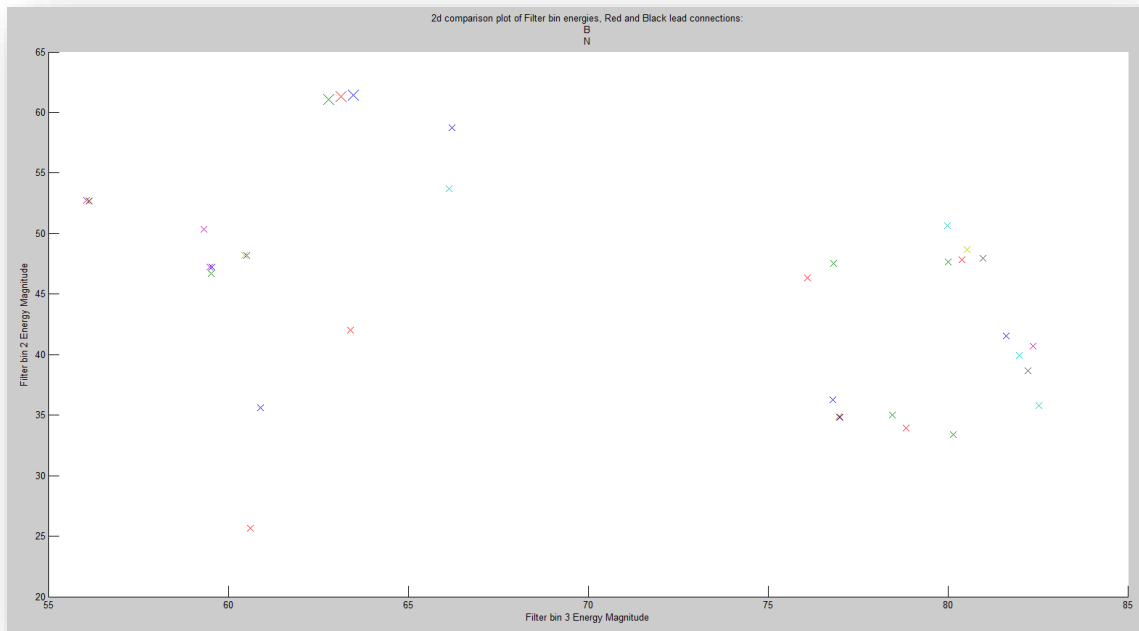

Figure 6.108 - Comparison plot 6 of the cepstrum coefficient 2 plotted against cepstrum coefficient 3

The figure above is the resulting output from the test subject and all APU transformers, resulting from processing baseline, 45% and 90% fault simulation data (from section 3.2.2) using the method detailed in section 4.4 above. *Settings -> 'f_min'=500, 'f_max'=750, 'M'=30, C-N phase test.*
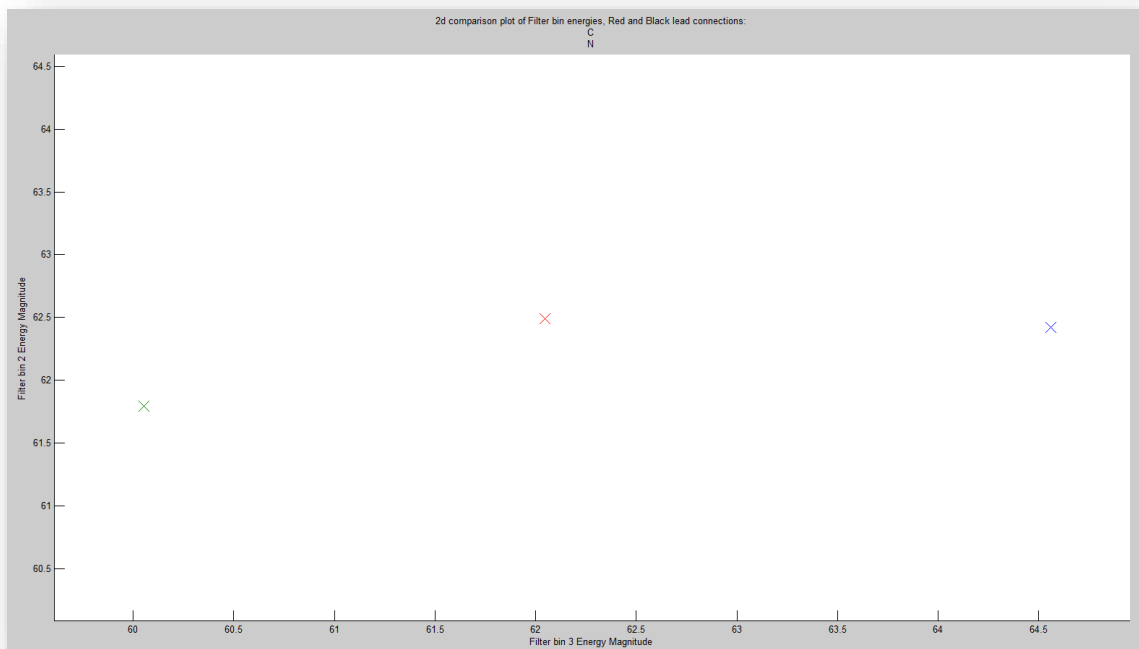
Figure 6.109 - Comparison plot 7 of the cepstrum coefficient 2 plotted against cepstrum coefficient 3

The figure above is the resulting output from all APU transformers, resulting from processing baseline, 45% and 90% fault simulation data (from section 3.2.2) using the method detailed in section 4.4 above. *Settings -> 'f_min'=500, 'f_max'=750, 'M'=30, A-'B phase' test.*
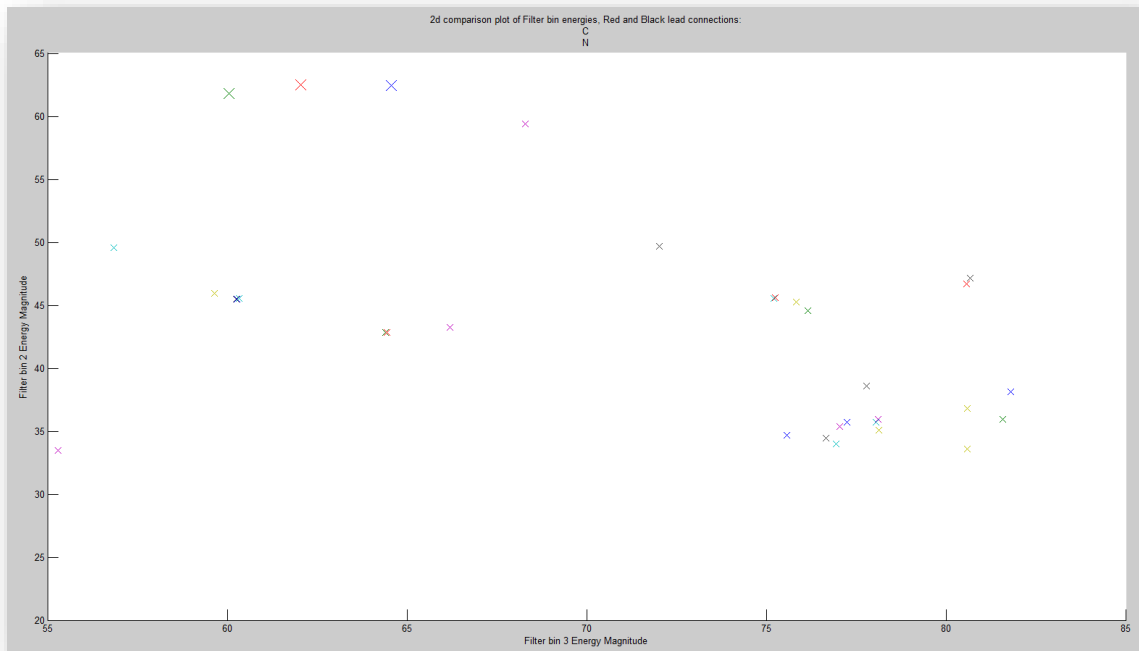

Figure 6.110 - Comparison plot 8 of the cepstrum coefficient 2 plotted against cepstrum coefficient 3

The figure above is the resulting output from all APU transformers, resulting from processing baseline, 45% and 90% fault simulation data (from section 3.2.2) using the method detailed in section 4.4 above. *Settings -> 'f_min'=500, 'f_max'=750, 'M'=30, B-'C phase' test.*
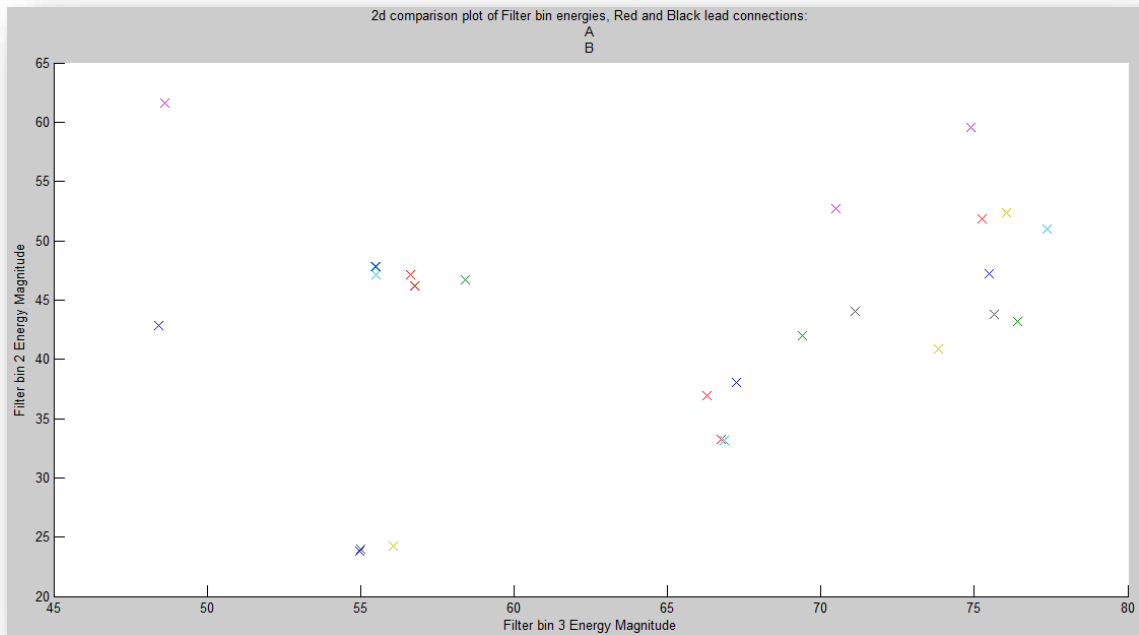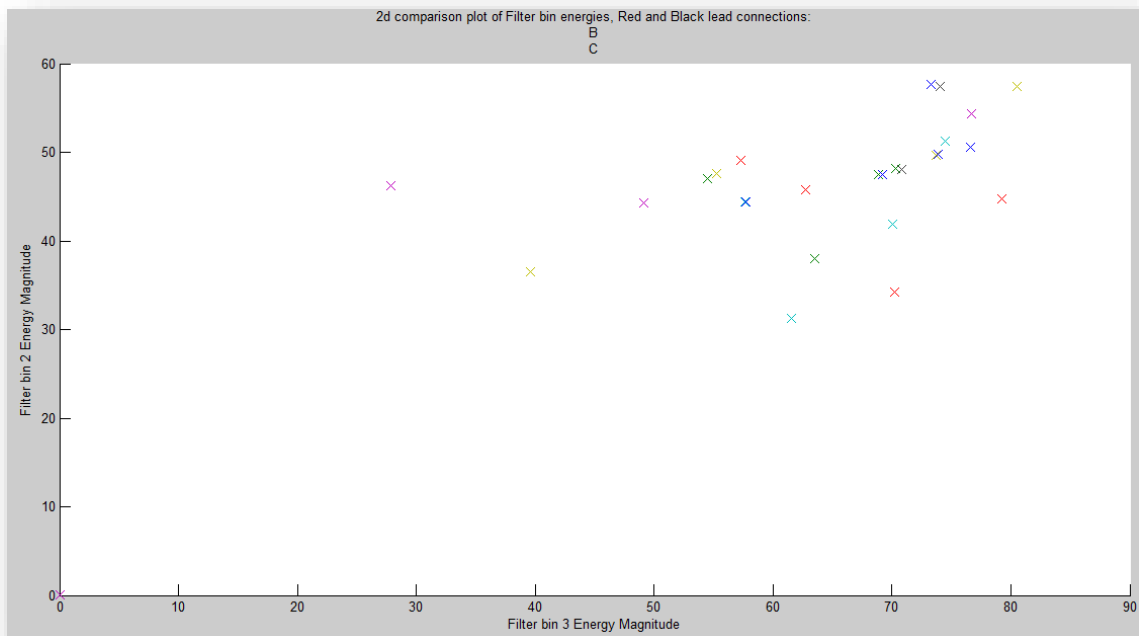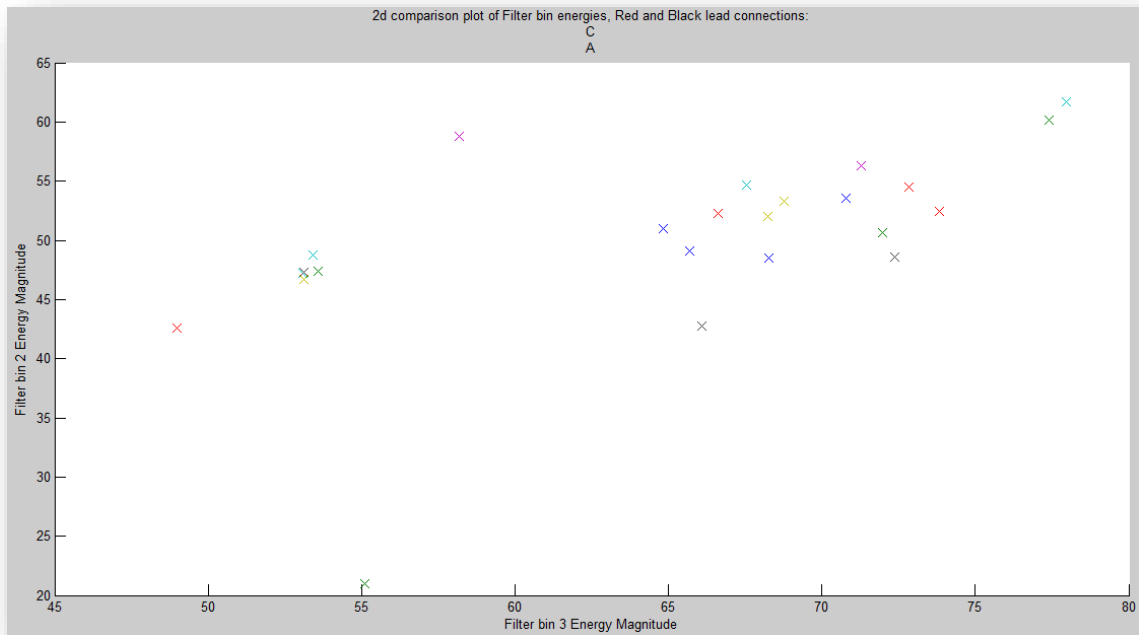

Figure 6.111 - Comparison plot 9 of the cepstrum coefficient 2 plotted against cepstrum coefficient 3

The figure above is the resulting output from all APU transformers, resulting from processing baseline, 45% and 90% fault simulation data (from section 3.2.2) using the method detailed in section 4.4 above. *Settings -> 'f_min'=500, 'f_max'=750, 'M'=30, C-'A phase' test.*

Bibliography

[1]   "IEEE Standard for Requirements, Terminology, and Test Procedures for Neutral Grounding Devices," *IEEE Std C57.32-2015 (Revision of IEEE Std 32-1972),* pp. 1-83, 2016.

[2]   EL-001, "AS/NZS 3000," in *Wiring Rules*, ed. Sydney, New South Wales: STANDARDS Australia, 2007.

[3]   J. R. BOYLE, "UNDERSTANDING ZIG-ZAG GROUNDING BANKS," ed: Georgia-Tech, 2008.

[4]   I. P. a. E. Society, "IEEE Standard for Requirements, Terminology, and Test Procedures for Neutral Grounding Devices," in *IEEE Std C57.32-2015 (Revision of IEEE Std 32-1972)*, ed. 3 Park Avenue, New York, NY 10016-5997, USA: IEEE, 2016.

[5]   Committee_EL-043, "Substations and high voltage installations exceeding 1 kV a.c.," in *Australian Standard® 2067*, ed. Sydney: Standards Australia, 2008.

[6]   (2017, 10/5/17). *Powerline Bushfire Safety Program, Reducing the risk of bushfires caused by powerlines.* Available: https://www.energy.vic.gov.au/safety-and-emergencies/powerline-bushfire-safety-program

[7]   L. Moodley, "Sweep frequency response analysis as a diagnostic tool to detect transformer mechanical integrity," B. d. Klerk, Ed., ed. Southern Africa: Congress The Association of Municipal Electricity Undertakings by eThekwini Electricity, 2006.

[8]   H. N. Amadi, "Analysis of Transformer Loadings and Failure Rate in Onitsha Electricity Distribution Network," vol. 4, F. I. Izuegbunam, Ed., ed. Department of Electrical & Electronic Engineering, Federal University of Technology, Owerri, Nigeria: ©Science and Education Publishing, 2016.

[9]   S. A. Ryder, "TRANSFORMER DIAGNOSTICS USING FREQUENCY RESPONSE ANALYSIS: RESULTS FOR FAULT SIMULATIONS," ed. SAINT-OUEN Cedex, France: ALSTOM TRANSFORMER RESEARCH CENTRE, 2003.

[10]   M. K. A. KRAETGE , J. L. VELÁSQUEZ, H. Viljoen , A. Dierks, "Aspects of the Practical Application of Sweep Frequency Response Analysis (SFRA) on Power Transformers," ed. South Africa: CIGRE, 2009.

[11]   A. R. Hambley, "Electrical Engineering Principles and Applications," ed. New Jersey: PEARSON, 2011.

[12]   C. Sweetser, "Sweep Frequency Response Analysis Transformer Applications," in *A Technical Paper from Doble Engineering*, D. T. McGrail, Ed., Version 1.0 ed. Massachusetts: Doble Engineering Company, 2004.

[13]   S. A. K. S.V.Kulkarni, "Transformer Engineering Design and Practice," ed. New York: Marcel Dekker, 2004.

[14]   M. E. team, "Sweep Frequency Response Analysis Application Overview," in *Internal document 1-4*, ed: Megger, 2010.

[15]   WG_A2.26, "Mechanical condition assessment of transformer windings using frequency response analysis using frequency response analysis (FRA)," in *Technical brochure 342*, ed: CIGRE, 2008.

[16]   I. P. a. E. Society, "IEEE Guide for the Application and Interpretation of Frequency Response Analysis for Oil-Immersed Transformers," in *IEEE Std C57.149*, ed. New York: IEEE, 2012.

[17]   D. E. team, "M5300 SFRA User Guide," in *72A-2498-01 Rev.A*, ed. Massachusetts: Doble Engineering Company, 2005.

[18]   L. Team, "FR Analyzer," ed: OMICRON, 2014.

[19]   T. McGrail, "SFRA Basic Analysis Volume 1," ed: Doble Engineering, 2003.

[20]   J. R. S. Sanchez, A. Avalos, C. Perez, "EXPERIENCES AND COMPARATIVES IN TESTS OF FIELD AND LABORATORY OF SWEEP IN THE FREQUENCY OF TRANSFORMERS USING METHODS OF SWEEP IN THE FREQUENCY AND IMPULSE," ed. Mexico: CIGRE, 2008.

[21]   B. Wright, "Zig – Zag Transformers," in *White Paper ZigZag_Transformers*, ed: GE, 2008.

[22] J. J, "Power Transformers Principles and Applications," J. Winders, Ed., ed. New York: MARCEL DEKKER, 2002.

[23] A. S. M. N. Hashemnia, A. Abu-Siada and Syed M. Islam, "Offline to Online Mechanical Deformation Diagnosis for Power Transformers," ed. Department of Electrical and Computer Engineering, Curtin University, Perth, WA, Australia: AUPEC, 2014.

[24] N. D. a. R. C. o. t. P. s. R. o. China, "Frequency Response Analysis on Winding Deformation of Power Transformers," in *DL 911/2004*, ed. China: PROFESSIONAL STANDARD OF THE PEOPLE'S REPUBLIC OF CHINA, 2004.

[25] S. R. Kulkarni, "Introduction to Electrical Signals and Systems," in *Chapter 5 Sampling and Quantization*, ed. New Jersey: Princeton University, 1999.

[26] F. Alagöz, "Feature Extraction: MFCC vectors," ed. Bebek, Istanbul, TURKEY: Computer Engineering Department, Boğaziçi University, 2014.

[27] K. Prahallad, "Speech Technology: A Practical Introduction," in *Topic: Spectrogram, Cepstrum and Mel-Frequency Analysis*, ed. International Institute of Information Technology Hyderabad: Carnegie Mellon University.

[28] U. Shrawankar, "TECHNIQUES FOR FEATURE EXTRACTION IN SPEECH RECOGNITION SYSTEM : A COMPARATIVE STUDY," D. V. Thakare, Ed., ed. Amravati, India: SGB Amravati University, 2010.

[29] R. R. D. Smita B. Magre, Pukhraj P. Shrishrimal, "A Comparative Study on Feature Extraction Techniques in Speech Recognition," Research Gate, 2013. Available: https://www.researchgate.net/publication/278549945_A_Comparative_Study_on_Feature_Extraction_Techniques_in_Speech_Recognition

[30] K. Rao, "Discrete cosine transform: algorithms, advantages, applications," P. Yip, Ed., ed. San Diego, CA, USA: Academic Press Professional, Inc., 1990.

[31] EL0008, "Power Transformers," in *AS/NZS 60076*, ed. Sydney: Standards Australia Limited, 2013.

[32] EL-008, "Power transformers Part 1.2: Minimum Energy Performance Standard (MEPS) requirements for distribution transformers " in *AS 2374.1.2—2003* ed. Sydney, NSW 2001, Australia: Standards Australia, 2001.

[33] P. T. EL/8, "Insulating liquids Part 2: Test methods Method 2.1: Determination of the breakdown voltage at power frequency " in *AS 1767.2.1—1999*, R. b. EL-008, Ed., ed. Homebush, NSW: Standards Association of Australia, 1999, Reconfirmed 2016.

[34] I. The MathWorks. (2017, 16/06/2017). *MATLAB*.

[35] H. Hermansky and L. A. Cox, "Perceptual Linear Predictive (PLP) Analysis-Resynthesis Technique," in *Final Program and Paper Summaries 1991 IEEE ASSP Workshop on Applications of Signal Processing to Audio and Acoustics*, 1991, pp. 0_37-0_38.

[36] EL/8, "Insulating liquids Part 2: Test methods Method 2.1: Determination of the breakdown voltage at power frequency," in *AS 1767.2.1*, ed. Sydney: Council of Standards Australia, 1999 (Reconfirmed 2016).

144